Theses and Dissertations   1. Thesis and Dissertation Collection, all items

2001-12

Characterization and performance of a liguid hydrocarbon-fueled pulse detonation rocket engine

Damphousse, Paul E.

Monterey, California. Naval Postgraduate School

http://hdl.handle.net/10945/6152

NAVAL POSTGRADUATE SCHOOL
Monterey, California

THESIS

CHARACTERIZATION AND PERFORMANCE OF A LIQUID HYDROCARBON-FUELED PULSE DETONATION ROCKET ENGINE

by

Paul E. Damphousse

December 2001

Thesis Advisor:	Christopher M. Brophy
Co-Advisor:	Jose O. Sinibaldi

THIS PAGE INTENTIONALLY LEFT BLANK

REPORT DOCUMENTATION PAGE		*Form Approved OMB No. 0704-0188*

Public reporting burden for this collection of information is estimated to average 1 hour per response, including the time for reviewing instruction, searching existing data sources, gathering and maintaining the data needed, and completing and reviewing the collection of information. Send comments regarding this burden estimate or any other aspect of this collection of information, including suggestions for reducing this burden, to Washington headquarters Services, Directorate for Information Operations and Reports, 1215 Jefferson Davis Highway, Suite 1204, Arlington, VA 22202-4302, and to the Office of Management and Budget, Paperwork Reduction Project (0704-0188) Washington DC 20503.

1. AGENCY USE ONLY *(Leave blank)*	2. REPORT DATE December 2001	3. REPORT TYPE AND DATES COVERED Master's Thesis

4. TITLE AND SUBTITLE CHARACTERIZATION AND PERFORMANCE OF A LIQUID HYDROCARBON-FUELED PULSE DETONATION ROCKET ENGINE	5. FUNDING NUMBERS N0001401WR20153
6. AUTHOR (S) Damphousse, Paul E.	

7. PERFORMING ORGANIZATION NAME(S) AND ADDRESS(ES) Naval Postgraduate School Monterey, CA 93943-5000	8. PERFORMING ORGANIZATION REPORT NUMBER

9. SPONSORING / MONITORING AGENCY NAME(S) AND ADDRESS(ES) Office of Naval Research Ballston Tower One 800 N. Quincy Street Arlington, VA 22217-5660	10. SPONSORING/MONITORING AGENCY REPORT NUMBER

11. SUPPLEMENTARY NOTES The views expressed in this thesis are those of the author and do not reflect the official policy or position of the U.S. Department of Defense or the U.S. Government.

12a. DISTRIBUTION / AVAILABILITY STATEMENT Approved for public release; distribution is unlimited.	12b. DISTRIBUTION CODE

13. ABSTRACT *(maximum 200 words)*

A liquid hydrocarbon-fueled PDRE was built and successfully tested at the Naval Postgraduate School's Rocket Propulsion and Combustion Laboratory. The first time use of a new electro-hydraulic liquid fuel injector was demonstrated to produce consistent atomization properties while allowing for varying fuel injection durations at frequencies up to 50Hz. Planar laser-induced fluorescence and high-speed imaging were used to characterize the injection flow paths of this injector.

Using gaseous ethylene as a baseline for comparison, the PDRE was operated at various equivalence ratios and frequencies up to 40 Hz. Operation in partial fill scenarios was successfully conducted and found to deliver a decreased impulse linearly related to the percentage fill.

A series of tests was conducted using liquid JP-10 and RP-1 fuels over varying oxidizer-to-fuel ratio. The higher pressures, wave speeds, and resulting impulse measurements revealed the benefits of using high energy density hydrocarbon fuels. The difficulty in detonating these fuels was demonstrated and overcome using a variety of different geometries and hardware configurations.

14. SUBJECT TERMS Detonation, Pulse Detonation Rocket Engine, Hydrocarbon Fuels, Space Propulsion	15. NUMBER OF PAGES
	16. PRICE CODE

17. SECURITY CLASSIFICATION OF REPORT Unclassified	18. SECURITY CLASSIFICATION OF THIS PAGE Unclassified	19. SECURITY CLASSIFICATION OF ABSTRACT Unclassified	20. LIMITATION OF ABSTRACT UL

i

THIS PAGE INTENTIONALLY LEFT BLANK

CHARACTERIZATION AND PERFORMANCE OF A LIQUID HYDROCARBON-FUELED PULSE DETONATION ROCKET ENGINE

Paul E. Damphousse
Major, United States Marine Corps
B.S., University of Arizona, 1989

Submitted in partial fulfillment of the
Requirements for the degree of

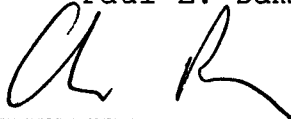MASTER OF SCIENCE IN ASTRONAUTICAL ENGINEERING

from the

NAVAL POSTGRADUATE SCHOOL
December 2001

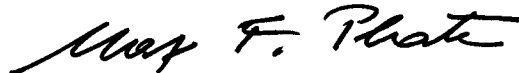Author: _____
Paul E. Damphousse

Approved by: _____
Christopher M. Brophy, Thesis Advisor

_____
Jose O. Sinibaldi, Co-Advisor

_____
Maximilian Platzer, Chairman
Department of Aeronautics and Astronautics

iii

THIS PAGE INTENTIONALLY LEFT BLANK

ABSTRACT

A liquid hydrocarbon-fueled PDRE was built and successfully tested at the Naval Postgraduate School's Rocket Propulsion and Combustion Laboratory. The first time use of a new electro-hydraulic liquid fuel injector was demonstrated to produce consistent atomization properties while allowing for varying fuel injection durations at frequencies up to 50Hz. Planar laser-induced fluorescence and high-speed imaging were used to characterize the injection flow paths of this injector.

Using gaseous ethylene as a baseline for comparison, the PDRE was operated at various equivalence ratios and frequencies up to 40 Hz. Operation in partial fill scenarios was successfully conducted and found to deliver a decreased impulse linearly related to the percentage fill.

A series of tests was conducted using liquid JP-10 and RP-1 fuels over varying oxidizer-to-fuel ratio. The higher pressures, wave speeds, and resulting impulse measurements revealed the benefits of using high energy density hydrocarbon fuels. The difficulty in detonating these fuels was demonstrated and overcome using a variety of different geometries and hardware configurations.

THIS PAGE INTENTIONALLY LEFT BLANK

TABLE OF CONTENTS

LIST OF FIGURES

LIST OF TABLES

THIS PAGE INTENTIONALLY LEFT BLANK

ACKNOWLEDGEMENTS

My sincere appreciation goes out to my thesis advisor, Professor Chris Brophy for his many hours of guidance, instruction, and advice over the last year. I also thank my co-advisor, Professor Jose Sinibaldi, for his expert opinion and sense of humor. The counsel of NASA Marshall's Dr. Noah Rhys was greatly appreciated. Mr. Harry Conner ("Master Chief of the Lab") and Mr. John Moulton provided valuable technical and hardware assistance in this effort.

I also thank my fiancée, Kathryn, for her unwavering support in my pursuit of this degree and all of my other life goals. Her encouragement became my strength.

This thesis is dedicated to the memories of my mother, Isabelle and father, Robert. I am truly blessed to have had such wonderful parents.

THIS PAGE INTENTIONALLY LEFT BLANK

I. INTRODUCTION

A. BACKGROUND

Inexpensive access to space remains a challenge in today's space launch industry. Launch costs to low Earth orbit (LEO) remain at roughly $10,000 per pound. NASA's Marshall Space Flight Center (MSFC) is investigating and developing advanced chemical propulsion systems that will eventually reduce launch costs by a factor of 100 while improving safety by a factor of 10,000. The goal is to make access to space as safe and cost effective as today's air transport systems.

An advanced propulsion system under investigation for these purposes is the pulse detonation rocket engine (PDRE). Unlike conventional rocket engines, which use constant pressure combustion, PDREs harness the energy release rate and thermodynamic characteristics of detonation waves to provide thrust. This enables PDREs to operate at higher thermodynamic efficiencies. Furthermore, since the reactants are injected into a PDRE at relatively low pressures, the need for massive turbomachinery (as used in conventional liquid-fueled rocket engines) is eliminated. Thus PDREs are potentially a simple and efficient alternative to today's conventional rocket engines.

The PDRE still requires extensive research before it can be considered as a viable option for space launch. Some areas that are being investigated are PDRE operation in a vacuum, partial-fill scenarios, and combined-cycle operations using both air and oxygen as oxidizers.

Additionally, the utilization and performance of liquid hydrocarbon fuels used in a PDRE is being characterized, since these fuels are attractive for volume-limited aerospace systems. The PDRE does have potential disadvantages, however, the primary being its relatively low specific impulse (I_{sp}) of roughly 120-200 seconds. Since these numbers represent nozzleless systems, improved nozzle design may help to offset this deficiency.

This work, conducted as part of an Office of Naval Research (ONR) program for the investigation of pulse detonation engine (PDE) design issues, involved the construction and operation of a PDRE at the Naval Postgraduate School's (NPS) Rocket Propulsion and Combustion Laboratory (RPCL). The overall goal of this work was the characterization of the performance of various liquid hydrocarbon fuels. In order to achieve this goal, an initial theoretical investigation was conducted using the Thermo-Equilibrium Program (TEP™), flow visualization was performed, and the performances of liquid hydrocarbon fuels were compared to those of gaseous hydrocarbons.

B. PDRE PRINCIPLES OF OPERATION

Before addressing the principles of operation of the PDRE, one must first make a distinction between the PDE and the PDRE. The PDE is a general term for all engines using pulsed detonations of a fuel/oxidizer mixture to produce thrust. Further, the PDE is usually considered an air-breathing device, using the surrounding air as an oxidizer. The PDRE is a subset of the PDE in which the oxidizer (usually O_2) is carried onboard. This thesis deals only

2

with the PDRE. Because of its more general nature, however, the term PDE is sometimes used to describe any pulse detonation engine.

The combustion cycle of the PDRE (Figure 1) involves the cyclical loading, detonating, and purging of a long, typically cylindrical detonation tube that is closed on one end and open on the other. A fuel/oxygen mixture is injected into the tube at or near the closed end. Once the tube is fully "charged", the reactive mixture is ignited near the closed end and a detonation wave eventually forms. Once the detonation wave reaches the open end of the tube, the pressure differential causes rarefaction waves to progress toward the closed end and the burned products are expelled. After the products are expelled, a new fuel/oxidizer charge is injected and the process is repeated.

The mechanics of a detonation wave are addressed in greater detail in the following chapter.

Each detonation wave formed by this process generates the high pressure needed to produce thrust. Due to the cyclical nature of the PDE, this thrust is produced in discrete bursts rather than in a continuous fashion as in a conventional rocket (or jet) engine. As the frequency of detonations increases, the thrust becomes quasi-steady and can be modeled as nearly continuous.
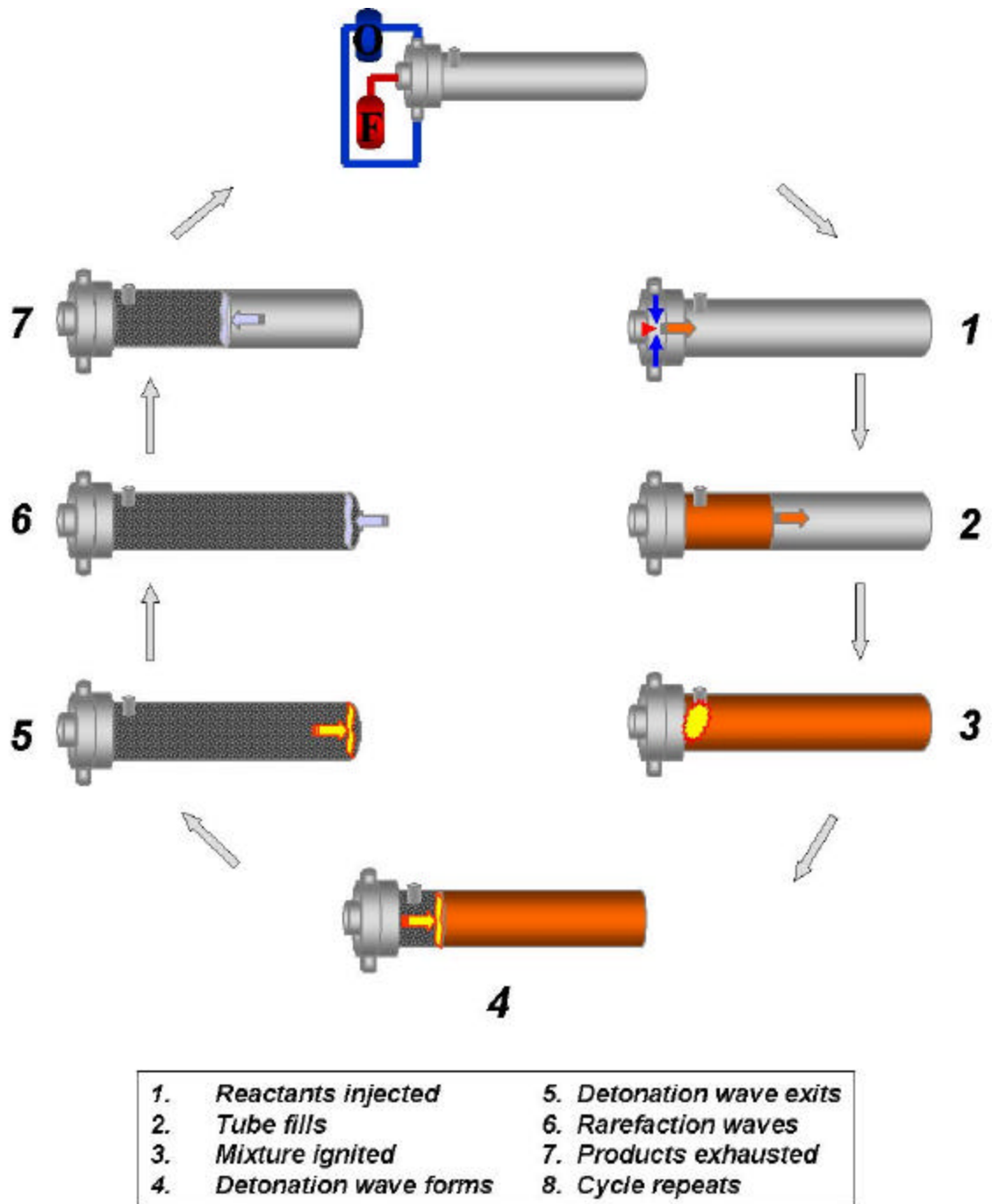
Figure 1.   PDRE Cycle

In order to overcome the unsteady thrust of the PDRE
while still taking advantage of its higher thermodynamic
efficiency, the operation of several PDREs in tandem will
be required. Rather than firing a single large PDRE,
future applications would "bundle" several smaller tubes
together around a central axis of thrust. Each of these
tubes will be fired in a sequence so as to minimize the
time in which thrust is not actually being produced.
Obviously, as the number of tubes increases, the ability to
achieve quasi-continuous thrust also increases.   An
artist's rendition of such a system is shown in Figure 2.

Figure 2.   PDRE-Propelled Spacecraft
(Courtesy of MSFC Website)

An inevitable effect of this type of geometry that
will need to be addressed is off-axis thrust effects.

Because the tubes are bundled around the axis of thrust, firing individual tubes will cause the overall thrust vector to vary. Although this may be desired for thrust vector control (TVC) purposes, it can be prevented by simultaneously firing tubes in opposing positions about the axis of thrust (i.e. 0° & 180° and 90° & 270° about the center axis). This geometry actually proves to be inherently advantageous for TVC applications.

Before such advanced applications of the PDRE can be undertaken, there are some basic issues that need further refinement. As stated above, when compared to a conventional chemical rocket engine, the PDRE is mechanically simple, lightweight, and highly reliable due to its independence from heavy turbomachinery. The PDRE does, however, have a high reliance on highly precise timing, injection, and ignition systems. The reactants must be injected into the combustion chamber at very precise and discrete intervals, ignition must occur in concert with this injection, and the hot combustion products must not ignite the unburned reactants in the following charge. Of these issues, precise injection seems to be the most challenging and is an area of investigation in this work.

II. DETONATION BACKGROUND

A. INTRODUCTION

In order to understand the combustion phenomena occurring within the PDRE, a discussion of the fundamental mechanics of detonation waves is presented.

B. DEFINITIONS

Several terms used to describe combustion processes are often mistakenly thought of as synonymous. Words such as deflagration, explosion, and detonation are sometimes used interchangeably when they actually have distinct meanings and describe very specific phenomena. Some very brief definitions are given below.

Combustion: A rapid chemical process by which a gas, liquid, or solid fuel is rapidly oxidized resulting in a release of heat and, quite often, light. During this process the transformation of chemically bound energy into heat leads to a significant temperature rise.

Combustion wave: A propagating area of localized combustion. The wave consists of a heating zone ahead of the wave, a reaction zone, and an equilibrium zone.

Deflagration: A combustion wave that propagates at a subsonic velocity sustained by a chemical reaction that occurs at nearly constant pressure. The combustor process that occurs inside rockets and gas turbines are typical examples.

Explosion (Thermal): An exothermic reaction where the rate at which energy is released exceeds the rate at which the surrounding environment can absorb that energy.   Despite being violent and rapid, the combustion event within an explosion occurs as a deflagration.

Detonation: A supersonic combustion event in which the combustion wave formed is composed of a strong shock sustained by the rapid energy release occurring in the highly compressed, high temperature region immediately behind the leading shock.   The close coupling of the strong shock wave with the rapid combustion region is known as a detonation wave.

The dramatic differences between a deflagration and detonation can be seen using a stationary one-dimensional model of a combustion wave propagating through a tube.   In Figure 3, a combustion wave is depicted with the reactants flowing into the wave from right to left.   The wave velocity (u_1) is considered subsonic in the case of a deflagration and supersonic in the case of a detonation. Using this depiction, a qualitative comparison of several deflagration and detonation thermodynamic ratios is given in Table 1. Note the dramatic increase in the velocity and pressure ratios of the detonation when compared to a deflagration.   It is the large increase in pressure, created by the detonation wave rather than a mechanical device, that make it an attractive mechanism for an advanced propulsion system.

8
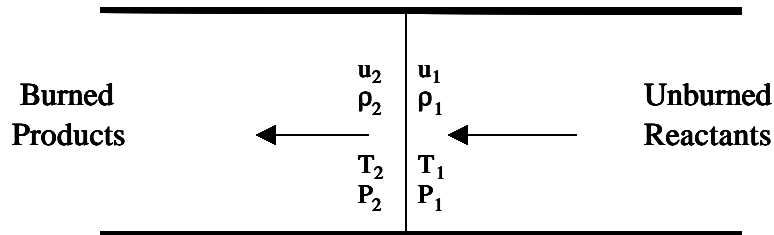
Where u=velocity
ρ=density
T=temperature
P=pressure

Figure 3.   Stationary One-Dimensional Wave

Table 1: Qualitative differences between detonations and deflagration in gases.[1]

Properties	Detonation	Deflagration
u_1/c_1	5-10	0.0001-0.03
u_2/u_1	0.4-0.7	4-16
P_2/P_1	13-55	~0.98
T_2/T_1	8-21	4-16
r_2/r_1	1.4-2.6	0.06-0.25

C.   DETONATION THEORY

With regard to the formation of a detonation, Glassman (Ref 1) offers the following description.

In a typical laboratory Bunsen burner, gaseous fuel enters the bottom of a vertical tube. Ports near the bottom of this tube allow air to be drawn in and mixed with

the passing fuel. This mixture is considered homogeneous when it exits the top of the tube where it is ignited. Within the flame that sits atop the burner is a boundary between the unburned and burned gases known as the luminous or reaction zone. This region, less that 1mm thick, is where most of the reaction and heat release take place within the flame. As the fuel/air mixture is continuously drawn into the reaction zone its temperature increases exponentially. The temperature continues to rise through the reaction zone until the adiabatic flame temperature is reached. The temperature profile of the gas as it passes through the reaction zone is shown in Figure 4 below.
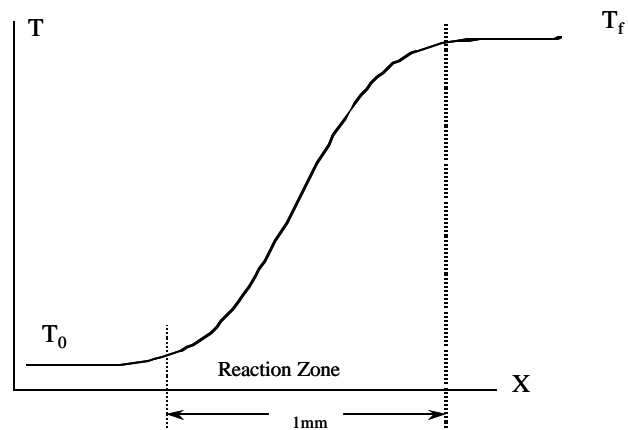
Figure 4.   Temperature Profile Through Reaction Zone of a Typical Flame[1]

Now consider the same fuel/air mixture used above, but stored uniformly in a horizontal tube that is open on both ends. If an ignition source is applied to one end a flame appears and propagates down the tube. This flame can be treated as a wave as it moves into the unburned reactants

at a speed of roughly 40 cm/s (see Figure 3). The temperature profile and thickness of the reaction zone of this wave are similar to those of the flame on the Bunsen burner.

Finally consider the case above where one end of the horizontal tube is closed with the reactants inside. The mixture is ignited, this time at the closed end, and again a flame forms. This flame accelerates as it propagates down the tube and eventually will attain a velocity of not tens of centimeters per second but rather *thousands of meters* per second. The combustion wave then travels at supersonic speeds with respect to the unburned reactants.

In order to determine the characteristics of this supersonic combustion wave, we can begin with the integrated conservation equations and state equations across the leading shock of the wave (see Figure 3).

$$\textit{Continuity} \qquad \rho_1 u_1 = \rho_2 u_2 \qquad\qquad (2.1)$$

$$\textit{Momentum} \qquad P_1 + \rho_1 u_1^2 = P_2 + \rho_2 u_2^2 \qquad\qquad (2.2)$$

$$\textit{Energy} \qquad c_{p_1} T_1 + \frac{1}{2} u_1^2 + q = c_{p_2} T_2 + \frac{1}{2} u_2^2 \qquad\qquad (2.3)$$

$$\textit{State}_1 \qquad P_1 = \rho_1 R T_1 \qquad\qquad (2.4)$$

$$\textit{State}_2 \qquad P_2 = \rho_2 R T_2 \qquad\qquad (2.5)$$

Where   Subscript 1 indicates unburned reactants

Subscript 2 indicates burned products

$P \equiv$ Pressure

$T \equiv$ Temperature

$\rho \equiv$ Density

$u \equiv$ Velocity of gases relative to wave

11

$$q \equiv \text{Chemical energy release}$$
$$R \equiv \text{Universal Gas Constant}$$
$$c_p \equiv \text{Specific heat at constant pressure}$$

In these equations there are five unknowns yet only four equations. Through algebraic manipulation (not shown) two new equations emerge:

$$\frac{g}{g-1}\left(\frac{P_2}{r_2} - \frac{P_1}{r_1}\right) - \frac{1}{2}(P_2 - P_1)\left(\frac{1}{r_1} + \frac{1}{r_2}\right) = q \tag{2.6}$$

$$gM_1^2 = \left(\frac{P_2}{P_1} - 1\right)\bigg/\left[1 - \frac{(1/r_2)}{(1/r_1)}\right] \tag{2.7}$$

Where $\gamma \equiv$ Ratio of specific heats
          $M \equiv$ Mach number of wave

Equation (2.6) is known as the Hugoniot relationship. This relationship states that for a given set of initial conditions (P_1, $1/\rho_1$), a family of solutions (P_2, $1/\rho_2$) exists for a given value of q. If we plot the pressure of the burned gases, P_2, versus their specific volume, $1/\rho_2$, we can see a graphical depiction of this family of solutions. This family of solutions, known as the Hugoniot plot (see Figure 5), shows all possible values of P_2 and $1/\rho_2$ for initial values of P_1 and $1/\rho_1$ at a given q. Figure 5 shows the Hugoniot plot for only one value of q.

12
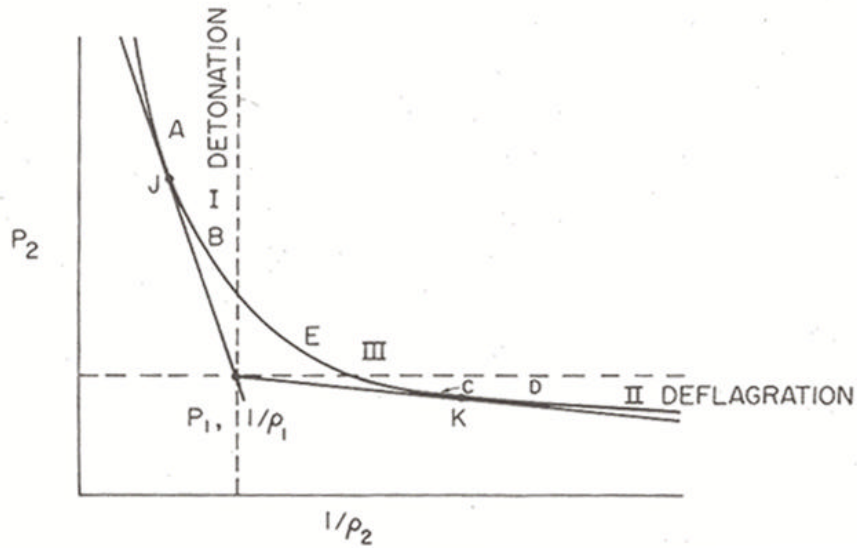
Figure 5.   The Hugoniot Plot[1]

To use the Hugoniot plot one first plots an initial
condition (P_1, $1/\rho_1$) of the unburned gases. The two dotted
lines passing through this point represent the conditions
of constant pressure and specific volume.   These lines
divide the curve into three major regions (I, II, III).
Next, two lines of tangency to the curve are drawn through
the initial condition.   These lines of tangency represent
Rayleigh flow.   The points of tangency (J, K) further
divide the three major regions of the curve into five
smaller sections (A, B, C, D, and E).

Using Equation 2.7 and the values of P_1, P_2, $1/\rho_1$, and
$1/\rho_2$ in region I, one finds that the values of M_1 in that
region are greater than 1.   This indicates that the waves
in that region are supersonic.   This region is therefore
called the "detonation branch."   In a similar fashion, one

13

finds that the values of M_1 in region II are less than 1 and therefore the waves are subsonic. This region is known as the "deflagration branch." Within this region, reactions occur at much lower rate than within the detonation region. The values for M_1 in region III are imaginary and, therefore, this region does not represent a physically real solution.

Concerning ourselves only with the detonation region we can further scrutinize sections A and B in this region. The wave velocity for points on the curve above point J (section A) is greater than the theoretical steady-state detonation velocity for the mixture. The resulting high temperatures in this region dramatically increase the sonic velocity. The Rayleigh condition allows this condition to exist only briefly. In this case rarefaction waves form and "catch up" to the detonation front. This reduces the pressure until P_2 and $1/\rho_2$ drop to point J, known as the Chapman-Jouguet (C-J) point. Here the velocity of the gases relative to the detonation wave is exactly sonic. Further, in section B, the burned gas velocity relative to the wave front slows down, but is *supersonic*. The Rayleigh condition dictates that it is impossible to maintain a supersonic velocity in a constant area duct with heat addition; sonic flow is the limit. Hence, a detonation wave in this region is rarely observed (the gas mixture requires extremely fast chemical kinetics)[7].

The upper Chapman-Jouguet point, then, represents the only steady-state solution in the detonation region. At this point the velocity of the burned gases with respect to

14

the detonation wave (u_2) is equal to the sonic velocity within the burned gases (a_2).

It can be shown that the velocity of the burned gases at point K in the deflagration region also equals the local sonic velocity and that solutions in section D are impossible. Therefore the only remaining sections of the Hugoniot curve where solutions can exist are in section A and C (see Figure 6). The solutions in section A are transitory in nature and they quickly drop to the C-J point.
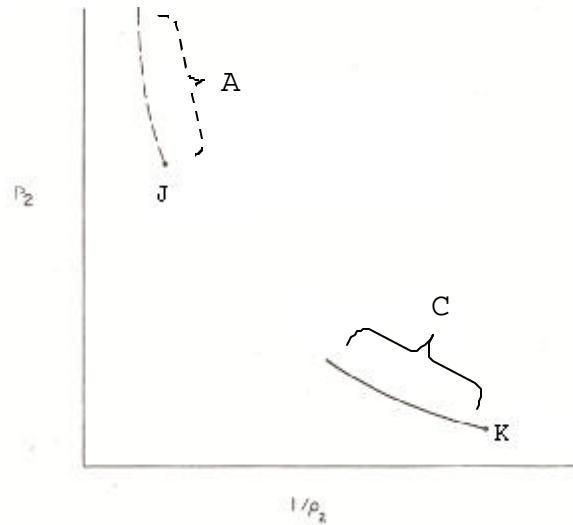
Figure 6.   Hugoniot Plot Showing the Only Experimentally Possible Results (Broken line indicates transient conditions)[1]

With the knowledge that the Chapman-Jouguet point is the only point on the Hugoniot plot were a steady state detonation solution can exist and that, at this point, u_2 equals a_2, the conservation of mass equation (Equation 2.1)

15

can be rewritten as follows to give an equation for the detonation velocity (u_1):

$$r_1 u_1 = r_2 u_2 = r_2 a_2 \quad \text{or} \quad u_1 = \frac{r_2}{r_1} a_2 = \frac{(1/r_1)}{(1/r_2)} a_2 \qquad (2.8)$$

where $a_2 \equiv$ Sonic velocity in the burned gases

D.   FORMATION AND STUCTURE OF THE DETONATION WAVE

The Hugoniot plot shows that, depending upon initial conditions, an explosive mixture can support either deflagration or detonation. With regard to the former, a subsonic combustion wave is formed and quickly attains a constant, subsonic velocity. In the case of a detonation, again a subsonic wave is formed, but this wave continues to accelerate until a supersonic detonation wave is formed. The formation of this wave is discussed below.

The example of a tube closed at one end and open on the other is again used. As the reactants are ignited at the closed end, a combustion wave forms. This initial deflagration leaves in its wake burned products with a specific volume 5-15 times that of the initial mixture. This rapid expansion generates compression waves that will accelerate the unburned reactants ahead of the flame due to compression heating. Each of these compression waves tends to heat up the reactants causing the local sonic velocity to increase thus allowing each succeeding wave to catch up with the leading wave. This preheating of the unburned reactants also increases the flame speed itself, which in turn increases the production and velocity of the burned

16

products.   Eventually turbulence ensues in the unburned
reactants further accelerating the entire process until a
shock is formed which is strong enough to ignite the
mixture itself.   The reaction zone immediately behind the
shock   continues   to   feed   compression   waves   forward
preventing the shock from decaying.   This sustainment
results in the formation of a stable detonation wave.   This
entire process is known as the deflagration-to-detonation
transition.

The process described above shows how a detonation
forms from a deflagration.   Direct initiation of a
detonation, however, is possible.   If a planar shock from
some other source is introduced to the unburned mixture,
the flame reaction is immediately started by the rapid
compression of the mixture.   The reaction zone behind the
shock is also immediately set up and sustains the shock as
described above.

The simplified structure of a typical detonation wave
is shown in Figure 6 below.   The structure of the
detonation wave consists of a shock traveling at the
detonation velocity, a region of heated and compressed
gases following the shock, and reaction region where the
chemical reaction progresses to the C-J conditions of
equilibrium.   In Figure 7, Plane 1 indicates the shock
front, Plane 1' the region immediately following the shock,
and Plane 2 the C-J conditions.
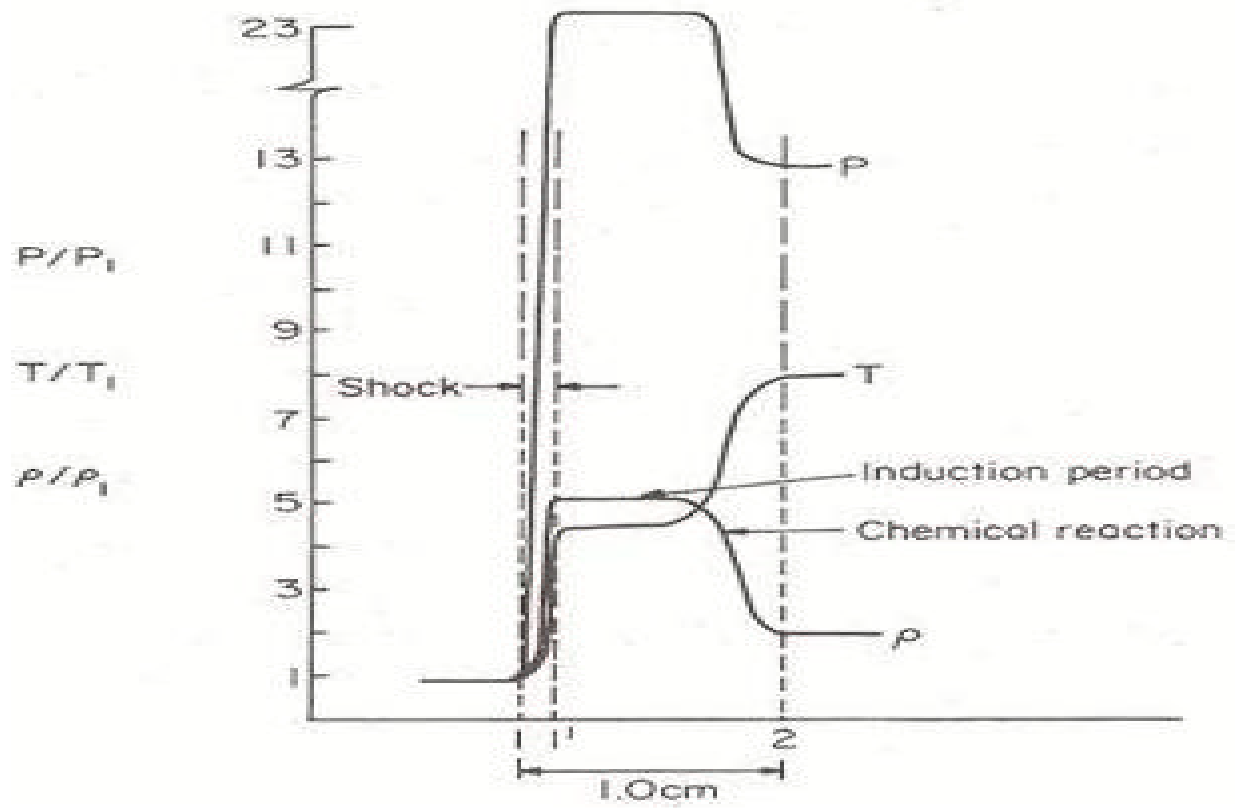
Figure 7.   The Variation of Physical Parameters in a Typical
                        Detonation Wave[1]

III. PRELIMINARY RESEARCH

A.   MARSHALL SPACE FLIGHT CENTER

The Propulsion Research Center (PRC) at NASA's Marshall Space Flight Center (MSFC) is actively investigating the PDRE concept. As part of the Advanced Space Transportation Program (ASTP), MSFC engineers, along with industry partners United Technology Research Corporation and Pratt & Whitney's Seattle Aerosciences Center (formerly Adroit Systems, Inc.), are developing pulse detonation technology that will eventually lead to the demonstration of a flight-qualified PDRE.

Initial research for this thesis was conducted at MSFC under the guidance of Dr. Noah Rhys. PDE fundamentals were reinforced, hardware configurations were discussed, and a preliminary list of test objectives was developed. An analysis of theoretical performance of several hydrocarbon fuels was also conducted, the results of which are discussed below.

B.   THERMO-EQUILIBRIUM PROGRAM

The Thermo-Equilibrium Program (TEP™)[2] is a Windows™-based software tool used to determine the products of combustion under thermodynamic equilibrium conditions. TEP™ can be used for several applications including temperature/pressure-based combustion, entropy/pressure-based combustion, and shock/detonation conditions. TEP™ contains thermodynamic information on over 1000 chemical species and elements, including ions. A reactants and ingredients library contains data on over 60 common fuels

and oxidizers, and allows information on new fuels to be added to the database as needed.

Chemical equilibrium is the state of a working fluid in which the mixture composition undergoes no further changes for a specified pressure and temperature. TEP™ uses the minimization of the Gibbs free energy to solve for the products of combustion that are in chemical equilibrium. This can be equated to finding the condition where the entropy of the products is at maximum.

The research conducted at Marshall used only the detonation application within TEP™. In this application, the Chapman-Jouguet detonation conditions are calculated for a moving wave propagating into a premixed combustible mixture in a shock tube. The tube is assumed to be closed on one end and open on the other. A Taylor-Zeldovich expansion was performed behind the detonation wave to account for the no-flow condition at the head end of the tube. Various hydrocarbon mixtures were analyzed using this approach.

1. TEP™ Input

Within the detonation application of TEP™, the user first chooses the reactants to be evaluated. A fuel and oxidizer are chosen from the master reactants file and a reference temperature, phase, and mole fraction for each reactant is entered.

A species library contained within the software is then selected. These libraries allow for the user to select the desired thermodynamic data set for a desired level of detail. A brief description of each library is

given within the software. The Master library was always selected for runs performed in this work.

The reactants mixture ratio is set next. TEP™ allows the mixture to be specified by an oxidizer-to-fuel ratio (O/F), equivalence ratio (ϕ), fuel percentage, or fuel-to-air ratio. A specific ratio/percentage or range of several of these values may be entered.

Finally, the operating conditions are input. These include the initial temperature and pressure of the unburned reactants. A specific pressure or range of pressures may be entered while only one temperature may be entered. Using the option/units menu, the user can specify English or metric units for these inputs.

2. TEP™ Output

TEP™ returns an output file containing the gas properties and composition of each user-specified detonation condition. The gas properties are arranged in a table containing rows that correspond to each gas property and columns that correspond to a user-specified initial gas pressure. If a range of gas properties such as ϕ were entered, several tables are produced in the output file. Gas species concentrations are listed in each table.

Within the gas properties section of the output file, each table is broken down into three subsections. These subsections contain the properties of the unburned gas, the properties of the burned gas, and the detonation parameters. The elements of each subsection are listed below.

21

Unburned Gas:

    Pressure, P1 (atm or psia)

    Temperature, T1 ($^\circ$K or $^\circ$R)

    Enthalpy, H1 (cal/g or btu/lbm)

    Molecular weight, M1 (g/mol)

    Ratio of specific heats (C_p/C_v), GAMMA1

    Sonic velocity, SON VEL1 (m/s or ft/s)

Burned Gas:

    P2, T2, H2, M2, GAMMA2, SON VEL2

    Density, Rho2 (kg/m3 or lbm/ft^3)

Detonation Parameters:

    Pressure ratio, P2/P1

    Temperature ratio, T2/T1

    Molecular weight ratio, M2/M1

    Density Ratio, Rho2/Rho1

    Detonation Mach number, MACH NO.

    Detonation velocity, DET VEL

These elements can be used to calculate other detonation properties such as head wall pressure (P3) and specific impulse (Isp) for the given conditions.

C.   THEORETICAL RESULTS

TEP™ was used to determine the theoretical performance of several different hydrocarbon fuels under varying initial conditions. All cases run used diatomic oxygen (O_2) as an oxidizer. All of the reactants were considered in a gaseous phase and the mixture was considered homogeneous. The gaseous phase was chosen to ensure uniformity of results as TEP™ had difficulty running some liquid fuels. The results closely match the performance

given by fuels in a liquid state since the heat of vaporization is nearly insignificant when compared to the heat of combustion.

The fuels chosen for analysis included JP-10, RP-1, ethylene, propane, methane, butane, and ethane. Graphite, heptane, and octane were also run but failed to give complete results. Hydrogen was also analyzed and its performance was compared to that of the hydrocarbon fuels. The TEP^{TM} output was compiled into several spreadsheets that are included in Appendix A.

The output from TEP^{TM} provided the means to calculate the performance of an ideal PDRE. In this ideal case the tube measures one meter in length and has a diameter of ten inches (0.254 m) giving an overall volume of 0.051 m^3. Each performance parameter is defined below and the calculated values of each are shown in the shaded areas of the performance spreadsheets (See Appendix A).

Detonation Time (s)

The time for the detonation to propagate from the closed end to the exit of the tube.

$$T_s = \frac{TubeLength}{DETVEL}$$

(3.1)

Rarefaction Time (s)

The time required for the rarefaction waves to propagate from the exit to the closed end of the tube at the local speed of sound.

$$T_r \cong \frac{TubeLength}{SONVEL2} \tag{3.2}$$

P₃ (atm)

The expanded pressure behind the detonation measured at the closed end of the tube calculated using the Taylor-Zeldovich isentropic expansion relation.

$$P_3 = P_2 \left[1 - \left(\frac{g_2 - 1}{2} \right) M_2 \right]^{\left(\frac{2g_2}{g_2 - 1} \right)} \tag{3.3}$$

F (N)

The force exerted by the detonation wave on the closed end of the tube.

$$F = P_3 * A \tag{3.4}$$

where $A \equiv$ Cross sectional area of tube

$P_3 \equiv$ Instantaneous head end pressure

Total Impulse (Iₜ)

The force integrated over the total cycle time (t_cycle).

$$I_t = \int_0^{t_{cycle}} F * dt \tag{3.5}$$

24

<u>Specific Impulse (I_{sp})</u>

The total impulse per unit weight of propellant.

$$I_{sp} = \frac{I_t}{W}$$ (3.6)

where W≡weight of the reactants

$$= r_1 * g_0 * vol$$

The compilation of TEP™ data is shown graphically in Appendix A. In these graphs the performance of the hydrocarbon fuels is compared to that of hydrogen fuel for a range of equivalence ratios. The P_2, P_3, F, detonation velocity and Mach number, total impulse, and specific impulse are plotted on separate graphs.

From the graphical representation it is evident that the hydrocarbon fuels all outperform hydrogen with regard to the force exerted on the head wall. This equates to greater thrust and total impulse that is also shown in their respective graphs. Hydrogen does outperform the hydrocarbons with respect to specific impulse, however. This is due to the lower molecular weight of hydrogen when compared to the heavier hydrocarbon molecules. This can be equated to a higher energy per unit mass for hydrogen. It is interesting to note that, while the hydrocarbons all attain a higher Mach number than hydrogen, hydrogen attains a higher overall detonation velocity. This results from the higher local sonic velocity of hydrogen at the chosen pressure and temperature.

With regard to sensitivity to changes in equivalence ratio, it appears that an increase in ϕ correlates to an increase in performance for the hydrocarbons within most of

the given range. A ϕ of roughly 2-2.1 gave the maximum performance. Hydrogen, on the other hand, actually decreased in all parameters except detonation velocity as ϕ increased.

In summary, this preliminary investigation made apparent the greater performance of several hydrocarbon fuels as compared to hydrogen when total impulse was the performance metric. It also showed that, per unit mass, hydrogen has a better performance but would ultimately require larger tanks. The data became a benchmark to which the actual results of hot fire were compared.

IV. EXPERIMENTAL SETUP

A. INTRODUCTION

This work was broken up into three distinct phases that were each completed in sequential order. The first phase encompassed flow visualization. In this phase, the fuel injection flow paths of the liquid fuel were characterized using several different injectors. The next phase involved the performance evaluation of gaseous ethylene. These data allow valving issues to be characterized and were used as a baseline comparison for the liquid fuel analysis that followed. Finally, several liquid hydrocarbon fuels were evaluated.

All phases of experimentation were run in Test Cell #2 at the RPCL and controlled from the safety of the lab's control room. An existing Visual Basic™ (VB™) code was modified to accommodate the control of each of the three phases (Figure 8). This code allowed the user to manually enter variables affecting the test conditions of the setup such as timing, fuel and oxidizer pressure, and purge rate. It also allowed the user to control the opening of the facility, the start/stop of test runs, and the real-time calibration of specific components. The specifics of the code's use in each phase are discussed in the sections of this chapter that follow.

Figure 8.   PC With VB™ Code Displayed

Timing for each sequence was provided by a Berkeley Nucleonics Corporation Model 500 pulse generator (hereafter referred to as the "BNC 500") accurate to 100 ns (Figure 9). This device produced TTL pulses that were sent to various components to control their timing. The pulse could be selected as either positive or negative.

Figure 9.   BNC 500 Pulse Generator and Data Acquisition
                         Break-Out Panel

        Electrical power for the test cell was provided
through two electrical cabinets, one providing 24VDC and
the other providing 110VAC (Figure 9). Observation of the
activity in and around the cell was provided via several
video cameras that were routed to two monitors mounted
inside the control room (Figure 10). The first monitor was
used to display one of several views of activity within the
test cell area. The second used to display activity on
the golf course that surrounds the RPCL. Care was taken to
ensure that the area immediately behind the test cell was
clear during all hot fire tests. Each video signal was
routed through a SVHS VCR to record test runs. Warning
lights and sirens were also controlled from this panel. An
emergency stop button was mounted on the wall immediately
above the PC that ran the VB™ code.

Figure 10.   Control Room Operations Panel

During the course of this research, a great deal of time and effort went into hardware drawings for components, buildup of hardware, and modification of existing hardware configurations. The experience gained in this process was, I feel, of equal value to the experimental results contained in the following chapter.

B.   LASER BACKGROUND

The environment within any combustor (to include the PDRE) is extremely hostile and flow measurements of the combustion process within prove difficult to accurately acquire.   Laser diagnostics are very attractive in the study of combustion processes for several reasons.   The first is the non-intrusive nature of the laser energy.   The laser eliminates the need for flow perturbing probes such as wires or thermocouples and replaces them with flow

measurements based on optical scattering, absorption, and emission[3]. The laser energy imparted on the overall flow is negligible. Second, the laser provides a means of depicting an extremely complex, three-dimensional flow in a point wise or planar fashion. The degree of space and time resolution afforded by the laser is normally achieved only by powerful computational fluid dynamic (CFD) codes. Finally, due to the lack of exposure to the combustion environment, the laser diagnostic hardware is unharmed during testing.

C.   LASER DIAGNOSTICS

The laser diagnostic method provides the best measurements with the least interference. Generally, optical methods are based on the principles of particle and molecular scattering or molecular absorption[3]. Simply put, as laser energy enters the combustion medium, one or more of several interactions can occur. Each photon may be transmitted, reflected, absorbed, or scattered by the medium. Several different characteristics of the flow can be determined through these interactions.

Optical scattering may be broken generally into Rayleigh and Raman scattering. A third type, Mie scattering, deals with particle scattering and will not be addressed here.

Rayleigh scattering is an elastic interaction that occurs between photons and the molecules of the medium. Because the interaction is elastic, no energy from the incoming photon is imparted upon the individual molecules and the photon is scattered at its original wavelength.

31

This lack of difference in wavelengths makes Rayleigh scattering ineffective at distinguishing individual gaseous species within the flow. The density of a *known* composition can, however, be obtained via Rayleigh scattering. Also, temperature measurements utilizing Rayleigh scattering are very difficult to obtain due to the high spectral resolution required. With this said, the primary advantage of Rayleigh over Raman scattering is that it is several times more intense and therefore much more easily detected.

Raman scattering, despite its lower intensity, has several advantages over Rayleigh scattering. These include the ability to identify specific species, accessibility to temperature information, its lack of interferences, and the capability to look at a medium not in chemical or thermal equilibrium[4]. In Raman scattering, an inelastic collision occurs between the incoming photon and the molecule. This results in an exchange of energy and the scattered photon undergoes a change in wavelength. From this change in wavelength and the associated redistribution of energy, the density of specific species and gas temperatures can be extracted.

Besides the scattering of incident radiation, another phenomenon, laser-induced fluorescence (LIF) has become useful in visualizing complex flow fields. LIF, as its name implies, uses the principle of chemical fluorescence to detect and image concentrations of specific species within the flow. Fluorescence involves the absorption of the incoming radiation at a particular wavelength and the subsequent emission of radiation at a separate, longer

wavelength[5] (Figure 11). The laser is used to excite a specific species within the medium from a quantum state *e* to an excited state, *e'*. From this excited state the medium emits photons of light at a longer wavelength, or it "fluoresces." A camera tuned to the emission wavelength can then image this fluorescence. The level of fluorescence is proportional to the number of molecules of the species present and therefore provides a qualitative image of its relative density[5].

A specific category of LIF, the planar LIF or PLIF, uses laser energy that has been manipulated to form a laser "sheet." This sheet can be used to fluoresce an area within the flow field that can then be imaged to provide a two-dimensional snapshot of the flow pattern. The use of PLIF in this thesis is further detailed in the flow visualization section that follows.
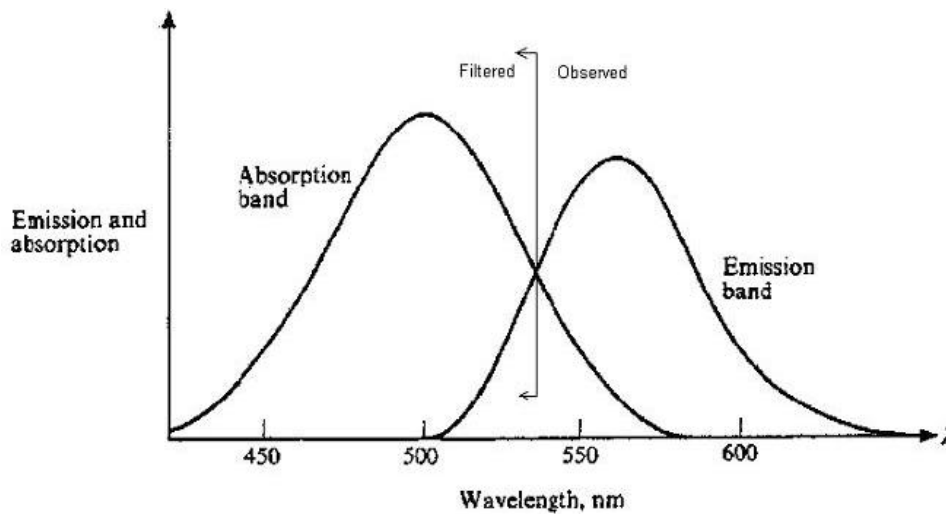
Figure 11.   Typical Absorption and Emission (Fluorescence)
Spectrum[4]

D.   FLOW VISUALIZATION

The characterization of fuel injection flow paths was essential in the overall design of a PDRE that would be successful in achieving the objectives of this work. In this phase, high-speed imaging and PLIF of liquid fuels were used to qualitatively characterize the behavior and performance of several different injectors. Several hardware and configuration decisions were made based on the data acquired during this phase.
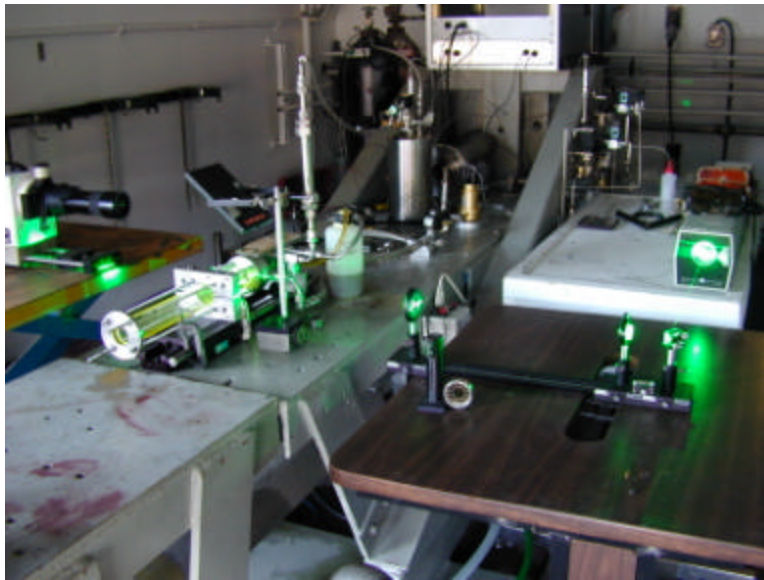
Figure 12.   Flow Visualization Setup

In order to closely approximate the behavior of the injector in the final experimental setup, a "cold fire" rig was developed with a similar geometry (Figure 12). In this configuration, the stainless steel tube of the final configuration was replaced with a clear acrylic tube. This allowed for the transmittance of the laser energy required

for the PLIF and for a variety of camera positions to record the injection sequence. Because the fuel to be imaged was not required to detonate, the ignition system was not included in this configuration. Its absence had no effect on the flow, however. All other hardware used in the final configuration was otherwise used in the flow visualization setup.
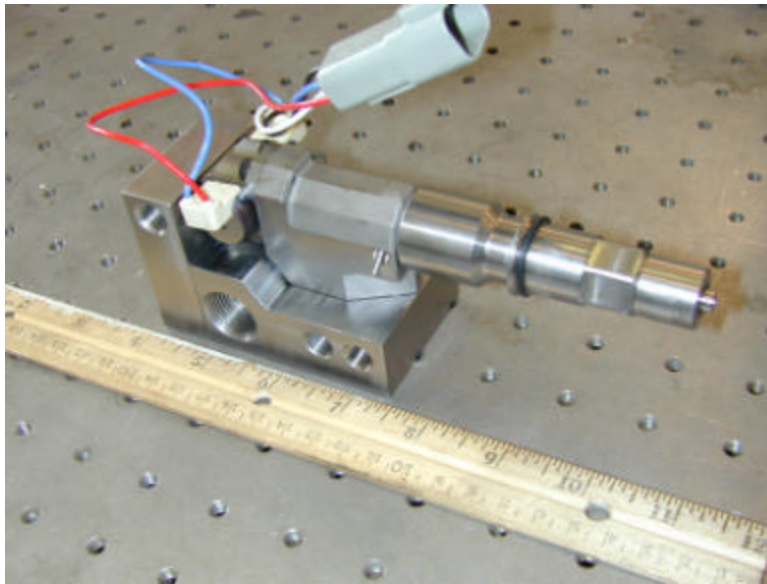
Figure 13.   Sturman Injector

Fuel was injected into the tube using one of several different Sturman injectors (Figure 13). These state of the art electro-hydraulic injectors, currently being tested for use in diesel and direct injection engines, were slightly modified for this application. Each injector was fitted with one of two different tips. The first tip had five holes drilled into an angled circular face (the "five-hole" injector). The second used an annular design that

injected the fuel in a hollow diverging spray cone (the "single-tip" injector).

Each injector used Mobil 1 synthetic motor oil as the hydraulic fluid. High pressure, gaseous nitrogen was used to pressurize both the fuel and oil reservoirs (Figure 14). The pressurized oil was then routed from the reservoir to the injector through a specially machined stainless steel block to which the injector was mounted.
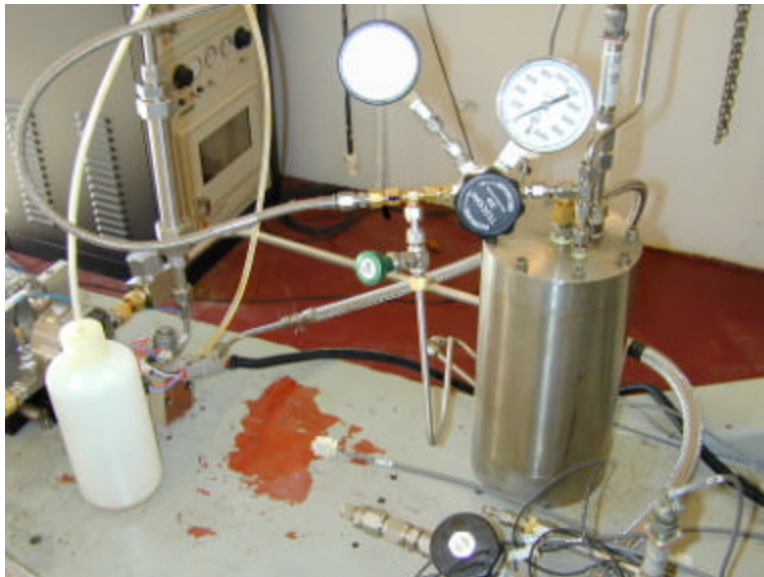
Figure 14.   Oil and Fuel Reservoirs

The performance of each injector is characterized in the following chapter.

A cylindrical fuel reservoir capable of holding 100 ml of liquid fuel was mounted above and adjacent to the injector (Figure 15). This reservoir was pressurized with

the same nitrogen as the oil, although the pressure was stepped down from 1500 psi to approximately 80 psi.

Figure 15.   Fuel Reservoir

Air was introduced into the tube via an annular inlet manifold through which the fuel injector protruded (Figure 16). The air flowed into the manifold through two ports at the 3- and 9-o'clock positions. Air was used for the flow visualization for cost reasons and, because no combustion was to take place, the effects were negligible. Air was flowed continuously while the fuel was pulsed. Four holes were drilled and tapped into this manifold into which four lengths of threaded rod were inserted. These rods were inserted into a similarly drilled and tapped stainless

steel flange fitted to the exit of the tube to hold the rig together in compression.
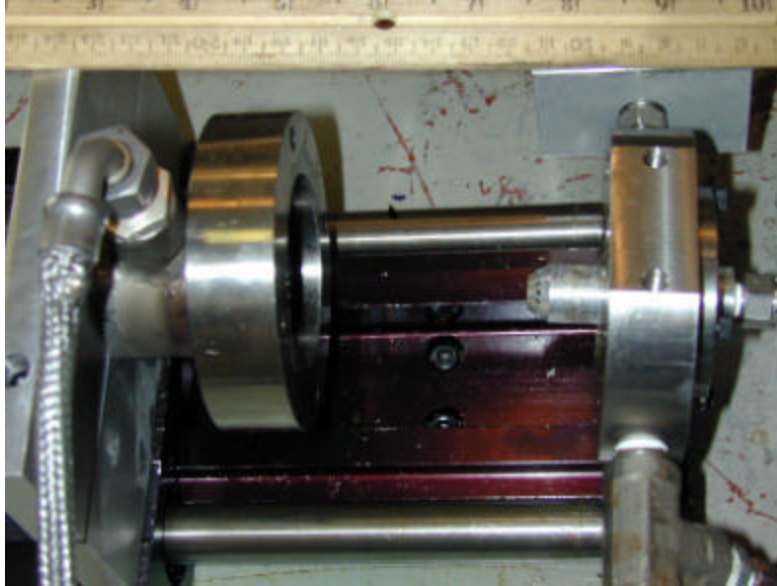
Figure 16.   Inlet Manifold

An argon-ion laser operating at 514 nm was used to create the laser sheet for the PLIF. The laser light was sent through a series of mirrors and other optical devices until a sheet was obtained that passed through the transparent tube at right angles to its longitudinal axis. At the open end of the tube was a mirror that directed an image of the laser sheet to a high-speed camera.

The injection patterns of both kerosene (RP-1) and JP-10 were imaged. Prior to the fuel being injected into the tube, a fluorescing dye was added. The dye used was P-576A pyro-methane from Exciton, Inc., which emitted from 552-608 nm when excited by the argon-ion 514 nm wavelength. Hence, the fluorescence observed indicates the presence of fuel.

38

A DRC Haddland Ultra 17 high-speed intensified CCD camera capable of up to 100 million frames per second was used for imaging the flow. A filter was installed that allowed only the fluorescing wavelengths to pass (see Figure 11). This was done to prevent the laser energy, which generally is an order of magnitude brighter than the fluorescence, from dominating the image. The resulting images show fuel concentrations at a specific time and location within the tube. Several images are taken looking down the length of the tube with the laser sheet placed in various locations. The laser sheet and camera are then rotated 90° and the tube is imaged from above, completing the overall three dimensional model (Figure 17).
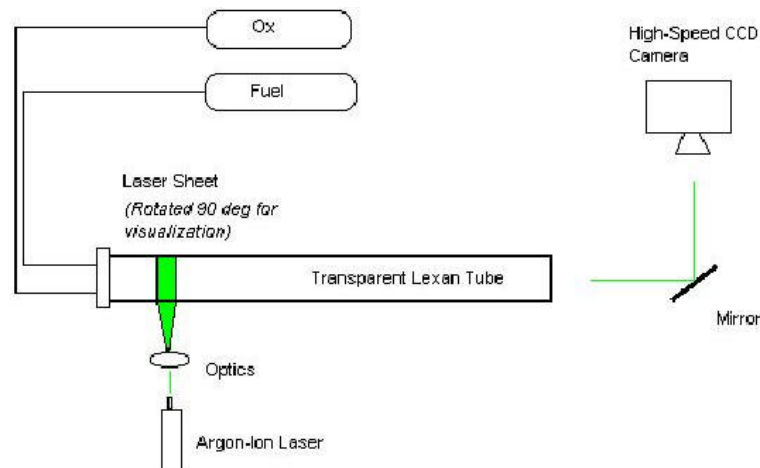
Figure 17.   Simplified PLIF Diagnostic

The imaging sequence was run from a PC inside the control room using the code provided by the camera's manufacturer. This code allowed the user to vary the

timing of the 17 images taken during each test run and the gain at which those images were taken. Once saved, the images were adjusted to optimize their brightness and contrast settings using the software and then animated in a multi-exposure stack. Each stack was then saved to the PC's hard drive for further analysis.

E.   GASEOUS FUELS

In order to provide a baseline of data to which the performance of liquid hydrocarbon fuels could be compared, a test matrix was performed using gaseous ethylene. This phase also served as a "shakedown" of the newly constructed PDRE, its components, and the software that supported their testing.

During this phase, the baseline PDRE was introduced (Figure 18). The rig was based on an 11″ stainless steel tube with an inside diameter of 1.5″. Welded to each end of this tube were stainless steel flanges. The first flange, at the head end of the tube, provided a mount for the inlet manifold through which the fuel and oxidizer would flow. This is the same manifold used in the flow visualization phase. The opposite flange, at the tube's exit, was cut with an o-ring groove and allowed for additional lengths of tube to be attached. A stainless steel port was welded to the tube at approximately 1.5″ from the inlet manifold to allow for the insertion of the igniter. Two ports were cut into the tube near the exit through which pressure sensors measured the speed of the detonation wave.
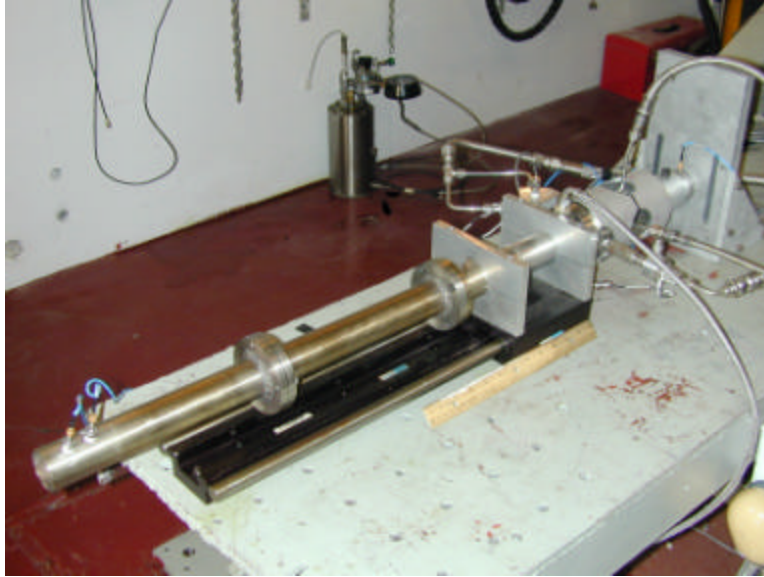
Figure 18.   Gaseous Setup

At the head end, two different stainless steel rings were used induce better mixing (Figure 19). The first was a straight ring that simply provided a smooth transition of the reactants from the inlet manifold to the tube. The second ring served as a collar for the fuel injector as it projected into the tube.   Drilled into the material surrounding the collar were twelve ¼" holes.   These holes increased the turbulence in the oxidizer as it passed from the inlet manifold into the detonation tube.   This turbulence resulted in better overall mixing of the reactants.
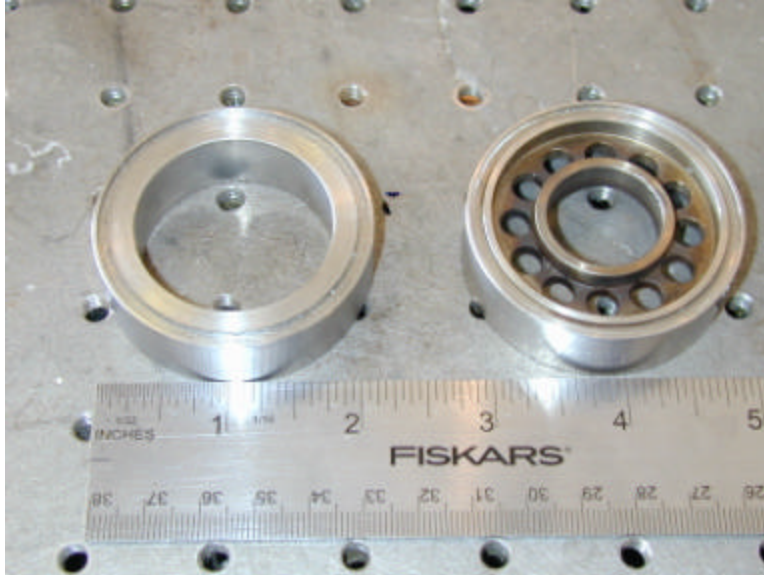
Figure 19.   Tube Inserts

During the later portion of the gaseous test matrix
the baseline tube was replaced with a tube with a different
internal geometry.   This tube had been used as a pre-
detonator (or initiator) in a five-inch PDE previously
tested at the RPCL.   The different geometry resulted from a
convergent/divergent, stepped insert placed inside the
first portion of the tube (Figure 20).
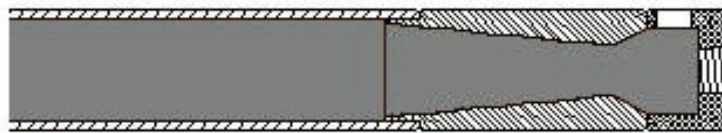
Figure 20.   Stepped Geometry Insert

42

Four Parker-Hannifin (PH) valves controlled both the fuel and the oxidizer flows (Figure 21). Three of these valves, one at the 3-o'clock position and two at the 9-o'clock position, were used to pulse the oxygen flowing into the inlet manifold. The fourth valve, attached to an aluminum injector that passed through the manifold along the tube's longitudinal axis, pulsed fuel into the tube. Purge air was flowed through the aluminum blocks that were used to mount the PH valves to the manifold.
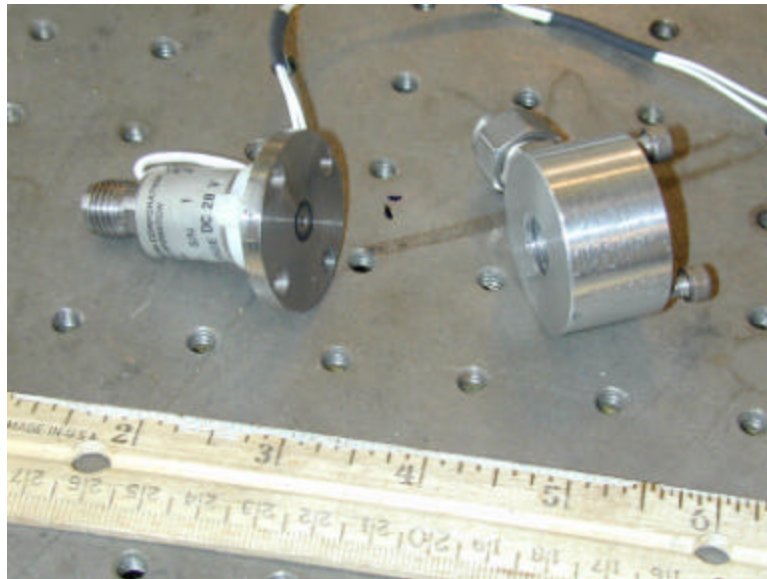
Figure 21.   Parker-Hannifin Valve with Aluminum Block

The aluminum injector was custom machined for this thesis (Figure 22). Perpendicular to the face of the tapered end, 16 holes were drilled through which the fuel was injected. The face was tapered at 30° to the longitudinal axis of the injector. This allowed for the fuel to be injected at 60° to the longitudinal axis of the

43

tube.   The injector passed through the manifold and was held in place by two small semi-circular plates that clamped the injector to the manifold.   An o-ring was placed between the injector and the manifold.
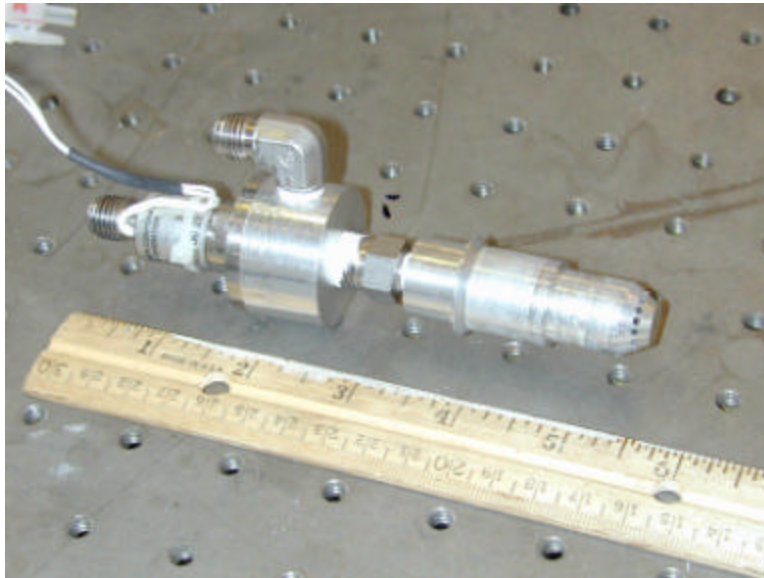
Figure 22.   Gaseous Injector

Two additional segments of main combustor tube were machined to provide additional length for the baseline PDRE (Figure 23).   Similar to the baseline tube, the second tube had two flanges (one with an o-ring groove) and two pressure ports.   The third tube had a single flange and two pressure ports.   Each of the flanges was drilled with four holes used to attach the segments together.   These geometries allowed for partial-fill operation with one, two, or three tube segments and for the pressure to be measured at three locations along the tube.   These pressure measurements were used to calculate detonation wave speed.

44

Figure 23.   Additional PDRE Segments

Two Kistler model 60381 piezoelectric pressure sensors
were inserted into the two ports at the exit of each tube
(Figure 24).   The high frequency pressure transducers were
filtered at 500kHz by a bank of Kistler 5010 amplifiers and
the amplified signals sent to a PC running the data
acquisition software where they were saved.   A third
pressure sensor was placed adjacent to the inlet manifold
where P_3 was measured.   This signal was amplified and
recorded in a similar fashion.
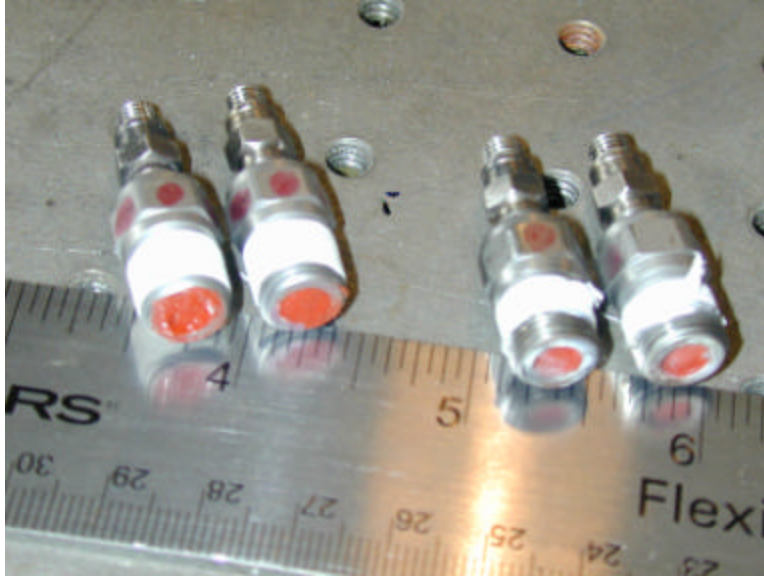
Figure 24.   Kistler Pressure Sensors

The sensors were exposed to extreme heat during the detonation process that, if not accounted for, would result in what is known "thermal dropout." This effect occurs when the thin solid-state diaphragm deforms due to heating rather than pressure. To offset this effect, the tips of the sensors were coated with a thin layer of insulating silicon (Figure 24).

In order to measure the thrust produced by the PDRE "thrust cage" was designed and fabricated (Figure 25). The thrust cage was a device that fit over the end of the inlet manifold and around the fuel injector. It was then bolted to a vertical plate that was fixed to the test stand. This cage was cut with four large holes that allowed the fuel, purge, and electrical lines to pass through. An annular Kistler load cell (Model #9061A) was placed around the bolt that attached the thrust cage to the plate (Figure 26).

The load cell signal was sent to the same bank of amplifiers and to the same data acquisition program used by the pressure sensors.
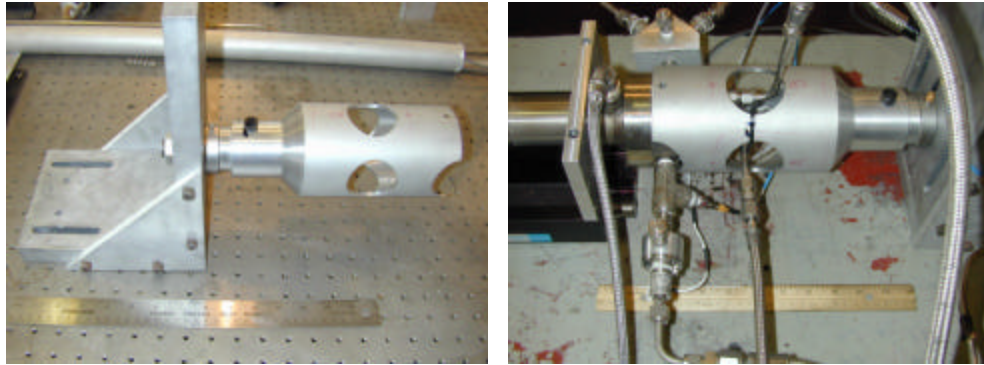
Figure 25.   Thrust Cage
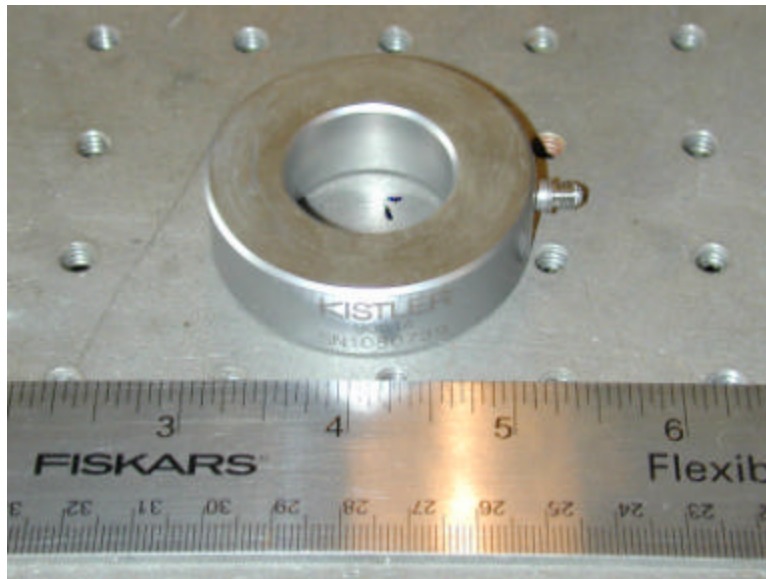
Figure 26.   Load Cell

The spark required to initiate combustion in the fuel/oxidizer mixture was provided via a Unison Industries Vision-2/50 Variable Ignition System (Figure 27). The ignition energy delivered by this system was held constant at 70MJ. A Champion igniter plug was mounted through the PDRE tube into the mixed reactants (Figure 28).

Figure 27.   Ignition System

Figure 28.   Champion Igniter Plug

F.   LIQUID FUELS

The baseline PDRE tube remained in place for the liquid fuel portion of this work. The gaseous injection system was replaced with one of the Sturman liquid injector systems tested during the flow visualization phase (Figure 29). Due to the size of this injector the thrust cage had to be removed and thrust measurements were therefore only determined from the integrated head wall pressure.
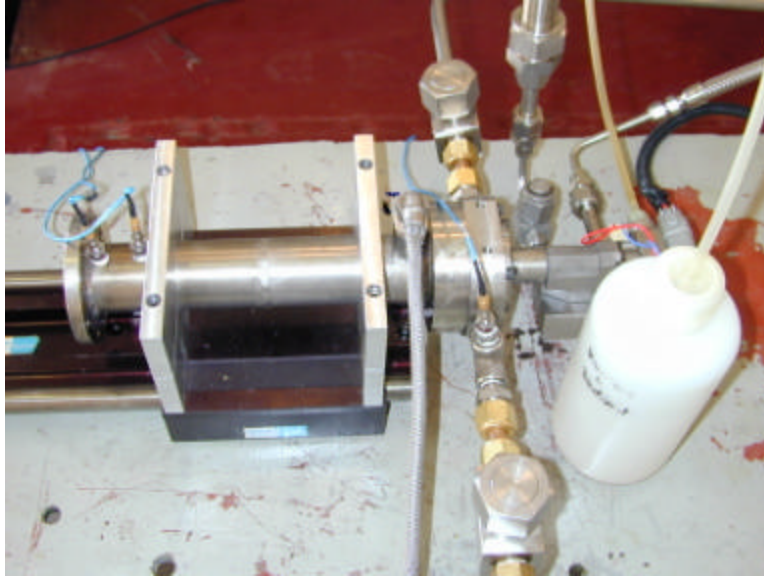
Figure 29.   Mounted Sturman Injector

The original design called for the oxidizer to be
delivered by four PH valves. After initial testing, and
following the catastrophic failure of one of the valves, it
became apparent that these valves were incapable of
delivering the required amount of oxygen for this phase.
The four PH valves were then replaced with two solenoid
valves capable of delivering the required oxygen mass flow
but only at frequencies below 10 Hz. These valves were
controlled by the BNC 500 and VB™ code in a similar fashion
as the PH valves. The air purge was eliminated during this
phase (Figure 30).
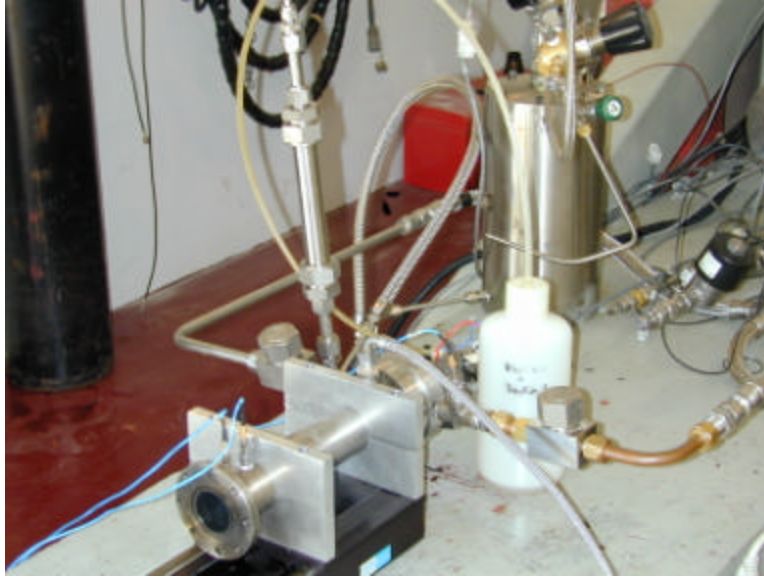
Figure 30.   Liquid PDRE Setup

V.   EXPERIMENTAL RESULTS

A.   INTRODUCTION

As discussed in the previous chapter, the experimental portion of this thesis was broken up into the flow visualization phase, the gaseous hot-fire phase, and the liquid hot-fire phase. Each of the first two phases was conducted so as to streamline the execution of the final, liquid hot-fire phase. For example, the flow visualization phase served not only to provide imaging of the liquid fuel injection pattern, but also to define the optimum operating range of the Sturman injectors. During the gaseous hot-fire phase, a wide range of equivalence ratios, injection/ignition times, and purge rates were explored to find the optimum operating conditions for this PDRE. The optimum conditions from each of the first two phases were then applied during the liquid hot-fire phase. This approach provided a focus of effort and minimized the amount of time needed for the final phase of experimentation.

B.   FLOW VISUALIZATION

Four of the Sturman injectors described in the experimental setup were characterized during this phase. Each injector was first imaged with the high-speed CCD camera in a stand-alone configuration. Based on the performance of each injector, one was chosen for use in the hot-fire configuration. This injector was then imaged inside the clear acrylic tube.

During the stand-alone imaging, the injector was mounted on the edge of the test cell table with the tip exposed to the surrounding environment. The fuel, oil, and electrical connections were made just as they would be in the final configuration. A black plate was placed around the injector tip to provide a background against which the fuel could be imaged. The laser was not used for the first portion of imaging and therefore the pyromethane dye was not added to the fuel.

Each of the four injectors was imaged with the camera positioned to the side and then at the end of the injector. A qualitative analysis was then conducted using the data obtained with the high-speed camera. From the analysis it was determined that the each of the "five-hole" injectors had problems directing the fuel in a uniform pattern. In the worse case, it appeared that one or more of the holes in the injector tip caused fuel to impinge on the plate *behind* the tip (see Figure 31). After some investigation it was determined that this injector was designed to be mounted at an angle in a diesel engine. The holes in the injector tip were therefore drilled at various angles resulting in the non-uniform pattern.

Due to the poor performance of the five-tip injectors, they were not tested further. The single-tip injector was used in the remainder of the experimental setups. This injector produced a much more uniform spray pattern and a wider dispersion of fuel (see Figure 32). The laser was introduced and the pyromethane dye was added to the fuel to provide imaging of this injector. Both JP-10 and kerosene (RP-1) were used as fuels. The oil to the injector was

53

varied to control the duration time of injection. A plot
of injection times is shown in Figure 33.
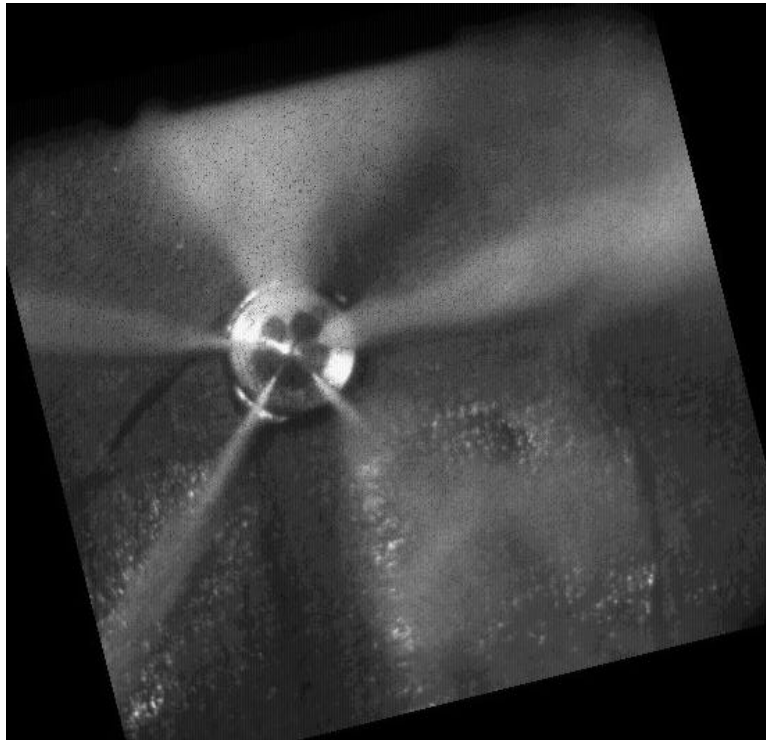
Figure 31.   "Five-Hole" Injector Pattern (Note the fuel
                   striking the black background)
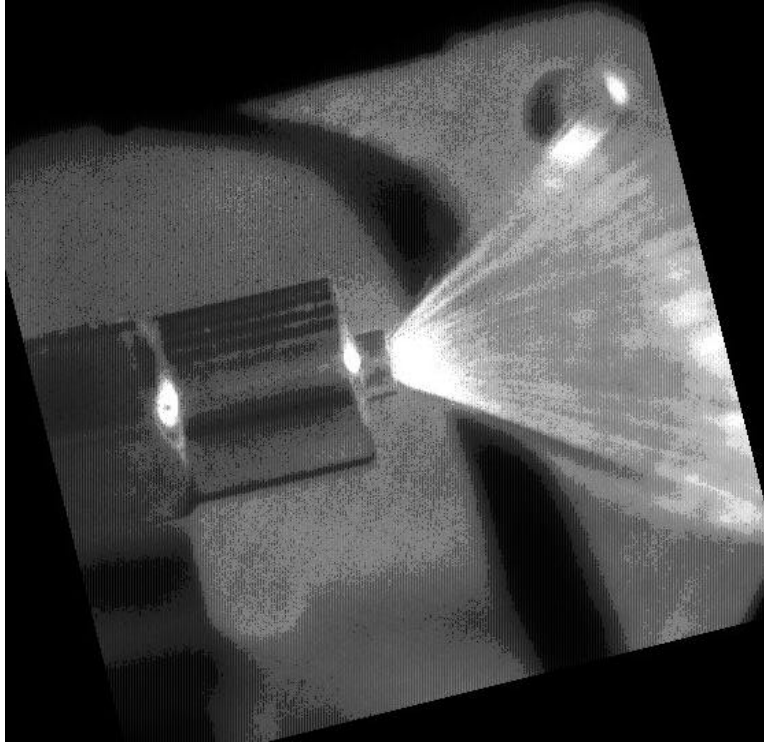
Figure 32.   Single-Tip" Injection Pattern
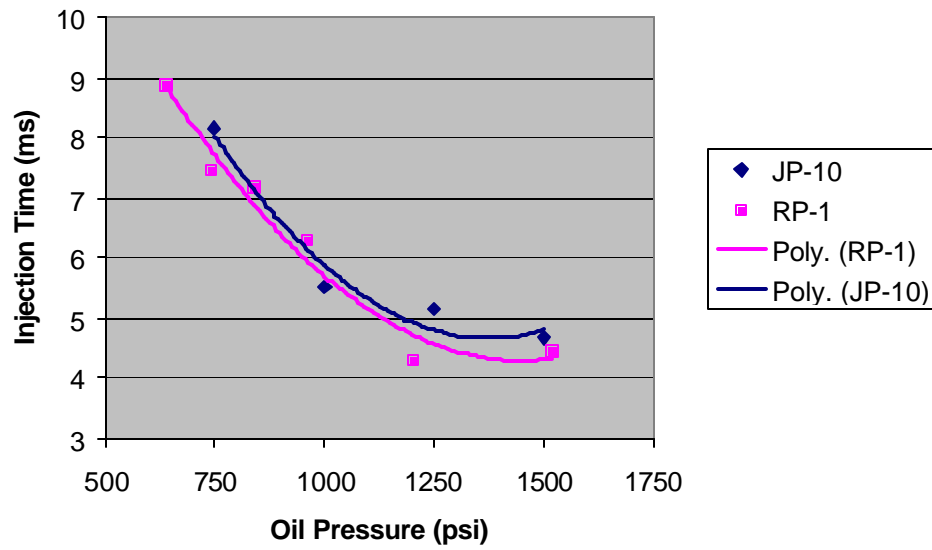
Figure 33.   Injection Time Vs. Oil Pressure

The injection time decreased with increasing oil pressure and eventually reached a minimum of roughly 4.3 ms at 1500 psi. From the qualitative analysis of the injection images it was determined that the minimum effective oil pressure was roughly 750 psi. At pressures below this value the injection pattern became erratic.

The injector was then mounted inside the acrylic tube for the cold-flow visualization. The laser sheet and camera were set up to provide cross-sectional images of the fuel injection pattern within the tube. Images were taken with and without air flowing into the tube. A set of images was created for a range of oil pressures from 900-1500 psi and a range of air pressures from 360-725 psi.

From the qualitative analysis of the images it was determined that this injector was more than sufficient to meet the requirements of the final experimental setup. However, because higher oil pressures were used to minimize injection times, fuel exiting the injector tip inevitably impinged upon the tube wall. This condition needed to be avoided not only to prevent hot spots along the tube wall, but also to minimize voids in the mixture downstream. Figure 34 shows an example of fuel hitting the tube wall. This image was taken without air flowing into the tube to better demonstrate the fuel impingement. A bright ring of fluorescing fuel is seen around the tube wall where the fuel accumulated. Also, a region is visible downstream of the fuel impingement in the center of the tube where a void existed in the mixture.
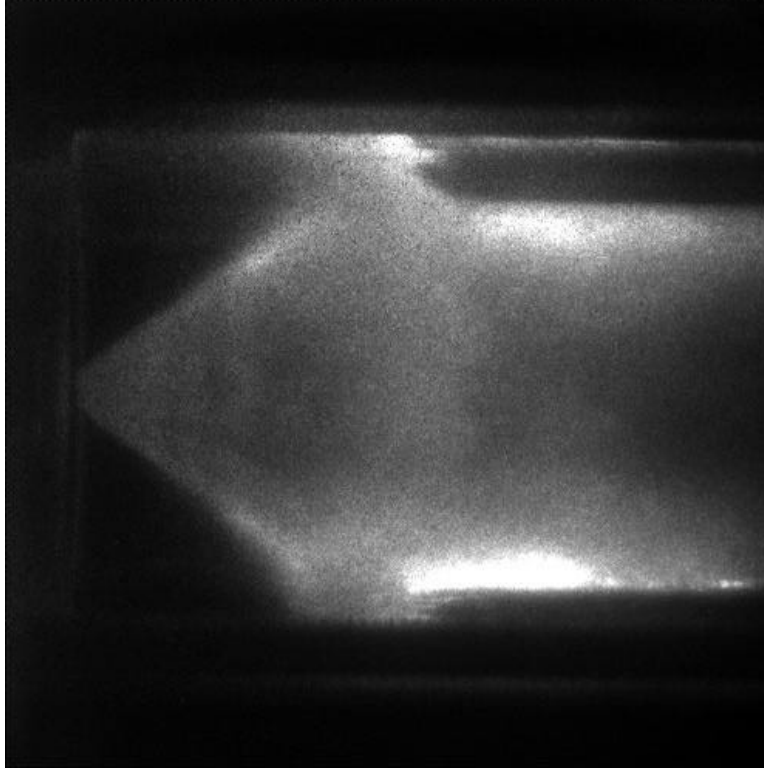
Figure 34.   Liquid Injection Showing Wall Impingement
        (Fuel injected from left; tube walls at top and bottom)

        Air flowing from the inlet manifold into the tube
was intended to redirect the fuel as it passed through the
injection stream.   The original geometry used the straight
insert   shown   in   Figure   19.   The   resulting   flow   was
predominately   uniform   and   added   the   majority   of   its
longitudinal momentum to the longitudinal component of the
injection   path.   This   served   only   to   push   the   wall
impingement further down the tube, not to minimize it.   The
straight   insert   was   replaced   with   the   insert   containing   12
holes.   Turbulence generated by this new geometry appeared
to impart a considerable amount of momentum on the fuel in
the   radial   direction   and   helped   to   reduce   the   amount   of

fuel on the wall. An image of the injection with air
flowing into the tube through the new geometry is shown in
Figure 35. Note that the downstream void in the mixture is
also minimized.
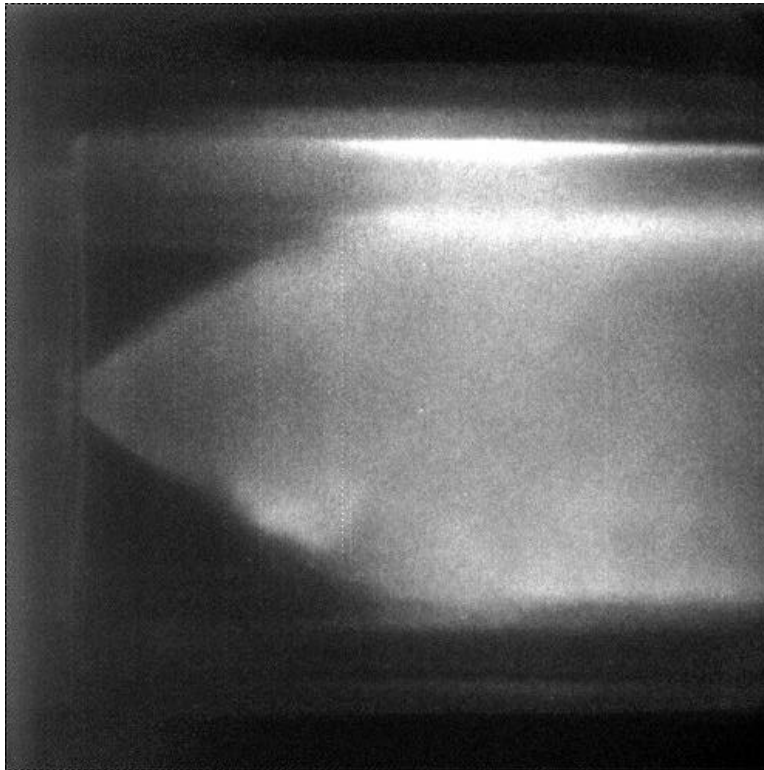
Figure 35.   Liquid Injection Showing Minimized Wall
                        Impingement

C.   GASEOUS FUELS

Gaseous ethylene (C_2H_4) was used during the gaseous
hot-fire phase to provide a baseline of experimental data.
The performance of the hot-fire setup was also
characterized under a wide variety of operating conditions.
A matrix of test objectives was established to include the
exploration of partial fill scenarios, sensitivity to

changes in equivalence ratio, and the effects of variations in injection and ignition timing. Flexibility was built into this matrix to explore areas of interest that arose during testing. Some of these included different hardware geometries and configurations, sensitivities to variations in the air purge, and placement of the sensors that detected detonation wave velocity.

The sensors discussed in Chapter IV were used to collect data on the four key performance metrics for the hot-fire phases. The load cell provided measurement of the instantaneous force (F) at the head wall. The pressure sensor at the head end of tube provided head wall pressure (P3) and the two sensors at the end of the tube provided indication of detonation wave passage ($Wave_1$ and $Wave_2$). These data were saved in one file for each run within the data acquisition program.

When the data was reduced, each of the data acquisition files was loaded into TecPlot 7.5™ for analysis. Each plot generated by TecPlot™ was screened for the results of that run. One particular event, whether it was a successful or failed detonation, from each run was selected for further analysis. The start/stop times and conditions for each event were recorded on a spreadsheet for each run (see Appendix C). The start time was defined by either the onset of load (F) or the passage of the detonation wave as recorded on the $Wave_1$ sensor, which ever came first. The stop time was defined as the time at which the load cell measurements decreased to zero. Examples of the TecPlot™ output are included in Figure 36.
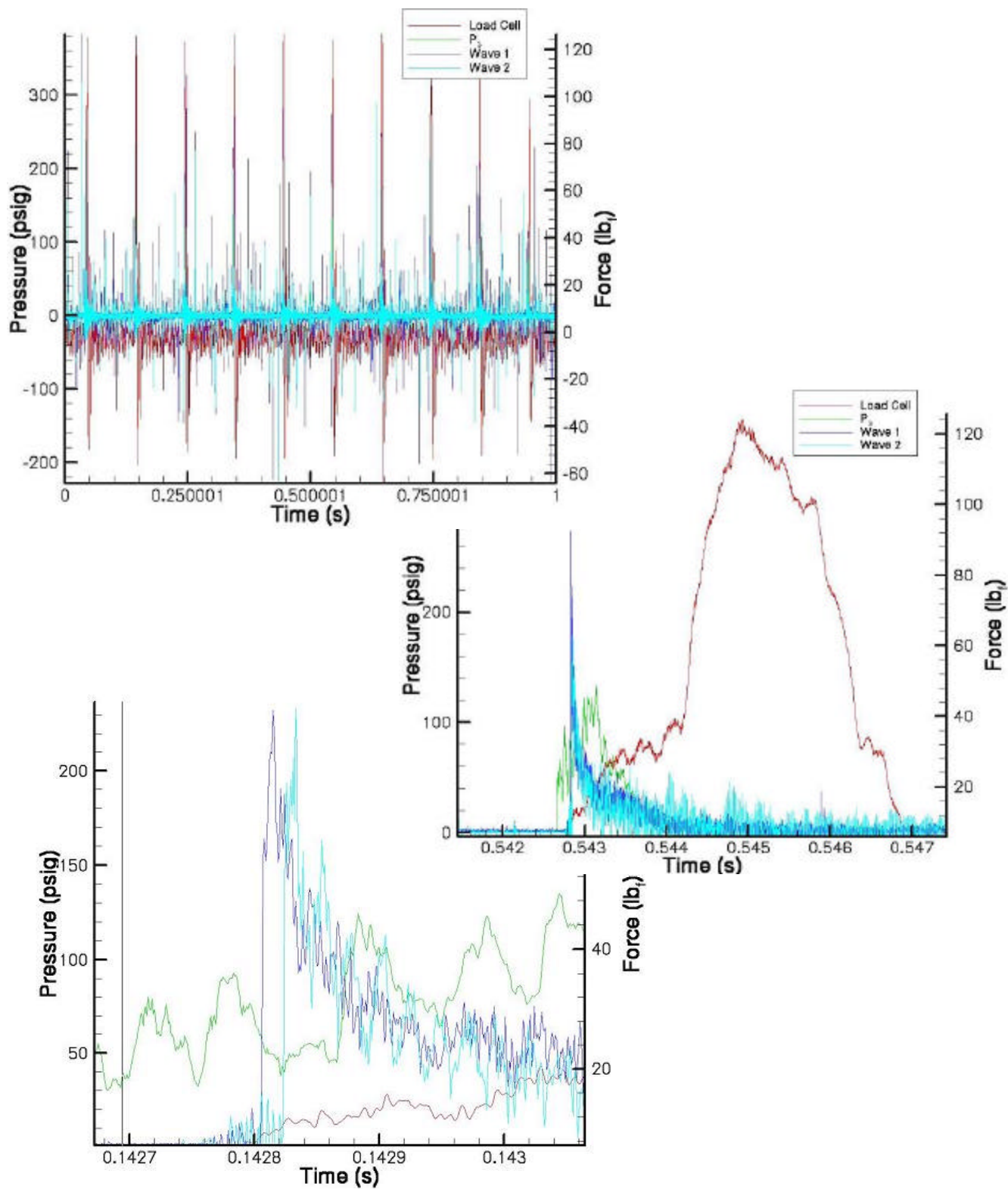
Figure 36.   TecPlot™ Output

60

The event start and stop times for each run were loaded into a MS-Visual C++™ program along with the associated ASCII data generated by TecPlot™ for each of the four run performance measurements. This program read the ASCII data for the entire run and eliminated all but the data that fell within the start and stop times. The total F and P_3 for this period was integrated over this period. The program also calculated the combustion wave speed using the time of passage at $Wave_1$ and $Wave_2$ and the user-defined value of the distance between each sensor (this distance varied slightly for each tube extension). A detonation velocity of zero was returned for any event in which neither $Wave_1$ or $Wave_2$ sensed a pressure rise of greater than 100 psi. The results of these calculations were output to an ASCII file that was then recorded into the run data spreadsheet (see Appendix C).

1. Correlation Between Force and Pressure Measurements

The total impulse per shot was determined through both the load cell and head end pressure measurements for each event. These were compared to determine the correlation between the two measurements. Each measured the same physical impulse but because the measurement came from two different types of sensors, some disagreement between the two was expected. A cursory inspection of the data revealed that each measurement of F was roughly twice that of P_3. This was thought to be a result of flexure in the vertical plate to which the thrust cage and load cell were mounted (see Figure 25). As the thrust cage transmitted the

61

load of a detonation to the plate, the plate would flex a small amount. Following the detonation, the plate deflected back to its resting state, and thus a second force, proportional to the detonation wave force, was recorded. The P_3 measurement, on the other hand, decayed with arrival of the rarefaction waves and, therefore, provided a measurement of the impulse that was believed to be more accurate.

The comparison of the two measurements is plotted in Figure 37. In this plot, the force recorded by the load cell is divided by two in order to offset the phenomenon discussed above. The plot contains all of the runs that were determined to be successful detonations. A handful of obviously anomalous events were discarded.
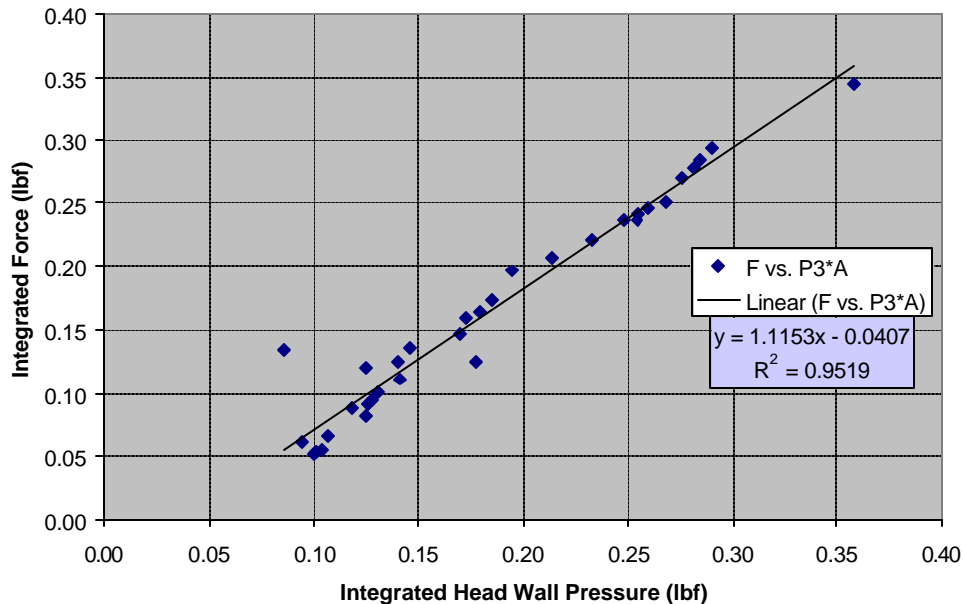
Figure 37. Force vs. Head Wall Pressure per Impulse(The plotted force is half that recorded by the load cell)

A close correlation between F and P_3*A is shown in the plot. A linear trendline is added to reinforce this correlation. The slope of the line shows that the load cell agrees with the P_3 measurement to within approximately 11%. However, P_3 is still considered the more accurate metric and is considered the primary measure of performance for this thesis.

2. Partial Fills

Partial fill scenarios were explored using both of the tube extensions shown in Figure 23 (also known as the "long tube"). The tube fill times were incrementally reduced for each run while the equivalence ratio, purge rate, and frequency were held constant. A plot of these partial fill runs is provided in Figure 38.
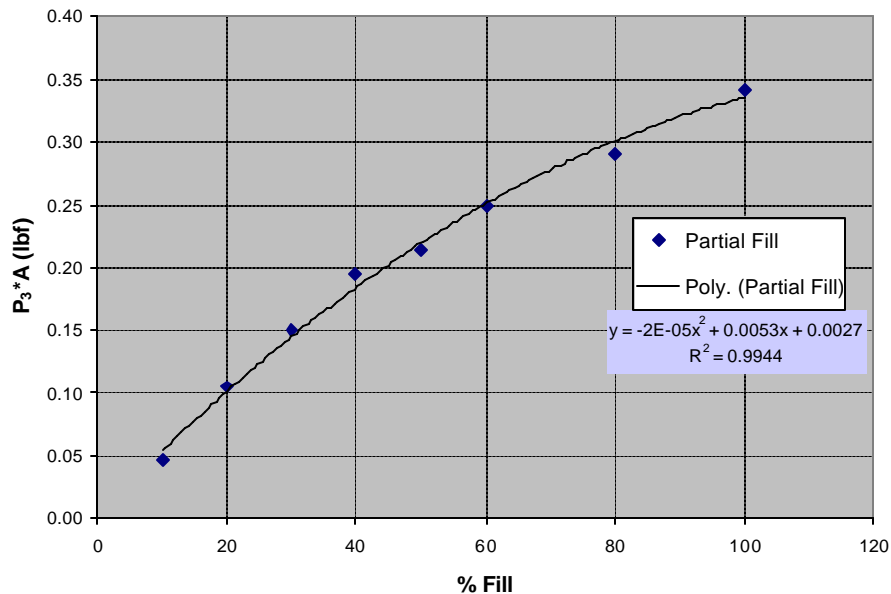
Figure 38.   Impulse vs. Percentage of Tube Filled

The head wall pressure decreased with decreasing fill percentage. As the fill percentage dropped below roughly 70%, the detonation wave decayed prior reaching the wave sensors. This being the case, the detonation wave still produced a fair amount of pressure prior to running out of reactants in the partially filled tube. It should be noted that, beyond a fill of 100%, the plot in Figure 38 will flatten as adding reactants to an already full tube has no additional effect on P_3. In fact, this situation has a detrimental effect on I_{sp}.

3.   Variation of Equivalence Ratio

From the theoretical data acquired in Chapter III it was determined that most hydrocarbon fuels give their best performance at an equivalence ratio (ϕ) of roughly 2.0. Due to hardware limitations, however, a ϕ range of 1.0 to 1.4 was attained with both hot-fire configurations. Values of 1.3 and 1.4 gave the best performance over the range evaluated.

The pressure, and therefore the mass flow rate ($\dot{m}$), of the oxygen was held constant for each of the test runs. Adjusting the fuel pressure prior to each run varied the fuel-to-oxidizer ratio (F/O) and, therefore, the value of ϕ. The VB™ control code was modified to display the current values of O/F and ϕ as the fuel pressure was varied. These calculations took into account the effects of the purge air on the values of O/F and ϕ.

The definition and calculation of ϕ is shown in Equations 5.1 and 5.2 below.

$$f = \frac{(F/O)}{(F/O)_{stoich}}$$
(5.1)

where $F/O = \dfrac{m_{fuel}}{m_{ox}} = \dfrac{\dot{m}_{fuel}}{\dot{m}_{ox}}$
(5.2)

and

$(F/O)_{stoich} \equiv$ Stoichiometric Fuel-to-Oxidizer Ratio for a given chemical reaction with a fuel 'A' and oxidizer 'B',

$$aA + bB \Leftrightarrow cC + dD$$
(5.3)

$$(F/O)_{stoich} = \frac{(a * W_A)}{(b * W_B)}$$
(5.4)

where W = Molecular weight of the reactants

and a,b,c,d = Stoichiometric molar concentration coefficients

The mass flow rate was calculated using the theoretical rate of flow of a compressible fluid in a closed channel[6]. This equation is shown below and a tabulation of applicable values of $\dot{m}$ is included in Appendix B.

$$\dot{m} = \frac{(A_2 P_t)\Gamma_2 K_2}{T_t^{1/2}}$$
(5.5)

where A_2 = Choke area

P_t = Upstream pressure

K = Compressibility factor*

Γ = Compressibility flow function*

65

A series of runs was conducted for a variety of tube lengths (to include the stepped geometry, indicated by the "tube 2" title) while φ was varied between 1.0 and 1.4. The frequency was held at 5 Hz for the long tube, 10 Hz for the medium tube, and 20 Hz for all others. The injection times were varied to ensure the tubes were full. Purge pressure was set at 20 psi for all runs except those with the second medium tube. The results of this series are plotted in Figures 39 and 40. (The base short tube returned zeros for all detonation velocities and is therefore not shown; missing data points represent problems with the results in the batch file).
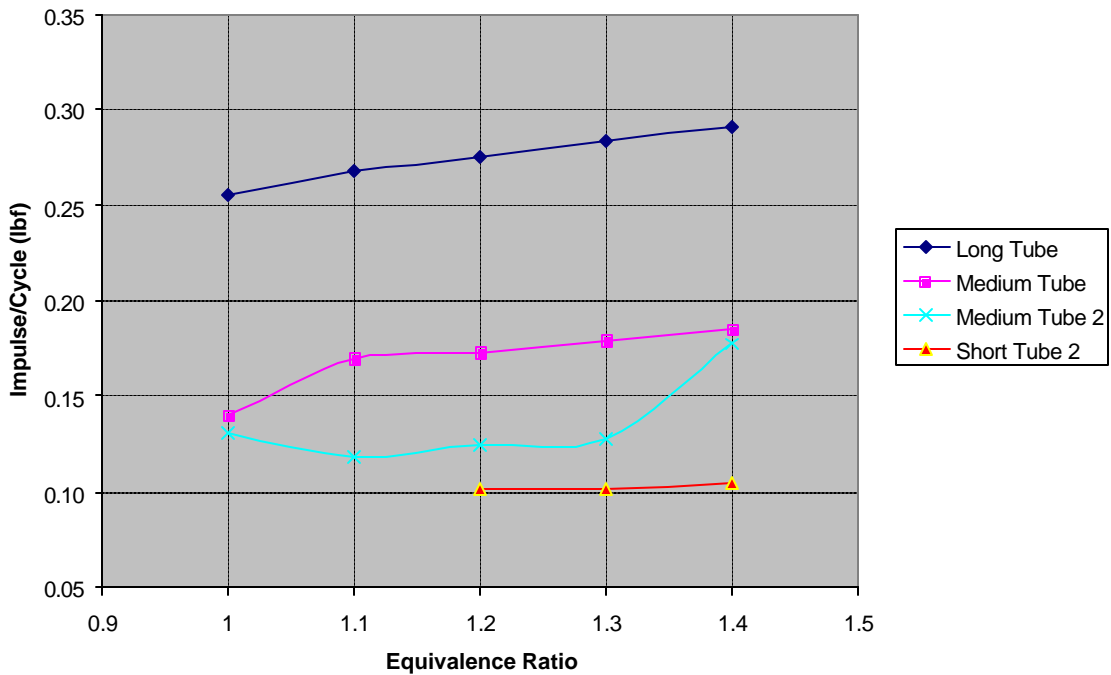
Figure 39.   Impulse per Cycle vs. Equivalence Ratio
                (Integrated head wall pressure)
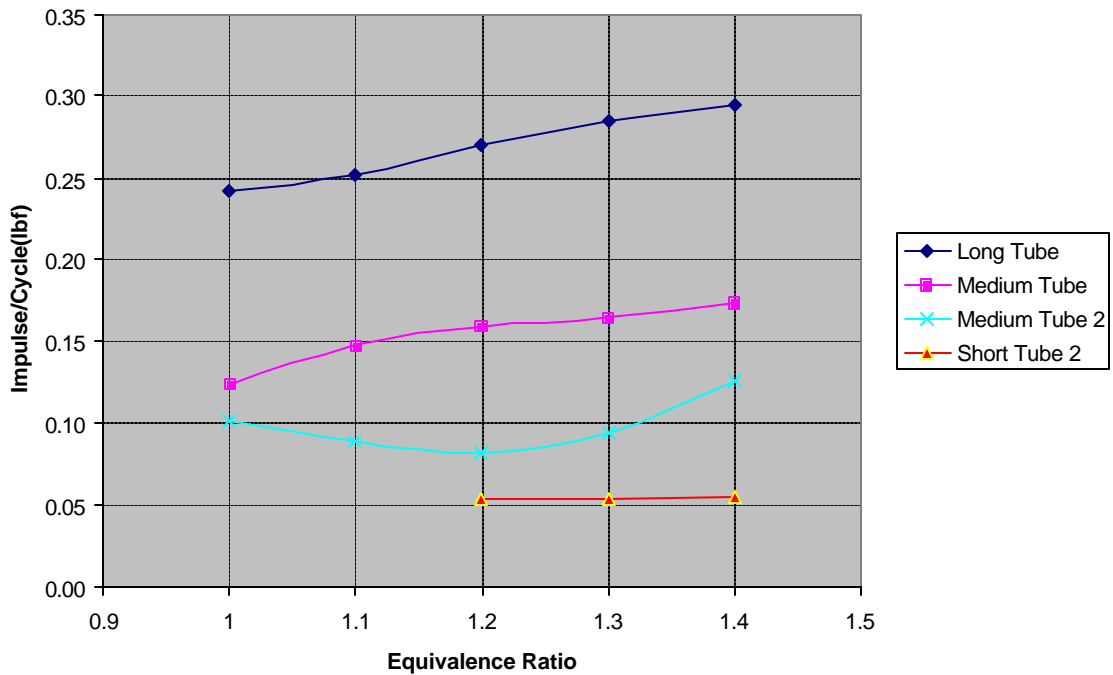
Figure 40.   Impulse per Cycle vs. Equivalence Ratio
(Load cell)

An increasing value of ϕ had a direct effect on the values of F and P_3 but a less obvious effect on the detonation velocity. The theoretical analysis conducted in Chapter III supports these results as the maximum performance was predicted at a ϕ of 2.0. Also, the tube length had a similar effect on the three measurements. This is rather intuitive because as the combustor length increases, the transit times for both the detonation and rarefaction waves also increase. This results in greater impulse per cycle. The longer tubes did not have an obvious effect on detonation velocity because a steady-state detonation wave should propagate at constant velocity, independent of tube length.

The experimental detonation velocities appear much lower than those predicted in the theoretical study. The explanation may be due to inaccuracies in calculating ϕ, specifically with regard to the effects of the purge air. The runs conducted with the second medium tube were performed with a purge of 40 psi, double that of all the other runs. With regard to the experimental plots, this higher purge rate seems to have degraded the performance of this particular configuration and may have had similar effects across the board. Those runs conducted with the base short tube that were not included were conducted with a single purge line through the fuel injector. Apparently this geometry was not conducive to producing successful detonations. There does exist the possibility that some of these events never completely evolved into detonations due to the short length of the detonation tubes.

D.   LIQUID FUELS

In order to provide the best chance of success, the highest turbulence-producing geometry was used to maximize the mixing for the liquid hot-fire testing. This included the use of the second short tube with the stepped geometry and the inlet insert with the 12 holes (see Figures 19 and 20). Extensions to the base tube were not used. Kerosene (RP-1) and JP-10 were the fuels evaluated. Testing of other liquid hydrocarbon fuels was planned but not accomplished due to time constraints. The failure of one of the high-speed Parker-Hannifin (PH) valves also contributed to the abbreviated test matrix.
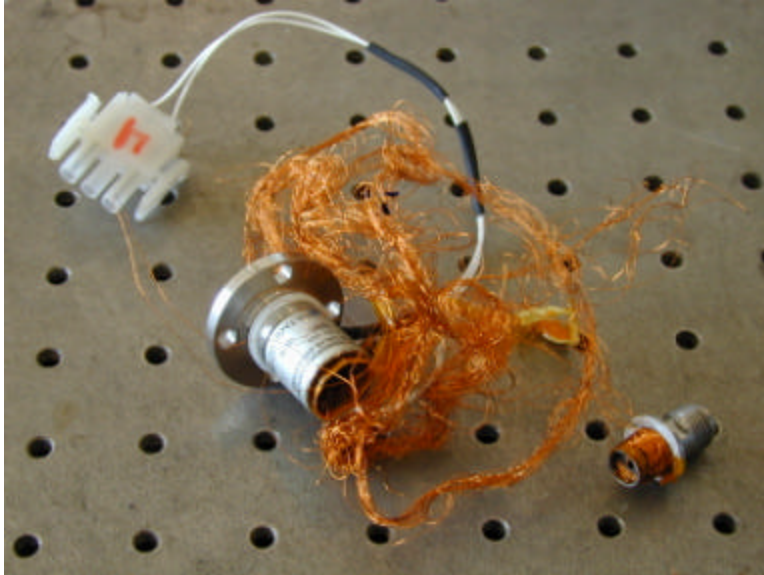
Figure 41.   Failed PH Valve

The failure of the PH valve (Figure 41) occurred during the shakedown of the liquid rig in preparation for the test matrix to come. Figure 41 shows the coil as it was ejected from the valve. After the failure of the valve, it was determined that the remaining three PH valves would not be able to provide the oxygen flow rate required to detonate the liquid fuels. After the failure, two solenoid valves were used to replace the four PH valves. These solenoids limited successful operation to a frequency of 5 Hz.

Other changes to the rig used in the gaseous phase included the elimination of the air purge. To compensate, oxygen was flowed continuously during firing. Due to the large size of the Sturman injector, the thrust cage and load cell had to be removed. Comparison of thrust calculated from load cell (force) and integrated head wall

pressure (P₃*A) data provided confidence that the P_3
measurements yielded the better metric. The removal of the
load cell therefore had a negligible impact on this phase.

During this phase the pressure of the oxygen was
varied from 120 to 200 psi in order to control the
equivalence ratio. Using the Sturman injector, the fuel
pressure was held constant. The value of $\dot{m}_{fuel}$ was
calculated by hand as follows:

$$\dot{m}_{fuel} = \frac{r_{fuel} * V_{inj}}{t_i} \qquad (5.6)$$

where r_{fuel} = Fuel density = 830 kg/m³ for RP-1

= 940 kg/m³ for JP-10

V_{inj} = Volume of fuel injected for each cycle

= 130 mm³

t_i = Injection time = 4.5 ms

This produced a range of φ from 1.0 to 1.4 for RP-1 and from
1.1 to 1.9 for JP-10.

As expected, the liquid fuels proved to be more
difficult to detonate than the gaseous fuels. Several runs
were made before finding a combination of injection and
ignition times that provided successful detonations (see
Appendix C). The results of this phase are plotted in
Figure 42. The theoretical values and polynomial
trendlines for each fuel are provided for reference in
Figure 43. Here, a handful of possibly anomalous events
were thrown out and the results were again plotted. The

70

plot shows the data for both RP-1 and JP-10 were lower than
theory predicted but did also show similar trends.
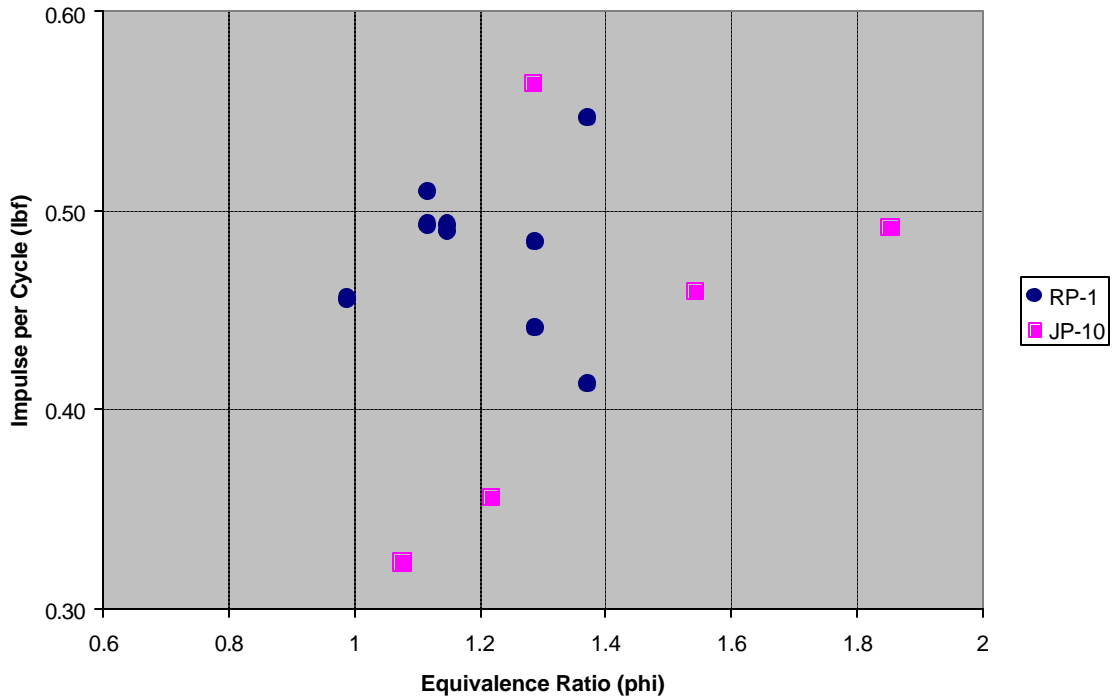
Figure 42.   Impulse per Cycle vs. Equivalence Ratio
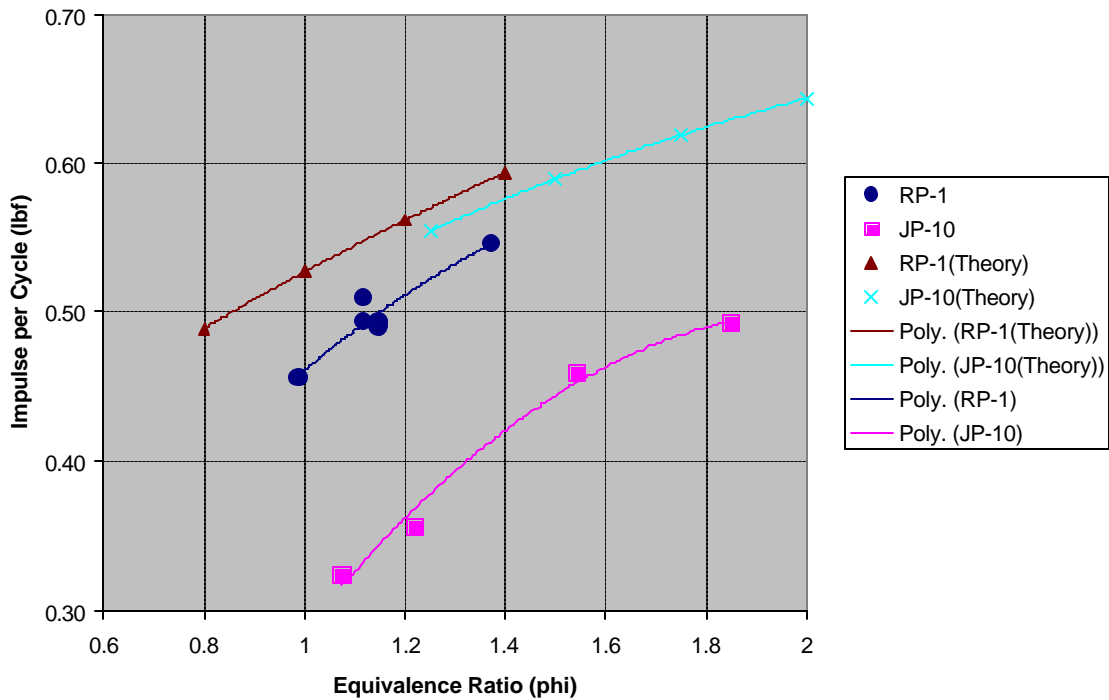
Figure 43.   Impulse per Cycle vs. Equivalence Ratio
       (Theoretical results shown and anomalies removed)

There was a wide dispersion of values for RP-1 but most fell within 15% of the predicted values. If the two lowest data points for RP-1 are ignored, the remaining values tend to track theory fairly well.

JP-10 also tracked theory but the majority of values were roughly 22% lower than predicted. At a ϕ of 1.3, JP-10 behaved nearly exactly as predicted. This ϕ may have provided the best mixture ratio for this configuration and resulted in near-ideal performance.

The lower than predicted values for this phase may have been a result of fuel impingement on the tube wall.

As graphically depicted during the flow visualization phase (see Figures 34 and 35), the momentum of the liquid fuel tends to carry to the tube wall. This can result in a lower than predicted value of ϕ as the fuel hitting the wall doesn't mix efficiently with the oxygen and is therefore not fully utilized during the combustion process. During several runs in this phase, liquid fuel was recorded dripping from the end of the tube by the remote camera. This indicates that the effective value of $\dot{m}_{fuel}$ was lower than calculated and reinforces the idea of fuel impingement. The stepped interior geometry of this configuration (see Figure 20), while beneficial in creating turbulence within the mixture, may have exacerbated this problem by limiting the distance from the injector to the tube wall.

VI. CONCLUSIONS

This work demonstrated the successful operation of a liquid-fueled pulse detonation rocket engine using two complex hydrocarbon fuels, namely JP-10 and RP-1. The importance of this success cannot be underestimated. If the PDRE is going to evolve into a viable alternative to the conventional rocket engine, the use of high energy density liquid fuels will have to be operationally realized. Some of the difficulties in achieving detonation with liquid fuels were experienced, the most notable being the tendency for fuel impingent on the tube walls due to improper oxygen-to-fuel momentum ratios during the injection process.

The first use of a Sturman fuel injector on a PDRE system was also demonstrated. This injector provided a factor of reliability proven by its diesel heritage. The properties of precise and predictable metering of fuel while maintaining constant atomization properties was one of the reasons it was selected for use in this system.

The ability of the PDRE to operate under partial fill scenarios was demonstrated. The demonstrated reduction in impulse with the partial fill scenarios was evident and was shown to be nearly linear with percentage fill. This ability is important for possible thrust vector control and throttling issues in future operational PDREs.

Several different geometries were used to accomplish the objectives of this work. Multiple tube segments allowed for the exploration of partial fill scenarios, while various internal geometries provided increased

turbulence to the reactants.   Care must be taken in the design of future PDREs to avoid fuel/wall interactions and mixture voids occasionally experienced during this work.

While the primary liquid phase was conducted at a frequency of 5 Hz, the preparatory gaseous phase achieved an operating frequency of 40 Hz.   Operation at this frequency was steady and reliable.   The key issue highlighted by this phase was the PDRE's sensitivity to the purge cycle. Air was used to blow down the tube following detonation and in preparation for a new charge of reactants.   While this practice is acceptable in the laboratory, an operational PDRE will require a more efficient means of achieving this buffer.

A.   FUTURE WORK

Future work in the pulse detonation area includes the possible use of a PDRE in a rocket-based combined cycle (RBCC) mode.   Like the strutjet, the PDRE here may be used inside an ejector setup.   Atmospheric air is flowed through a duct containing the PDRE.   Firing inside this duct, the PDE would impart additional momentum to the airflow.   As the upper region of the atmosphere is reached, the intake of the duct would be closed and the PDRE would opporate as the primary propulsion unit using the onboard oxidizer to continue into the vacuum of space.

Perhaps the most promising area of future research involves the use an adaptive exit nozzle with a PDRE.   In this application the thermal energy of the exhausted reactants is further converted to kinetic energy through an adaptive converging-diverging nozzle.   Because the burned

combustion products are exiting the tube at just below the sonic velocity, only a very slight amount of convergence at the exit is required to choke the flow. The convergence may help to provide a degree of backpressure during the fill process and would have little effect on the remaining portion of the cycle. It is estimated that if the thermal energy can be further converted to kinetic energy at the exhaust plane, the thrust could be improved by up to $\approx 40\%$. This is an area of future work at the RPCL.

While a great deal of refinement remains, the PDRE provides a promising alternative to some of today's prohibitively expensive and risky space launch systems. It is my sincere hope that this work provides a contribution to the goal of safe, simple, and reliable access to space.

Hydrocarbon Fuel Comparisons Used in a Pulse Detonation Rocket Engine

<u>Assumptions</u>:

1. All reactions consist of a hydrocarbon fuel mixed with pure oxygen as an oxidizer (a hydrogen reaction is provided for reference).
2. Ambient conditions for all reactions are one atmosphere pressure and a temperature of 300 degrees Kelvin.
3. Reactants are considered in a gaseous state. The mixture in considered homogenous.
4. Performance calculations are based on a one meter tube with a diameter of five inches (volume=$0.051m^3$).

H2/O2

Phi		0.8	0.9	1	1.1	1.2	1.3	1.4	1.5	1.6	1.7	1.8	1.9	2
O/F		9.921	8.8183	7.964	7.215	6.6137	6.105	5.6689	5.291	4.9603	4.6685	4.4091	4.1771	3.9682

Unburned Gas

P1	(atm)	1	1	1	1	1	1	1	1	1	1	1	1	1
T1	(deg K)	300	300	300	300	300	300	300	300	300	300	300	300	300
H1	(cal/g)	0.97	1.04	1.1	1.16	1.22	1.28	1.33	1.39	1.44	1.5	1.55	1.6	1.65
M1	(kg/kmol)	13.548	12.724	12.01	11.386	10.834	10.345	9.906	9.512	9.155	8.83	8.534	8.262	8.013
Gamma1		1.4008	1.4011	1.4014	1.4016	1.4018	1.4019	1.4021	1.4022	1.4023	1.4025	1.4026	1.4026	1.4027
Sonic Vel1	(m/sec)	507.8	524.1	539.5	554.1	568.1	581.4	594.2	606.4	618.1	629.4	640.3	650.7	660.8

Burned Gas

P2	(atm)	18.52	18.643	18.716	18.747	18.74	18.701	18.634	18.542	18.43	18.302	18.16	18.008	17.847
T2	(deg K)	3649	3671	3681	3681	3672	3656	3634	3608	3578	3546	3511	3475	3438
H2	(J/kg)	2.49E+06	2.67E+06	2.84E+06	3.00E+06	3.16E+06	3.30E+06	3.43E+06	3.56E+06	3.67E+06	3.78E+06	3.88E+06	3.98E+06	4.06E+06
M2	(kg/kmol)	16.353	15.355	14.475	13.696	13.002	12.38	11.82	11.315	10.856	10.438	10.057	9.707	9.385
Rho2	(kg/m^3)	1.01	0.95	0.897	0.85	0.809	0.772	0.739	0.709	0.681	0.657	0.634	0.613	0.594
Gamma2(SF)		1.2174	1.2176	1.2181	1.2187	1.2195	1.2205	1.2215	1.2226	1.2238	1.225	1.2263	1.2276	1.2289
Gamma2(S)		1.1288	1.1288	1.1291	1.1296	1.1304	1.1315	1.1328	1.1345	1.1363	1.1384	1.1407	1.1431	1.1456
Sonic Vel2	(m/sec)	1447	1498	1545.1	1588.7	1629.2	1666.8	1701.7	1734.3	1764.7	1793.1	1819.7	1844.6	1868

Detonation Parameters

P2/P1		18.52	18.643	18.716	18.747	18.74	18.701	18.634	18.542	18.43	18.302	18.16	18.008	17.847
T2/T1		12.16333	12.23667	12.27	12.27	12.24	12.18667	12.11333	12.02667	11.92667	11.82	11.70333	11.58333	11.46
M2/M1		1.207042	1.206775	1.205246	1.202881	1.200111	1.196713	1.193216	1.18955	1.1858	1.182106	1.178463	1.174897	1.171222
Rho2/Rho1		1.8381	1.8383	1.8383	1.838	1.8374	1.8365	1.8354	1.8339	1.8323	1.8304	1.8284	1.8263	1.824
Mach #		5.2373	5.2546	5.26651	5.2698	5.2695	5.2649	5.2566	5.2451	5.231	5.2147	5.1966	5.177	5.1562
Det Vel	(m/sec)	2659.8	2753.8	2840.4	2920.1	2993.5	3061.1	3123.3	3180.6	3233.4	3282.2	3327.2	3368.8	3407.3
Det Time	(sec)	3.76E-04	3.63E-04	3.52E-04	3.42E-04	3.34E-04	3.27E-04	3.20E-04	3.14E-04	3.09E-04	3.05E-04	3.01E-04	2.97E-04	2.93E-04
Raref Time	(sec)	6.91E-04	6.68E-04	6.47E-04	6.29E-04	6.14E-04	6.00E-04	5.88E-04	5.77E-04	5.67E-04	5.58E-04	5.50E-04	5.42E-04	5.35E-04
Tot Time	(sec)	1.07E-03	1.03E-03	9.99E-04	9.72E-04	9.48E-04	9.27E-04	9.08E-04	8.91E-04	8.76E-04	8.62E-04	8.50E-04	8.39E-04	8.29E-04
P3	(atm)	6.353322	6.392628	6.413975	6.42272	6.420066	6.407201	6.386658	6.359818	6.327198	6.290175	6.249477	6.206117	6.160713
F3	(N)	32831.27	33034.39	33144.7	33189.89	33176.17	33109.69	33003.53	32864.83	32696.27	32504.95	32294.64	32070.57	31835.95
Tot Imp	(N-sec)	35.03271	34.04825	33.12052	32.25723	31.44621	30.6805	29.96133	29.28282	28.63999	28.0312	27.45349	26.90607	26.38625
Spec Imp	(sec)	127.4331	131.6887	135.6694	139.4166	142.7527	145.8804	148.7333	151.3921	154.0221	156.0929	158.2487	160.2222	161.9485

Methane/O2

Phi		0.8	0.9	1	1.1	1.2	1.3	1.4	1.5	1.6	1.7	1.8	1.9	2	Phi
O/F		4.9864	4.4324	3.9891	3.6265	3.3243	3.0686	2.8494	2.6594	2.4932	2.3465	2.2162	2.0995	1.9946	O/F

Unburned Gas

P1	(atm)	1	1	1	1	1	1	1	1	1	1	1	1	1	P1
T1	(deg K)	300	300	300	300	300	300	300	300	300	300	300	300	300	T1
H1	(cal/g)	-185.75	-204.73	-222.96	-240.46	-257.3	-273.49	-289.09	-304.12	-318.61	-332.59	-346.09	-359.12	-371.73	H1
M1	(kg/kmol)	27.44	27.047	26.68	26.337	26.015	25.713	25.429	25.161	24.907	24.668	24.441	24.225	24.021	M1
Gamma1		1.364	1.3615	1.3593	1.3572	1.3553	1.3535	1.3519	1.3503	1.3489	1.3475	1.3462	1.345	1.3439	Gamma1
Sonic Vel1	(m/sec)	352.1	354.3	356.5	358.5	360.5	362.4	364.1	365.9	367.5	369.1	370.7	372.1	373.6	Sonic Vel1

Burned Gas

P2	(atm)	27.319	28.316	29.202	29.98	30.649	31.202	31.629	31.928	32.086	32.102	31.978	31.721	31.339	P2
T2	(deg K)	3662	3700	3726	3740	3742	3732	3710	3676	3629	3571	3501	3420	3331	T2
H2	(J/kg)	1.06E+06	1.08E+06	1.09E+06	1.11E+06	1.11E+06	1.11E+06	1.10E+06	1.09E+06	1.07E+06	1.03E+06	9.90E+05	9.40E+05	8.80E+05	H2
M2	(kg/kmol)	22.715	21.837	21.036	20.301	19.623	18.994	18.406	17.856	17.339	16.852	16.393	15.959	15.55	M2
Rho2	(kg/m^3)	2.07	2.04	2.01	1.98	1.96	1.94	1.91	1.89	1.87	1.85	1.82	1.8	1.78	Rho2
Gamma2(SF)		1.2191	1.2196	1.2203	1.2212	1.2224	1.2237	1.2253	1.2271	1.2292	1.2315	1.2341	1.2369	1.24	Gamma2(SF)
Gamma2(S)		1.1297	1.1303	1.1312	1.1322	1.1335	1.1353	1.1376	1.1406	1.1447	1.1497	1.1558	1.1629	1.1709	Gamma2(S)
Sonic Vel2	(m/sec)	1230.5	1261.9	1290.7	1316.9	1340.6	1361.9	1380.8	1397.3	1411.4	1423.2	1432.5	1439.5	1444.2	Sonic Vel2

Detonation Parameters

P2/P1		27.319	28.316	29.202	29.98	30.649	31.202	31.629	31.928	32.086	32.102	31.978	31.721	31.339	P2/P1
T2/T1		12.20667	12.33333	12.42	12.46667	12.47333	12.44	12.36667	12.25333	12.09667	11.90333	11.67	11.4	11.10333	T2/T1
M2/M1		0.827806	0.807372	0.788456	0.770817	0.754296	0.738692	0.723819	0.70967	0.69615	0.683152	0.670717	0.658782	0.64735	M2/M1
Rho2/Rho1		1.8528	1.8535	1.8538	1.8538	1.8534	1.8526	1.8511	1.8492	1.8464	1.8427	1.8381	1.8329	1.8268	RHO2/RHO1
Mach #		6.4747	6.6008	6.7119	6.809	6.8927	6.963	7.0191	7.0621	7.0905	7.1043	7.1039	7.09	7.0626	Mach #
Det Vel	(m/sec)	2279.8	2339	2392.6	2441.2	2484.7	2523	2556	2583.9	2606	2622.4	2633.1	2638.5	2638.3	Det Vel
Det Time	(sec)	4.39E-04	4.28E-04	4.18E-04	4.10E-04	4.02E-04	3.96E-04	3.91E-04	3.87E-04	3.84E-04	3.81E-04	3.80E-04	3.79E-04	3.79E-04	Det Time
Raref Time	(sec)	8.13E-04	7.92E-04	7.75E-04	7.59E-04	7.46E-04	7.34E-04	7.24E-04	7.16E-04	7.09E-04	7.03E-04	6.98E-04	6.95E-04	6.92E-04	Raref Time
Tot Time	(sec)	1.25E-03	1.22E-03	1.19E-03	1.17E-03	1.15E-03	1.13E-03	1.12E-03	1.10E-03	1.09E-03	1.08E-03	1.08E-03	1.07E-03	1.07E-03	Tot Time
P3	(atm)	9.172344	9.491263	9.778148	10.02794	10.24203	10.42343	10.5675	10.67275	10.74086	10.77353	10.76622	10.72199	10.64512	P3
F3	(N)	47398.78	49046.81	50529.31	51820.11	52926.48	53863.84	54608.37	55152.24	55504.22	55673.01	55635.23	55406.67	55009.47	F3
Tot Imp	(N-sec)	59.31069	59.83657	60.26776	60.57738	60.78065	60.89964	60.91313	60.81515	60.62427	60.34798	59.96703	59.48952	58.94027	Tot Imp
Spec Imp	(sec)	106.1089	108.6651	111.0997	113.3624	114.8786	116.24	117.9963	118.9309	119.6442	120.1452	121.0518	121.0786	120.9049	Spec Imp

Propane/O2

Phi		0.8	0.9	1	1.1	1.2	1.3	1.4	1.5	1.6	1.7	1.8	1.9	2	Phi
O/F		4.5353	4.0313	3.6282	3.2954	3.0235	2.7909	2.5916	2.4188	2.2676	2.1432	2.0157	1.9096	1.8141	O/F
Unburned Gas															**Unburned Gas**
P1	(atm)	1	1	1	1	1	1	1	1	1	1	1	1	1	P1
T1	(deg K)	300	300	300	300	300	300	300	300	300	300	300	300	300	T1
H1	(cal/g)	-101.16	-111.33	-121.07	-130.39	-139.32	-147.89	-156.12	-164.04	-171.64	-178.96	-186.02	-192.81	-199.37	H1
M1	(kg/kmol)	33.668	33.844	34.015	34.18	34.34	34.495	34.645	34.791	34.932	35.069	35.201	35.33	35.455	M1
Gamma1		1.3055	1.2984	1.2918	1.2857	1.28	1.2747	1.2698	1.2652	1.2609	1.2568	1.253	1.2494	1.246	Gamma1
Sonic Vel1	(m/sec)	311	309.3	307.8	306.3	304.9	303.6	302.4	301.2	300.1	299	298	297	296.1	Sonic Vel1
Burned Gas															**Burned Gas**
P2	(atm)	32.58	34.362	36.04	37.612	39.073	40.412	41.615	42.663	43.54	44.23	44.724	45.017	45.116	P2
T2	(deg K)	3748	3794	3828	3851	3863	3865	3855	3833	3800	3754	3696	3626	3547	T2
H2	(J/kg)	1.38E+06	1.42E+06	1.47E+06	1.51E+06	1.54E+06	1.57E+06	1.60E+06	1.61E+06	1.62E+06	1.62E+06	1.61E+06	1.59E+06	1.56E+06	H2
M2	(kg/kmol)	23.961	23.127	22.365	21.663	21.015	20.41	19.845	19.313	18.811	18.335	17.884	17.455	17.048	M2
Rho2	(kg/m^3)	2.54	2.55	2.57	2.58	2.59	2.6	2.61	2.62	2.63	2.63	2.64	2.64	2.64	Rho2
Gamma2(SF)		1.2242	1.2251	1.2262	1.2275	1.2289	1.2305	1.2323	1.2342	Jan-00	1.2386	1.2412	1.244	1.247	Gamma2(SF)
Gamma2(S)		1.1323	1.1333	1.1345	1.1359	1.1374	1.1392	1.1414	1.1442	1.1478	1.1522	1.1576	1.1639	1.1711	Gamma2(S)
Sonic Vel2	(m/sec)	1213.4	1243.3	1270.7	1295.7	1318.6	1339.2	1357.8	1374.2	1388.4	1400.4	1410.3	1417.9	1423.2	Sonic Vel2
Detonation Parameters															**Detonation Parameters**
P2/P1		32.58	34.362	36.04	37.612	39.073	40.412	41.615	42.663	43.54	44.23	44.724	45.017	45.116	P2/P1
T2/T1		12.49333	12.64667	12.76	12.83667	12.87667	12.88333	12.85	12.77667	12.66667	12.51333	12.32	12.08667	11.82333	T2/T1
M2/M1		0.711685	0.683341	0.6575	0.633792	0.611969	0.59168	0.57281	0.555115	0.538503	0.522826	0.508054	0.494056	0.480835	M2/M1
Rho2/Rho1		1.8561	1.8567	1.857	1.857	1.8567	1.8561	1.855	1.8535	1.8512	1.8483	1.8445	1.8401	1.835	RHO2/RHO1
Mach #		7.242	7.4625	7.6666	7.8553	8.029	8.1874	8.3302	8.4566	8.5658	8.6571	8.73	8.7846	8.821	Mach #
Det Vel	(m/sec)	2252.3	2308.4	2359.6	2406.1	2448.2	2485.7	2518.7	2546.9	2570.2	2588.4	2601.3	2609	2611.6	Det Vel
Det Time	(sec)	4.44E-04	4.33E-04	4.24E-04	4.16E-04	4.08E-04	4.02E-04	3.97E-04	3.93E-04	3.89E-04	3.86E-04	3.84E-04	3.83E-04	3.83E-04	Det Time
Raref Time	(sec)	8.24E-04	8.04E-04	7.87E-04	7.72E-04	7.58E-04	7.47E-04	7.36E-04	7.28E-04	7.20E-04	7.14E-04	7.09E-04	7.05E-04	7.03E-04	Raref Time
Tot Time	(sec)	1.27E-03	1.24E-03	1.21E-03	1.19E-03	1.17E-03	1.15E-03	1.13E-03	1.12E-03	1.11E-03	1.10E-03	1.09E-03	1.09E-03	1.09E-03	Tot Time
P3	(atm)	10.82418	11.39688	11.93403	12.43481	12.90253	13.33008	13.71929	14.06498	14.36209	14.60857	14.8057	14.94698	15.0034	P3
F3	(N)	55934.75	58894.23	61669.99	64257.81	66674.77	68884.17	70895.47	72681.83	74217.18	75490.91	76509.55	77239.65	77686.23	F3
Tot Imp	(N-sec)	70.93204	72.88229	74.66808	76.29934	77.79901	79.14899	80.36112	81.42766	82.33122	83.07176	83.66259	84.07976	84.33221	Tot Imp
Spec Imp	(sec)	103.6027	106.068	107.8387	109.7675	111.4748	112.9365	114.159	115.1394	115.8305	116.6893	116.8334	117.1358	117.1619	Spec Imp

Ethane/O2

Phi		0.8	1	1.2	1.4	1.6	1.8	2	2.2	2.4	2.6	Phi	
O/F		4.6556	3.7245	3.1037	2.6603	2.378	2.0692	1.8622	1.6929	1.5519	1.4325	O/F	
Unburned Gas												**Unburned Gas**	
P1	(atm)	1	1	1	1	1	1	1	1	1	1	P1	(atm)
T1	(deg K)	300	300	300	300	300	300	300	300	300	300	T1	(deg K)
H1	(cal/g)	-117.31	-140.51	-161.83	-181.48	-199.65	-216.51	-232.2	-246.82	-260.49	-273.29	H1	(cal/g)
M1	(kg/kmol)	31.64	31.57	31.506	31.448	31.394	31.334	31.297	31.254	31.214	31.177	M1	(kg/kmol)
Gamma1		1.3274	1.3169	1.3079	1.3	1.2931	1.287	1.2816	1.2767	1.2723	1.2684	Gamma1	
Sonic Vel1	(m/sec)	323.5	322.6	321.8	321.1	320.5	320	319.6	319.2	318.9	318.6	Sonic Vel1	(m/sec)
Burned Gas												**Burned Gas**	
P2	(atm)	30.938	33.844	36.302	38.266	39.638	40.332	40.336	39.705	38.514	36.824	P2	(atm)
T2	(deg K)	3726	3802	3832	3817	3756	3647	3496	3312	3102	2874	T2	(deg K)
H2	(J/kg)	1.32E+06	1.41E+06	1.47E+06	1.51E+06	1.53E+06	1.51E+06	1.45E+06	1.36E+06	1.24E+06	1.09E+06	H2	(J/kg)
M2	(kg/kmol)	23.565	21.942	20.571	19.387	18.345	17.414	16.58	15.829	15.151	14.536	M2	(kg/kmol)
Rho2	(kg/m^3)	2.38	2.38	2.38	2.37	2.36	2.35	2.33	2.31	2.29	2.27	Rho2	(kg/m^3)
Gamma2(SF)		1.223	1.2248	1.2274	1.2305	1.2345	1.2393	1.245	1.2516	1.2591	1.2676	Gamma2(SF)	
Gamma2(S)		1.1316	1.1336	1.1363	1.1403	1.1466	1.1565	1.17	1.1865	1.2058	1.228	Gamma2(S)	
Sonic Vel2	(m/sec)	1219.7	1277.9	1326.6	1366.2	1397.1	1419.1	1432.2	1436.6	1432.8	1420.8	Sonic Vel2	(m/sec)
Detonation Parameters												**Detonation Parameters**	
P2/P1		30.938	33.844	36.302	38.266	39.638	40.332	40.336	39.705	38.514	36.824	P2/P1	
T2/T1		12.421	12.673	12.772	12.724	12.519	12.157	11.654	11.039	10.341	9.58	T2/T1	
M2/M1		0.7448	0.695	0.6529	0.6165	0.5843	0.5556	0.5297	0.5065	0.4854	0.4662	M2/M1	
Rho2/Rho1		1.8552	1.8561	1.8558	1.8541	1.8501	1.8432	1.8336	1.8216	1.8077	1.7922	Rho2/Rho1	
Mach #		6.9948	7.3535	7.6507	7.8885	8.064	8.1733	8.217	8.1983	8.1231	7.9935	Mach #	
Det Vel	(m/sec)	2262.7	2371.9	2461.8	2533.1	2584.8	2615.7	2626.1	2616.9	2590.1	2546.3	Det Vel	(m/sec)
Det Time	(sec)	4.42E-04	4.22E-04	4.06E-04	3.95E-04	3.87E-04	3.82E-04	3.81E-04	3.82E-04	3.86E-04	3.93E-04	Det Time	(sec)
Raref Time	(sec)	8.20E-04	7.83E-04	7.54E-04	7.32E-04	7.16E-04	7.05E-04	6.98E-04	6.96E-04	6.98E-04	7.04E-04	Raref Time	(sec)
Tot Time	(sec)	1.26E-03	1.20E-03	1.16E-03	1.13E-03	1.10E-03	1.09E-03	1.08E-03	1.08E-03	1.08E-03	1.10E-03	Tot Time	(sec)
P3	(atm)	10.3077	11.2378	12.02381	12.65649	13.12155	13.40466	13.4974	13.41079	13.15476	12.73949	P3	(atm)
F3	(N)	53265.79	58072.17	62133.92	65403.39	67806.58	69269.58	69748.81	69301.27	67978.18	65832.28	F3	(N)
Tot Imp	(N-sec)	67.21203	69.92684	72.07619	73.69199	74.76662	75.29456	75.26032	74.72198	73.68968	72.18875	Tot Imp	(N-sec)
Spec Imp	(sec)	104.7181	109.0007	112.3329	115.2301	117.1526	118.04	118.3792	117.7742	116.2675	113.9176	Spec Imp	(sec)

Butane(C4H10)/O2

Phi		0.8	1	1.2	1.4	1.6	1.8	2	2.2	2.4	2.6	Phi	
O/F		4.473	3.5784	2.982	2.556	2.2365	1.988	1.7892	1.6265	1.491	1.3763	O/F	
Unburned Gas												**Unburned Gas**	
P1	(atm)	1	1	1	1	1	1	1	1	1	1	P1	(atm)
T1	(deg K)	300	300	300	300	300	300	300	300	300	300	T1	(deg K)
H1	(cal/g)	-93.97	-112.42	-129.31	-144.85	-159.19	-172.46	-184.79	-196.25	-206.96	-216.96	H1	(cal/g)
M1	(kg/kmol)	34.862	35.482	36.07	36.629	37.159	37.665	38.146	38.605	39.044	39.463	M1	(kg/kmol)
Gamma1		1.2903	1.2745	1.2611	1.2495	1.2394	1.2305	1.2227	1.2157	1.2093	1.2037	Gamma1	
Sonic Vel1	(m/sec)	303.8	299.3	295.3	291.7	288.4	285.5	282.8	280.3	278	275.8	Sonic Vel1	(m/sec)
Burned Gas												**Burned Gas**	
P2	(atm)	33.534	37.341	40.746	43.67	45.971	47.494	48.165	48.018	47.123	45.537	P2	(atm)
T2	(deg K)	3759	3842	3881	3875	3823	3721	3573	3387	3174	2939	T2	(deg K)
H2	(J/kg)	1.40E+06	1.49E+06	1.57E+06	1.63E+06	1.66E+06	1.65E+06	1.61E+06	1.53E+06	1.42E+06	1.28E+06	H2	(J/kg)
M2	(kg/kmol)	24.184	22.604	21.266	20.104	19.075	18.15	17.314	16.556	15.868	15.241	M2	(kg/kmol)
Rho2	(kg/m^3)	2.63	2.68	2.72	2.76	2.8	2.82	2.84	2.86	2.87	2.88	Rho2	(kg/m^3)
Gamma2(SF)		1.2248	1.227	1.2297	1.2331	1.2372	1.2422	1.248	1.2548	1.2625	1.2712	Gamma2(SF)	
Gamma2(S)		1.1326	1.135	1.138	1.1421	1.1485	1.1583	1.1719	1.1885	1.2079	1.2302	Gamma2(S)	
Sonic Vel2	(m/sec)	1209.8	1266.5	1314	1352.9	1383.4	1405.3	1418	1421.9	1417.3	1404.5	Sonic Vel2	(m/sec)
Detonation Parameters												**Detonation Parameters**	
P2/P1		33.534	37.341	40.746	43.67	45.971	47.494	48.165	48.018	47.123	45.537	P2/P1	
T2/T1		12.53	12.80667	12.93667	12.91667	12.74333	12.40333	11.91	11.29	10.58	9.796667	T2/T1	
M2/M1		0.693707	0.637055	0.589576	0.548855	0.513335	0.48188	0.453888	0.428856	0.406413	0.38621	M2/M1	
Rho2/Rho1		1.8566	1.8575	1.8572	1.8555	1.8518	1.8451	1.8356	1.8239	1.8103	1.795	Rho2/Rho1	
Mach #		7.3928	7.8593	8.2636	8.6061	8.8815	9.0824	9.2054	9.2533	9.2306	9.1401	Mach #	
Det Vel	(m/sec)	2246.2	2352.5	2440.3	2510.4	2561.7	2592.7	2602.8	2593.3	2565.7	2521	Det Vel	(m/sec)
Det Time	(sec)	4.45E-04	4.25E-04	4.10E-04	3.98E-04	3.90E-04	3.86E-04	3.84E-04	3.86E-04	3.90E-04	3.97E-04	Det Time	(sec)
Raref Time	(sec)	8.27E-04	7.90E-04	7.61E-04	7.39E-04	7.23E-04	7.12E-04	7.05E-04	7.03E-04	7.06E-04	7.12E-04	Raref Time	(sec)
Tot Time	(sec)	1.27E-03	1.21E-03	1.17E-03	1.14E-03	1.11E-03	1.10E-03	1.09E-03	1.09E-03	1.10E-03	1.11E-03	Tot Time	(sec)
P3	(atm)	11.12614	12.34411	13.43355	14.37193	15.13683	15.69506	16.01953	16.11043	15.97784	15.63115	P3	(atm)
F3	(N)	57495.16	63789.09	69418.9	74268.02	78220.73	81105.4	82782.14	83251.87	82566.71	80775.15	F3	(N)
Tot Imp	(N-sec)	73.12115	77.48189	81.27709	84.47956	87.07708	88.99616	90.18454	90.65242	90.4373	89.5526	Tot Imp	(N-sec)
Spec Imp	(sec)	103.1731	107.3384	110.9223	113.5179	115.1067	116.3866	116.5072	115.5514	114.019	111.5606	Spec Imp	(sec)

Ethylene/O2

Phi		0.8	0.9	1	1.1	1.2	1.3	1.4	1.5	1.6	1.7	1.8	1.9	2	Phi	
O/F		4.2773	3.802	3.4218	3.1107	2.8515	2.6322	2.4442	2.2812	2.1386	2.0128	1.901	1.801	1.7109	O/F	
Unburned Gas															**Unburned Gas**	
P1	(atm)	1	1	1	1	1	1	1	1	1	1	1	1	1	P1	
T1	(deg K)	300	300	300	300	300	300	300	300	300	300	300	300	300	T1	
H1	(cal/g)	84.82	93.18	101.15	108.78	116.07	123.06	129.75	136.18	142.34	148.27	153.97	159.46	164.74	H1	
M1	(kg/kmol)	31.168	31.089	31.013	30.94	30.872	30.806	30.744	30.684	30.627	30.572	30.52	30.469	30.421	M1	
Gamma1		1.3474	1.3435	1.3398	1.3364	1.3332	1.3302	1.3274	1.3248	1.3223	1.3199	1.3177	1.3156	1.3136	Gamma1	
Sonic Vel1	(m/sec)	328.4	328.3	328.3	328.2	328.2	328.2	328.2	328.2	328.2	328.2	328.2	328.2	328.2	Sonic Vel1	
Burned Gas															**Burned Gas**	
P2	(atm)	30.536	31.95	33.265	34.486	35.614	36.65	37.589	38.427	39.159	39.781	40.287	40.676	40.949	P2	
T2	(deg K)	3846	3897	3937	3967	3989	4002	4007	4004	3992	3973	3945	3909	3866	T2	
H2	(J/kg)	2.17E+06	2.30E+06	2.42E+06	2.53E+06	2.64E+06	2.74E+06	2.83E+06	2.91E+06	2.99E+06	3.06E+06	3.12E+06	3.17E+06	3.22E+06	H2	
M2	(kg/kmol)	24.229	23.403	22.651	21.963	21.33	20.745	20.201	19.695	19.221	18.776	18.358	17.963	17.591	Rho2	
Rho2	(kg/m^3)	2.34	2.34	2.33	2.33	2.32	2.32	2.31	2.3	2.3	2.29	2.28	2.28	2.27	M2	
Gamma2(SF)		1.2352	1.2372	1.2392	1.2413	1.2434	1.2455	1.2476	1.2497	1.252	1.2542	1.2566	1.259	1.2615	Gamma2(SF)	
Gamma2(S)		1.1359	1.1374	1.139	1.1407	1.1424	1.1442	1.1462	1.1484	1.1508	1.1537	1.157	1.1609	1.1652	Gamma2(S)	
Sonic Vel2	(m/sec)	1224.4	1254.8	1282.9	1308.8	1332.7	1354.7	1374.8	1393.7	1409.8	1424.6	1437.8	1449.3	1459.2	Sonic Vel2	
Detonation Parameters															**Detonation Parameters**	
P2/P1		30.536	31.95	33.265	34.486	35.614	36.65	37.589	38.427	39.159	39.781	40.287	40.676	40.949	P2/P1	
T2/T1		12.82	12.99	13.12333	13.22333	13.29667	13.34	13.35667	13.34667	13.30667	13.24333	13.15	13.03	12.88667	T2/T1	
M2/M1		0.777368	0.752774	0.730371	0.709858	0.690917	0.673408	0.657071	0.641865	0.627584	0.614157	0.601507	0.58955	0.578252	M2/M1	
Rho2/Rho1		1.8515	1.8517	1.8515	1.8512	1.8508	1.8501	1.8492	1.8481	1.8467	1.845	1.8428	1.8403	1.8373	RHO2/RHO1	
Mach #		6.9038	7.0772	7.2361	7.3819	7.5154	7.6372	7.7474	7.8462	7.9335	8.0095	8.074	8.127	8.1689	Mach #	
Det Vel	(m/sec)	2267.1	2323.5	2375.4	2423	2466.6	2506.4	2542.4	2574.8	2603.5	2628.46	2649.6	2667.1	2681	Det Vel	(m/sec)
Det Time	(sec)	4.41E-04	4.30E-04	4.21E-04	4.13E-04	4.05E-04	3.99E-04	3.93E-04	3.88E-04	3.84E-04	3.80E-04	3.77E-04	3.75E-04	3.73E-04	Det Time	(sec)
Raref Time	(sec)	8.17E-04	7.97E-04	7.79E-04	7.64E-04	7.50E-04	7.38E-04	7.27E-04	7.18E-04	7.09E-04	7.02E-04	6.96E-04	6.90E-04	6.85E-04	Raref Time	(sec)
Tot Time	(sec)	1.26E-03	1.23E-03	1.20E-03	1.18E-03	1.16E-03	1.14E-03	1.12E-03	1.11E-03	1.09E-03	1.08E-03	1.07E-03	1.06E-03	1.06E-03	Tot Time	(sec)
P3	(atm)	10.07979	10.52091	10.93018	11.30811	11.65744	11.97868	12.27049	12.54563	12.76389	12.96396	13.13383	13.27171	13.37844	P3	
F3	(N)	52088.06	54367.6	56482.5	58435.49	60240.72	61900.73	63408.7	64830.47	65958.33	66992.25	67870.07	68582.58	69134.1	F3	
Tot Imp	(N-sec)	65.51734	66.72672	67.8053	68.76514	69.62458	70.39038	71.06261	71.69564	72.12008	72.51257	72.81932	73.03547	73.16476	Tot Imp	
Spec Imp	(sec)	103.6155	105.5396	107.6942	109.201	111.0184	112.197	113.7035	115.1466	115.7406	116.771	117.6389	117.828	118.3633	Spec Imp	

Head Wall Pressure
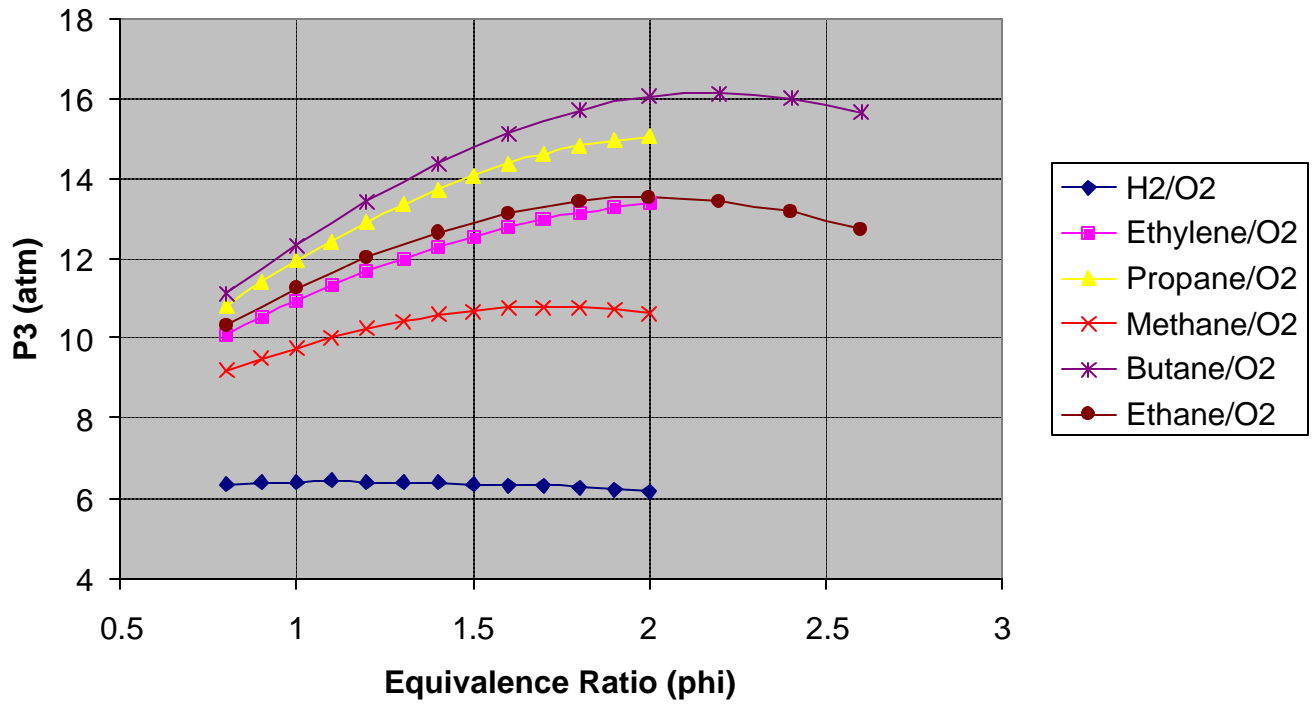
Force
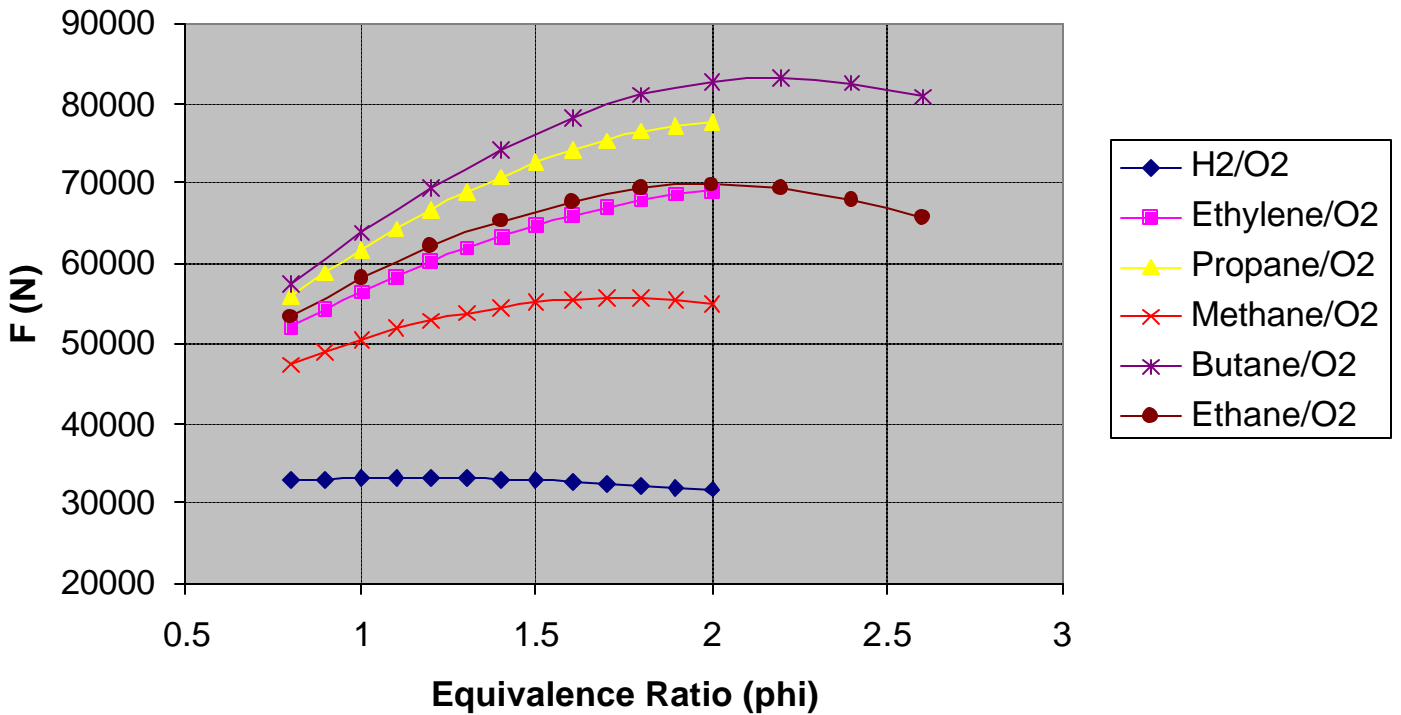
Detonation Velocity
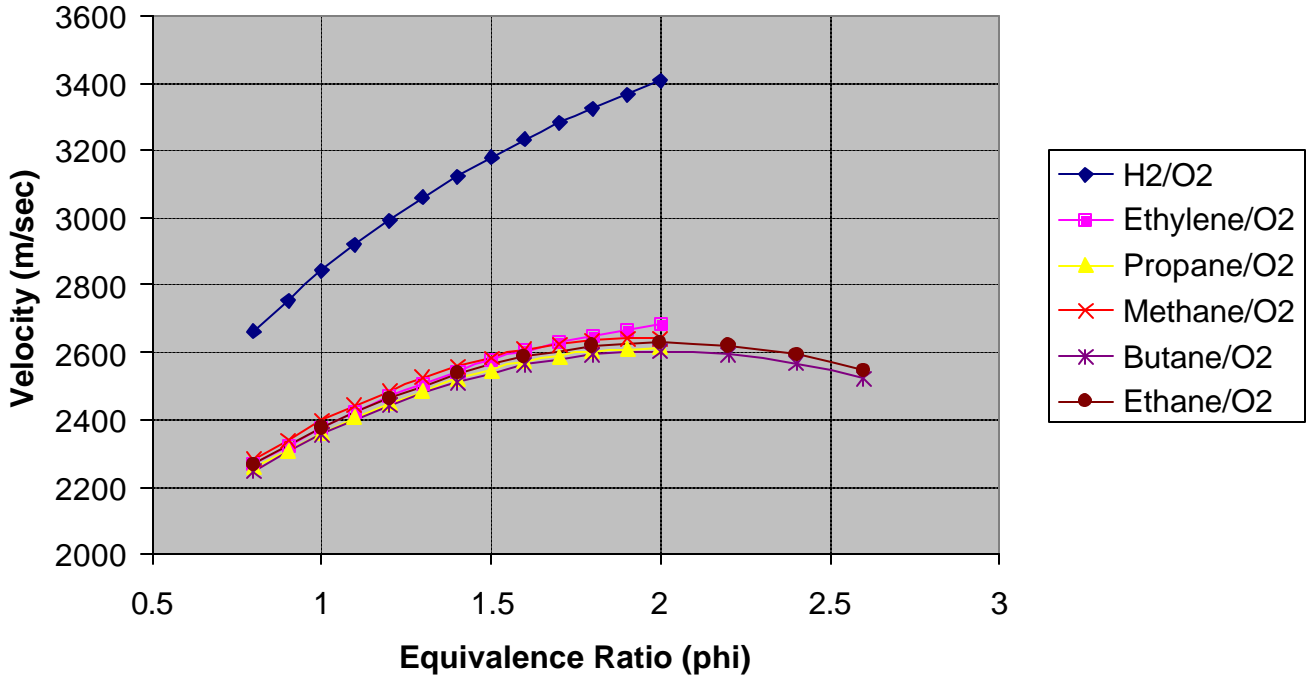
Detonation Mach Number
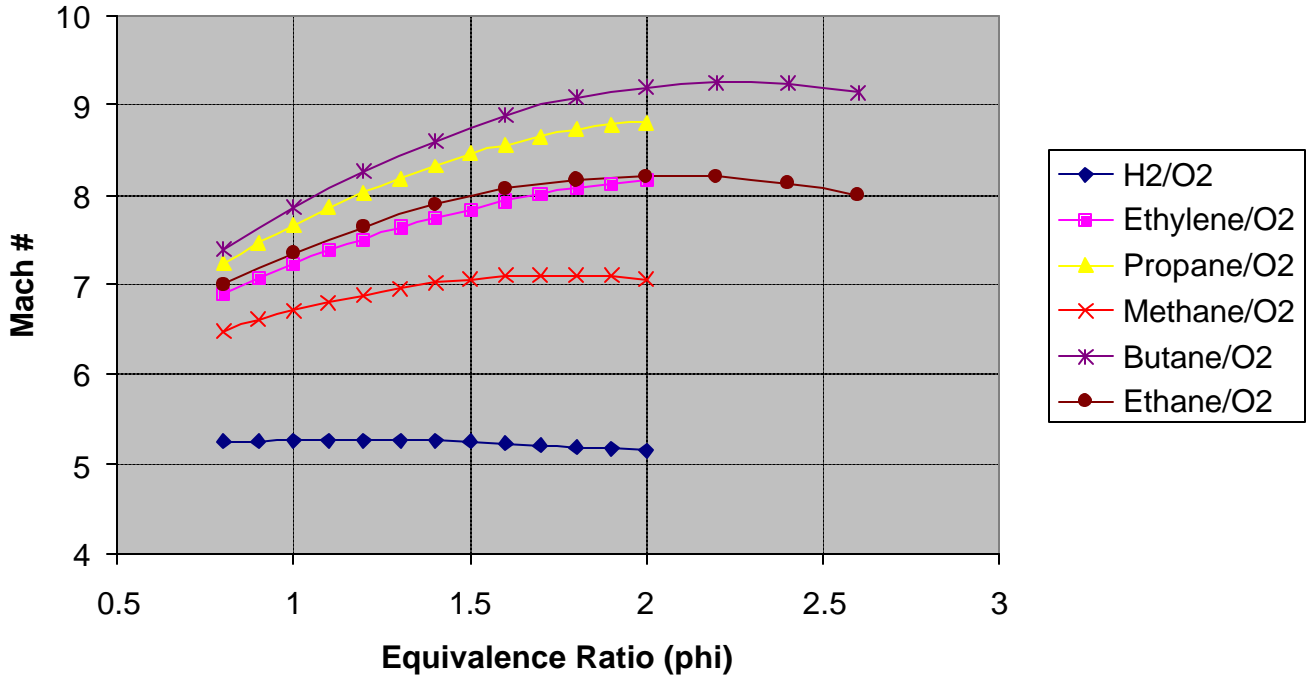
Pressure Following Wave
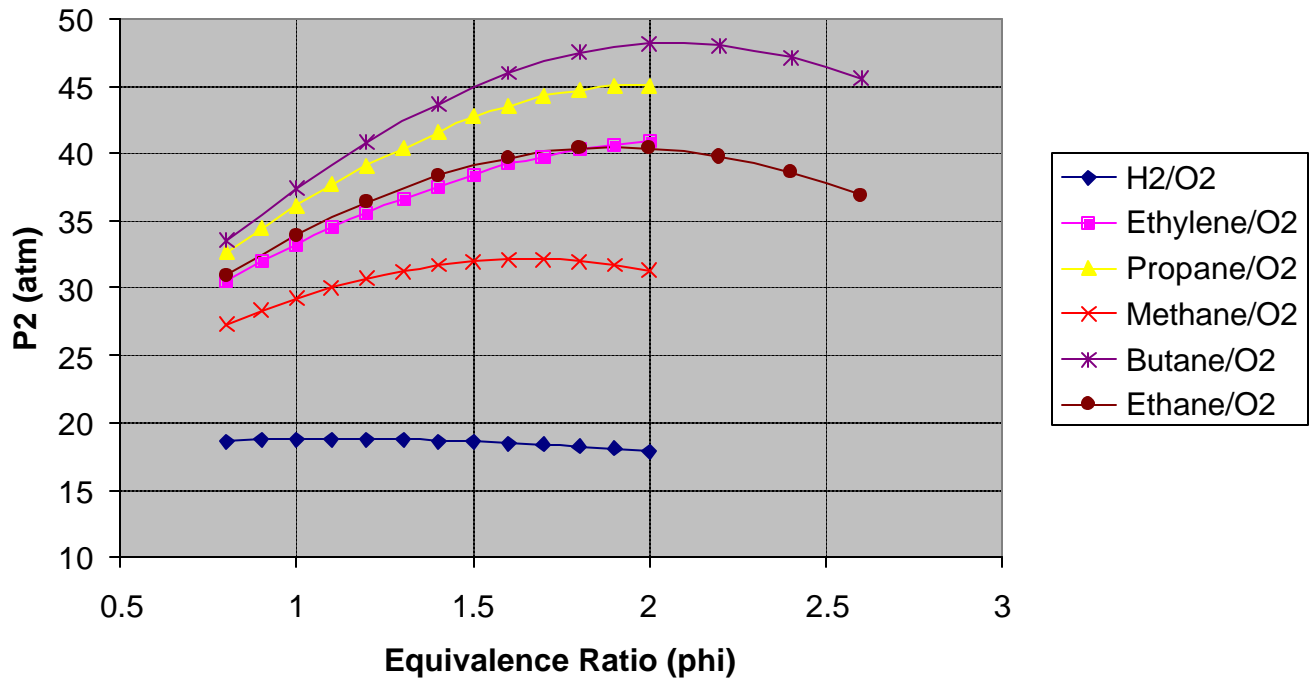
Total Impulse
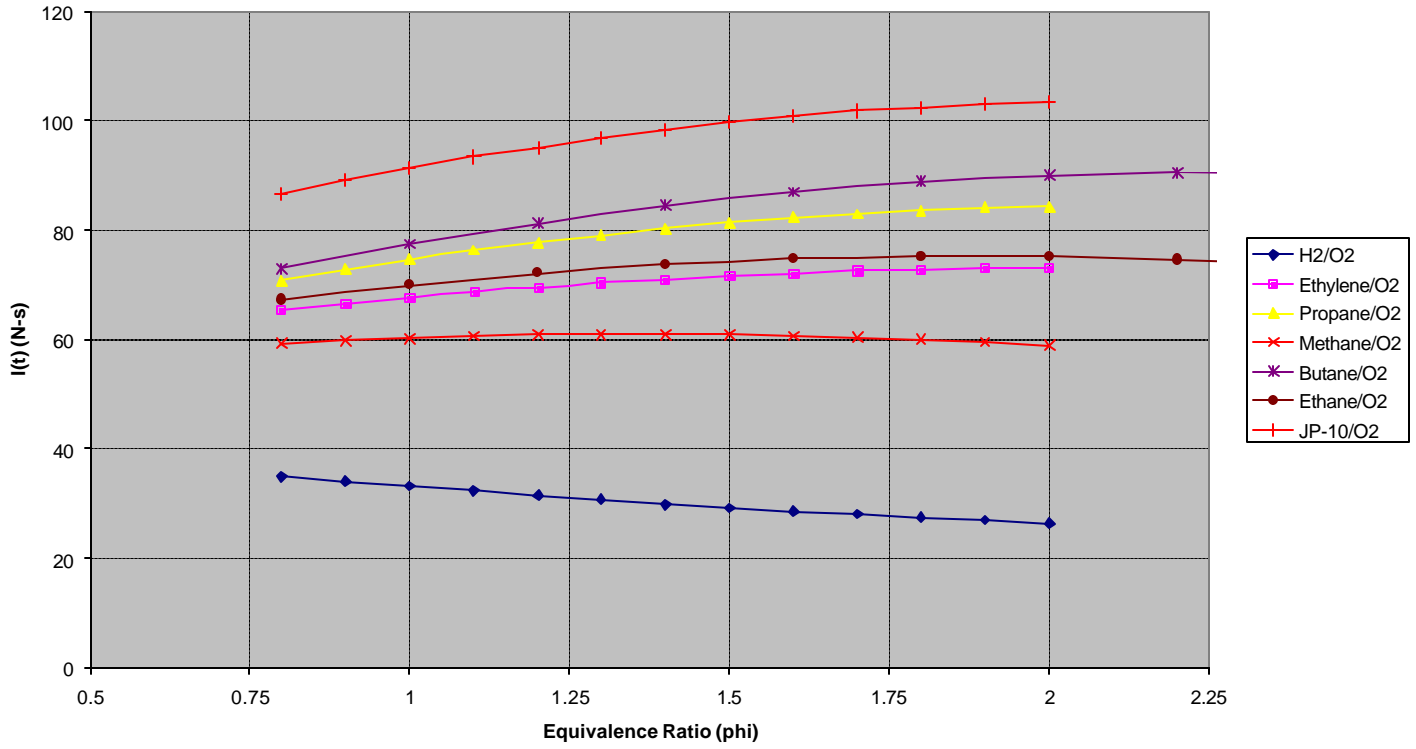
Specific Impulse
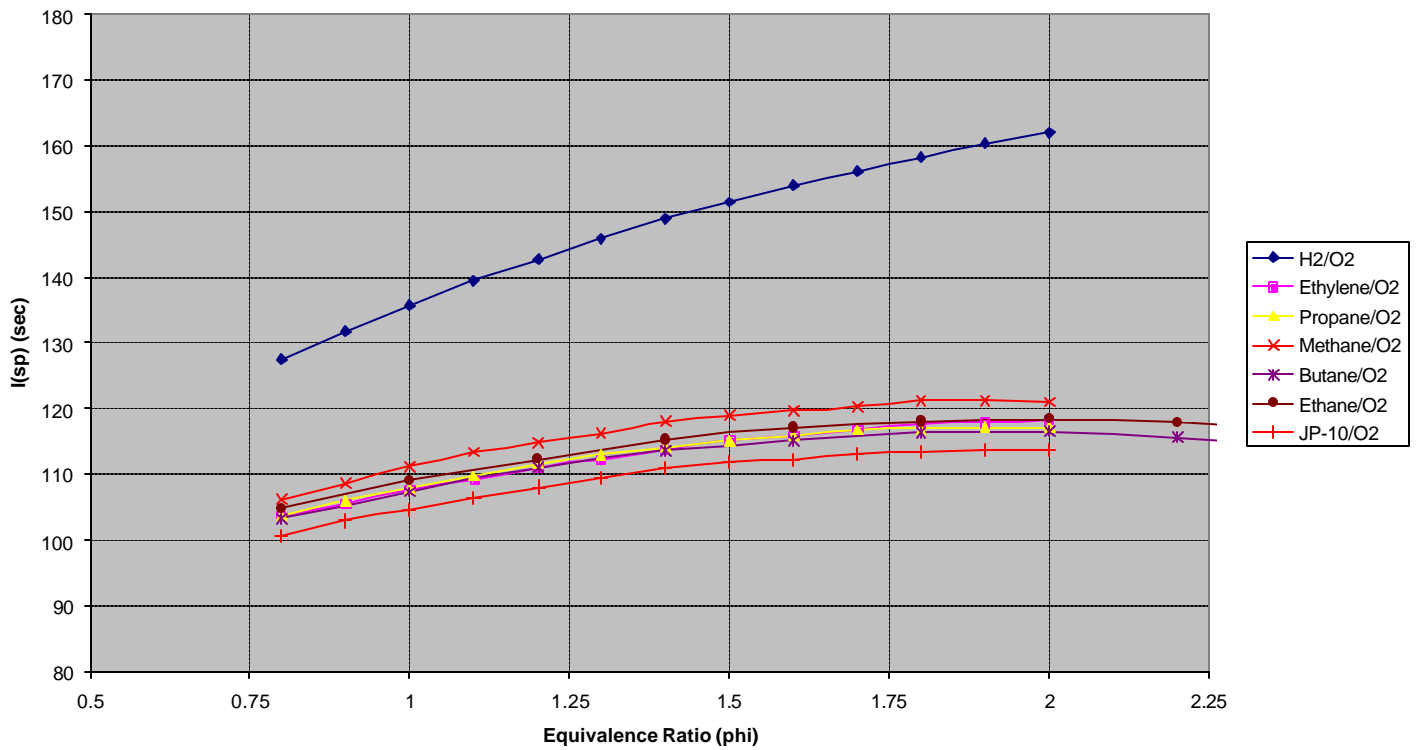
APPENDIX B: MASS FLOW RATE TABLES

Gas	O$_2$	
γ	1.393	
R	259.83	J/kg-K
K	0.042405619	sec-K$^{1/2}$/m
Γ	1	
g$_c$	1	
T$_t$=(K)	285	deg-K

Mass Flow Rate (mdot)(kg/sec)

		d$_2$ 0.001	0.002	0.003	0.004	0.005	0.003968
		A$_2$ 7.85398E-07	3.14159E-06	7.06858E-06	1.25664E-05	1.9635E-05	1.23661E-05
Upstream Pressure(p$_t$)							
(psia)	(kPa)						
45	310.264065	0.0006121	0.0024484	0.005508899	0.009793599	0.015302499	0.009637528
55	379.211635	0.000748122	0.002992489	0.006733099	0.011969954	0.018703054	0.011779201
65	448.159205	0.000884144	0.003536577	0.007957299	0.01414631	0.022103609	0.013920874
75	517.106775	0.001020167	0.004080666	0.009181499	0.016322665	0.025504164	0.016062547
85	586.054345	0.001156189	0.004624755	0.010405699	0.01849902	0.028904719	0.01820422
95	655.001915	0.001292211	0.005168844	0.011629899	0.020675376	0.032305275	0.020345893
105	723.949485	0.001428233	0.005712933	0.012854099	0.022851731	0.03570583	0.022487566
115	792.897055	0.001564255	0.006257022	0.014078299	0.025028086	0.039106385	0.024629239
125	861.844625	0.001700278	0.00680111	0.015302499	0.027204442	0.04250694	0.026770912
135	930.792195	0.0018363	0.007345199	0.016526698	0.029380797	0.045907496	0.028912585
145	999.739765	0.001972322	0.007889288	0.017750898	0.031557152	0.049308051	0.031054258
155	1068.687335	0.002108344	0.008433377	0.018975098	0.033733508	0.052708606	0.033195931
165	1137.634905	0.002244366	0.008977466	0.020199298	0.035909863	0.056109161	0.035337604
175	1206.582475	0.002380389	0.009521555	0.021423498	0.038086219	0.059509716	0.037479277
185	1275.530045	0.002516411	0.010065643	0.022647698	0.040262574	0.062910272	0.039620949
195	1344.477615	0.002652433	0.010609732	0.023871898	0.042438929	0.066310827	0.041762622
205	1413.425185	0.002788455	0.011153821	0.025096098	0.044615285	0.069711382	0.043904295
215	1482.372755	0.002924477	0.01169791	0.026320297	0.04679164	0.073111937	0.046045968
300	2068.4271	0.004080666	0.016322665	0.036725996	0.06529066	0.102016657	0.064250188
400	2757.9028	0.005440888	0.021763553	0.048967995	0.087054214	0.136022209	0.085666918
500	3447.3785	0.00680111	0.027204442	0.061209994	0.108817767	0.170027761	0.107083647

O$_2$
Upstream Pressure vs. Mass Flow Rate
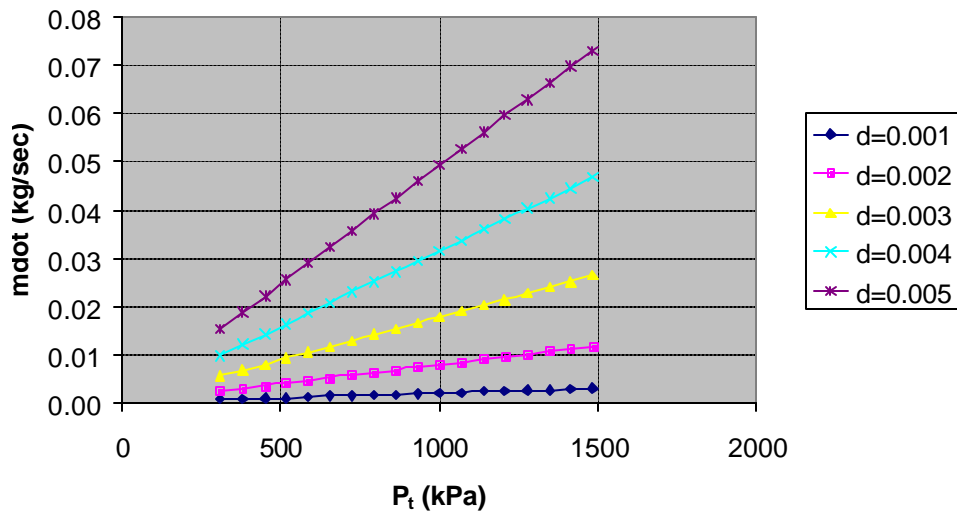
Gas	Air	
γ	1.4	
R	289	J/kg-K
K	0.040278321	sec-K$^{1/2}$/m
Γ	1	
g$_c$	1	
T$_r$(K)	292	deg-K

Mass Flow Rate (mdot)(kg/sec)

		d$_2$	0.001	0.002	0.003	0.004	0.005	0.002286
		A$_2$	7.85398E-07	3.14159E-06	7.06858E-06	1.25664E-05	1.9635E-05	4.10433E-06
Upstream Pressure(p$_t$)								
(psia)	(kPa)							
45	310.264065		0.000574383	0.00229753	0.005169444	0.009190122	0.014359566	0.003001606
55	379.211635		0.000702023	0.002808093	0.006318209	0.011232371	0.01755058	0.00366863
65	448.159205		0.000829664	0.003318655	0.007466974	0.013274621	0.020741595	0.004335654
75	517.106775		0.000957304	0.003829217	0.008615739	0.01531687	0.023932609	0.005002677
85	586.054345		0.001084945	0.00433978	0.009764505	0.017359119	0.027123624	0.005669701
95	655.001915		0.001212586	0.004850342	0.01091327	0.019401369	0.030314638	0.006336725
105	723.949485		0.001340226	0.005360904	0.012062035	0.021443618	0.033505653	0.007003748
115	792.897055		0.001467867	0.005871467	0.0132108	0.023485867	0.036696668	0.007670772
125	861.844625		0.001595507	0.006382029	0.014359566	0.025528117	0.039887682	0.008337796
135	930.792195		0.001723148	0.006892591	0.015508331	0.027570366	0.043078697	0.009004819
145	999.739765		0.001850788	0.007403154	0.016657096	0.029612615	0.046269711	0.009671843
155	1068.687335		0.001978429	0.007913716	0.017805861	0.031654865	0.049460726	0.010338867
165	1137.634905		0.00210607	0.008424278	0.018954627	0.033697114	0.05265174	0.01100589
175	1206.582475		0.00223371	0.008934841	0.020103392	0.035739363	0.055842755	0.011672914
185	1275.530045		0.002361351	0.009445403	0.021252157	0.037781613	0.05903377	0.012339937
195	1344.477615		0.002488991	0.009955965	0.022400922	0.039823862	0.062224784	0.013006961
205	1413.425185		0.002616632	0.010466528	0.023549688	0.041866111	0.065415799	0.013673985
215	1482.372755		0.002744273	0.01097709	0.024698453	0.04390836	0.068606813	0.014341008
300	2068.4271		0.003829217	0.01531687	0.034462957	0.06126748	0.095730437	0.020010709
400	2757.9028		0.005105623	0.020422493	0.04595061	0.081689973	0.127640583	0.026680946
500	3447.3785		0.006382029	0.025528117	0.057438262	0.102112466	0.159550728	0.033351182
560	3861.06392		0.007147873	0.028591491	0.064330854	0.114365962	0.178696816	0.037353324
150	1034.21355		0.001914609	0.007658435	0.017231479	0.03063374	0.047865219	0.010005355
674	4647.066218		0.008602975	0.034411901	0.077426778	0.137647604	0.215074382	0.044957394
300	2068.4271		0.003829217	0.01531687	0.034462957	0.06126748	0.095730437	0.020010709
366	2523.481062		0.004671645	0.018686581	0.042044808	0.074746325	0.116791133	0.024413065
800	5515.8056		0.010211247	0.040844986	0.09190122	0.163379946	0.255281166	0.053361892

AIR
Upstream Pressure vs. Mass Flow Rate
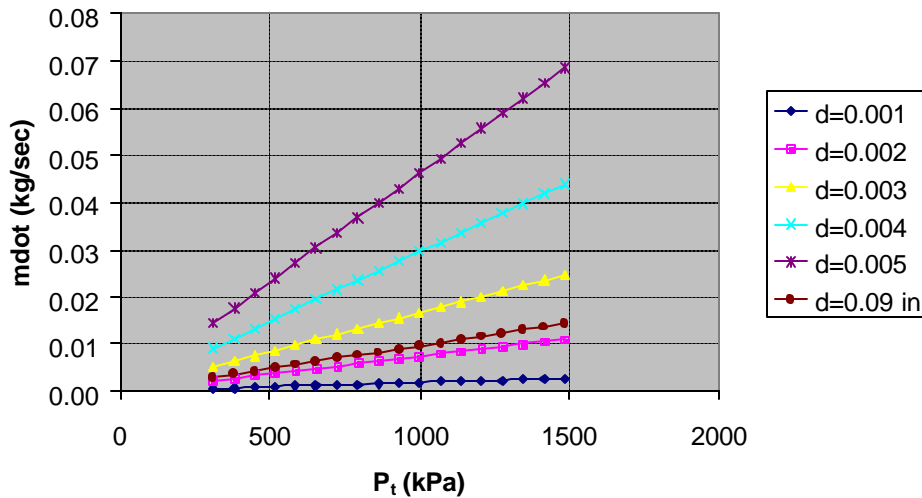
Gas	N₂
γ	1.4
R	296.8 J/kg-K
K	0.039745534 sec-K$^{1/2}$/m
Γ	1
g_c	1
T_t=(K)	285 deg-K

Mass Flow Rate (mdot)(kg/sec)

	d_2	0.001	0.002	0.003	0.004	0.005
	A_2	7.85398E-07	3.14159E-06	7.06858E-06	1.25664E-05	1.9635E-05

Upstream Pressure(p_t)						
(psia)	(kPa)					
45	310.264065	0.000573703	0.002294813	0.005163329	0.009179251	0.01434258
55	379.211635	0.000701193	0.002804771	0.006310735	0.011219085	0.01752982
65	448.159205	0.000828682	0.00331473	0.007458141	0.013258918	0.020717059
75	517.106775	0.000956172	0.003824688	0.008605548	0.015298752	0.023904299
85	586.054345	0.001083662	0.004334646	0.009752954	0.017338585	0.027091539
95	655.001915	0.001211151	0.004844605	0.010900361	0.019378419	0.030278779
105	723.949485	0.001338641	0.005354563	0.012047767	0.021418252	0.033466019
115	792.897055	0.00146613	0.005864521	0.013195173	0.023458086	0.036653259
125	861.844625	0.00159362	0.00637448	0.01434258	0.025497919	0.039840499
135	930.792195	0.00172111	0.006884438	0.015489986	0.027537753	0.043027739
145	999.739765	0.001848599	0.007394397	0.016637392	0.029577586	0.046214979
155	1068.687335	0.001976089	0.007904355	0.017784799	0.03161742	0.049402219
165	1137.634905	0.002103578	0.008414313	0.018932205	0.033657254	0.052589459
175	1206.582475	0.002231068	0.008924272	0.020079611	0.035697087	0.055776699
185	1275.530045	0.002358558	0.00943423	0.021227018	0.037736921	0.058963938
195	1344.477615	0.002486047	0.009944189	0.022374424	0.039776754	0.062151178
205	1413.425185	0.002613537	0.010454147	0.023521831	0.041816588	0.065338418
215	1482.372755	0.002741026	0.010964105	0.024669237	0.043856421	0.068525658
300	2068.4271	0.003824688	0.015298752	0.034422191	0.061195006	0.095617198
400	2757.9028	0.005099584	0.020398335	0.045896255	0.081593342	0.127489597
500	3447.3785	0.00637448	0.025497919	0.057370319	0.101991677	0.159361996

N₂
Upstream Pressure vs. Mass Flow Rate
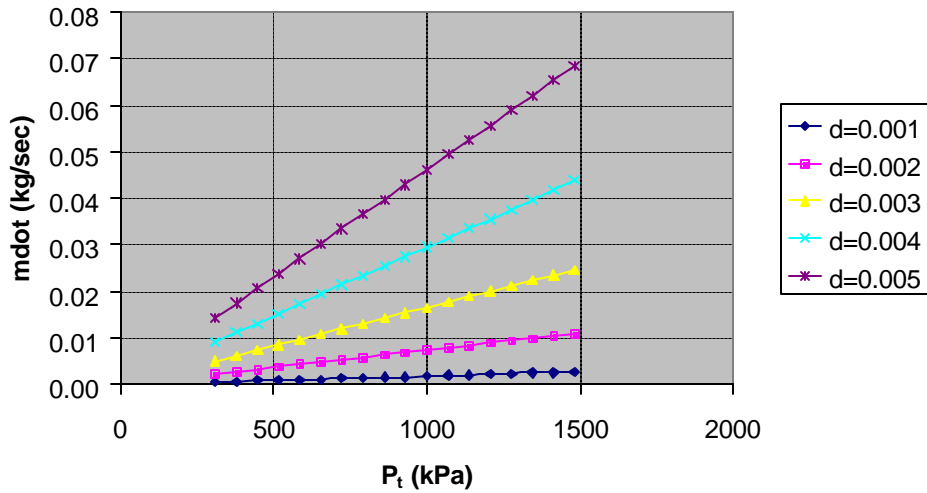
Gas	Ethylene(C2H4)	
γ	1.237	
R	296.37	J/kg-K
K	0.038083302	sec-K$^{1/2}$/m
Γ	1	
g_c	1	
T_t=(K)	285	deg-K

Mass Flow Rate (mdot)(kg/sec)

	d_2	0.001	0.002	0.003	0.004	0.005
	A_2	7.85398E-07	3.14159E-06	7.06858E-06	1.25664E-05	1.9635E-05

Upstream Pressure(p_t)						
(psia)	(kPa)					
45	310.264065	0.00054971	0.002198839	0.004947389	0.008795358	0.013742746
55	379.211635	0.000671868	0.00268747	0.006046808	0.010749882	0.01679669
65	448.159205	0.000794025	0.003176101	0.007146228	0.012704406	0.019850634
75	517.106775	0.000916183	0.003664732	0.008245648	0.01465893	0.022904577
85	586.054345	0.001038341	0.004153363	0.009345068	0.016613453	0.025958521
95	655.001915	0.001160499	0.004641994	0.010444487	0.018567977	0.029012465
105	723.949485	0.001282656	0.005130625	0.011543907	0.020522501	0.032066408
115	792.897055	0.001404814	0.005619256	0.012643327	0.022477025	0.035120352
125	861.844625	0.001526972	0.006107887	0.013742746	0.024431549	0.038174296
135	930.792195	0.00164913	0.006596518	0.014842166	0.026386073	0.041228239
145	999.739765	0.001771287	0.007085149	0.015941586	0.028340597	0.044282183
155	1068.687335	0.001893445	0.00757378	0.017041006	0.030295121	0.047336127
165	1137.634905	0.002015603	0.008062411	0.018140425	0.032249645	0.05039007
175	1206.582475	0.002137761	0.008551042	0.019239845	0.034204169	0.053444014
185	1275.530045	0.002259918	0.009039673	0.020339265	0.036158693	0.056497957
195	1344.477615	0.002382076	0.009528304	0.021438684	0.038113217	0.059551901
205	1413.425185	0.002504234	0.010016935	0.022538104	0.040067741	0.062605845
215	1482.372755	0.002626392	0.010505566	0.023637524	0.042022265	0.065659788
300	2068.4271	0.003664732	0.01465893	0.032982591	0.058635718	0.091618309
400	2757.9028	0.00488631	0.019545239	0.043976789	0.078180957	0.122157746
500	3447.3785	0.006107887	0.024431549	0.054970986	0.097726197	0.152697182

C$_2$H$_4$
Upstream Pressure vs. Mass Flow Rate

88
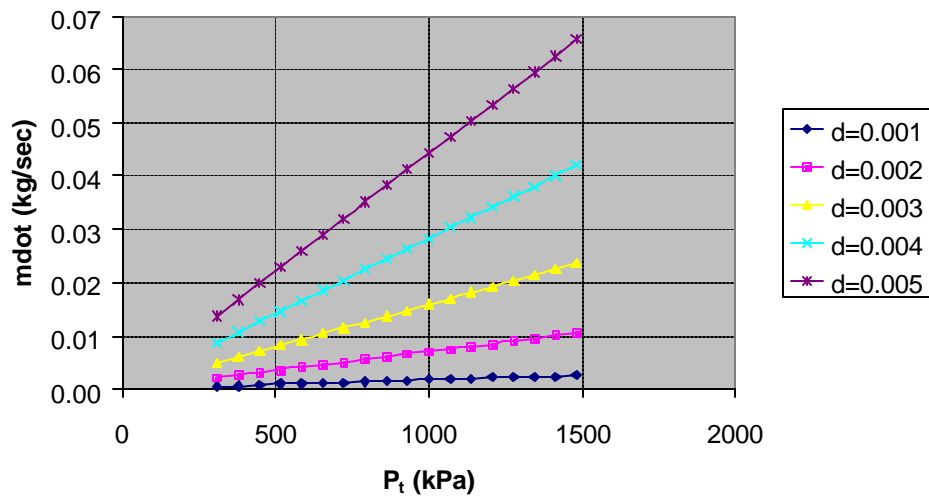
APPENDIX C: RUN DATA

Gas, Short Tube

LONG TUBE
MED TUBE
SHORT TUBE

Sensors=0.9791"=24.87mm

Run:	Comments	Event Start	Event End	O₂:	Pressures Fuel:	Purge(set):	O/F:	Ψ:	O₂ Fill:	Timing Fuel Fill:	Delay	Spark:	Freq:
3	Phi variation	0.172538	0.175639	156	162	20	3.41	1	20	20	0	21	20
4	Phi variation	0.872505	0.875954	156	180	20	3.07	1.1	20	20	0	21	20
5	Phi variation	0.522419	0.525984	156	194	20	2.87	1.2	20	20	0	21	20
6	Phi variation	0.172546	0.175703	156	214	20	2.63	1.3	20	20	0	21	20
7	Phi variation	0.922542	0.925746	156	229	20	2.45	1.4	20	20	0	21	20
8	Problem loading	NA	NA	156	229	18	2.45	1.4	20	20	0	21	20
9	Freq variation	0.522285	0.525568	156	214	20	2.64	1.3	20	20	0	21	10
10	Freq variation	0.272452	0.275437	156	214	20	2.64	1.3	20	20	0	21	20
11	Freq variation	Bad data	Bad data	156	214	20	2.64	1.3	20	20	0	21	30
12	High purge, freq	0.588577	0.591549	156	214	45	2.64	1.3	20	20	0	21	30
13	Timing variation	Bad data	Bad data	156	214	20	2.64	1.3	15	15	0	16	30
14	Timing variation	0.11233	0.116187	156	214	20	2.64	1.3	10	10	0	11	30
15	Higher purge	0.112434	0.116255	156	214	30	2.64	1.3	10	10	0	11	30

Gas, Med Tube

LONG TUBE
MED TUBE
SHORT TUBE

Sensors=0.9760"=24.79mm

Run:	Comments	Event Start	Event End	O₂:	Pressures Fuel:	Purge(set):	O/F:	Ψ:	O₂ Fill:	Timing Fuel Fill:	Delay	Spark:	Freq:
14	Phi, spark variation	0.342419	0.347713	174	181	20	3.34	1	40	40	0	41	10
15	Phi, spark variation	0.5425	0.547867	174	202	20	3.01	1.1	40	40	0	41	10
16	Phi, spark variation	0.347345	0.352917	174	202	20	3.01	1.1	45	45	0	46	10
17	Phi, spark variation	0.447515	0.45269	174	215	20	2.86	1.2	45	45	0	46	10
18	Phi, spark variation	0.547359	0.552772	174	233	20	2.64	1.3	45	45	0	46	10
19	Phi, spark variation	0.447205	0.452844	174	253	20	2.45	1.4	45	45	0	46	10
20	Phi, spark variation	0.346302	0.351734	174	233	20	2.68	1.3	45	45	0	45	10
1*	*	0.447408	0.451736	175	180	20	3.36	1	45	45	0	46	10
2**	**	NA	NA	156	232	20	2.44	1.4	10	10	0	11	5

* Add for 16_R14-20
** ReRun of 16_R5

Run:	Comments	Event Start	Event End	O₂:	Pressures Fuel:	Purge(set):	O/F:	Ψ:	O₂ Fill:	Timing Fuel Fill:	Delay	Spark:	Freq:
16	Phi variation	0.247515	0.251674	156	160	20	3.42	1	45	45	0	46	10
17	Phi variation	0.947376	0.951687	156	179	20	3.1	1.1	45	45	0	46	10
18	Phi variation	0.347623	0.351652	156	195	20	2.86	1.2	45	45	0	46	10
19	Phi variation	0.647385	0.651455	156	213	20	2.61	1.3	45	45	0	46	10
20	Phi variation	0.247451	0.251306	156	228	20	2.45	1.4	45	45	0	46	10
20	Phi variation	0.047456	0.051542	156	256	20	2.24	1.53	45	45	0	46	10

Gas, Long Tube

LONG TUBE
MED TUBE
SHORT TUBE

Sensors=0.9516"=24.17mm

Run:	Comments	Event Start	Event End	O₂:	Fuel:	Purge(set):	O/F:	Φ:	O₂ Fill:	Fuel Fill:	Delay	Spark:	Freq:
1	Exploratory	0.142321	0.148183	119	128	134	3.35	1.02	40	40	0	41	10
2	Exploratory	0.142703	0.147957	115	130	202	2.29	1.5	40	40	0	41	10
3	Exploratory	0.199512	0.207215	115	130	202	2.29	1.5	60	60	0	60	10
4	Exploratory	0.652498	0.657734	?	?	?	?	?	?	?	0	?	?
1	Purge variation	0.104562	0.109225	174	255	10	2.45	1.4	100	100	0	101	5
2	Purge variation	0.502192	0.509199	174	255	20	2.45	1.4	100	100	0	101	5
3	Purge variation	0.502349	0.510148	174	255	30	2.45	1.4	100	100	0	101	5
4	Purge variation	0.160171	0.167922	174	255	40	2.45	1.4	100	100	0	101	5
5	Purge variation	0.302292	0.310655	172	254	50	2.46	1.39	100	100	0	101	5
6	Partial fill series	0.093813	0.098922	175	254	20	2.46	1.39	90	90	0	91	5
7	Partial fill series	0.082387	0.088716	175	254	20	2.46	1.39	80	80	0	81	5
8	Partial fill series	Problem	Problem	175	254	20	2.46	1.39	70	70	0	71	5
9	Partial fill series	0.66244	0.668397	175	254	20	2.46	1.39	60	60	0	61	5
10	Partial fill series	0.052263	0.057757	175	254	20	2.46	1.39	50	50	0	51	5
11	Higher freq, purge	0.652386	0.658309	174	239	40	?	?	50	50	0	51	10
12	Higher freq, purge	0.952324	0.958547	174	239	40	?	?	50	50	0	51	10
3	Part Fill Threshold*	0.172429	0.177481	?	?	?	?	?	?	?	0	?	?
4	Part Fill Threshold*	0.52265	0.527786	174	256	50	2.45	1.4	20	20	0	21	20
5	Part Fill Threshold*	0.874255	0.880105	174	259	50	2.43	1.4	22	22	0	23	20
6	Part Fill Threshold*	0.876309	0.881963	174	261	50	?	?	24	24	0	25	20
7	Part Fill Threshold*	0.128553	0.133658	174	255	50	2.49	1.37	26	26	0	27	20
8	Part Fill Threshold*	0.07719	0.082814	173	256	50	2.47	1.39	25	25	0	26	20

*Frequency=20Hz

Run:	Comments	Event Start	Event End	O₂:	Fuel:	Purge(set):	O/F:	Φ:	O₂ Fill:	Fuel Fill:	Delay	Spark:	Freq:
1	Partial fill series	0.052369	0.058685	174	257	20(26)	2.44	1.4	50	50	0	51	5
2	Partial fill series	0.642326	0.64826	174	257	20(26)	2.44	1.4	40	40	0	41	5
3	Partial fill series	0.832374	0.838191	174	257	20(26)	2.44	1.4	30	30	0	31	5
4	Partial fill series	0.222491	0.228103	174	257	20(26)	2.44	1.4	20	20	0	21	5
5	Partial fill series	0.613199	0.617777	174	257	20(26)	2.44	1.4	10	10	0	11	5
6	Phi variation	0.272587	0.279536	174	239	20(26)	2.62	1.3	70	70	0	71	5
7	Phi variation	0.271373	0.280129	174	215	20(26)	2.87	1.2	70	70	0	71	5
8	Phi variation	0.272475	0.279042	174	197	20(26)	3.11	1.1	70	70	0	71	5
9	Phi variation	0.472498	0.478998	174	179	20(26)	3.4	1	70	70	0	71	5
10	No purge	0.072409	0.077826	174	180	0	3.38	1	70	70	0	71	2
11	No purge	0.531103	0.537162	174	180	0	3.36	1	100	70	30	101	2
12**	AlternateWav1,2**	0.072214	0.079829	174	235	20	2.63	1.3	70	70	0	71	5
13**	AlternateWav1,2**	0.072553	0.079027	174	181	20	3.41	1	70	70	0	71	5

Gas, Short Tube 2

LONG TUBE
MED TUBE
SHORT TUBE

Sensors=1.0309"=26.185mm

Run:	Layout Saved?	Event Start	Event End	O₂:	Fuel:	Purge(set):	O/F:	Φ:	O₂ Fill:	Fuel Fill:	Delay	Spark:	Freq:
1	Phi variation	0.122482	0.126233	157	162	20	3.42	1	20	20	0	21	20
2	Phi variation	0.320835	0.326357	157	178	20	3.11	1.1	20	20	0	21	20
3	Phi variation	0.621772	0.62643	157	197	20	2.85	1.2	20	20	0	21	20
4	Phi variation	0.421025	0.426459	157	211	20	2.63	1.3	20	20	0	21	20
5	Phi variation	0.071776	0.076354	157	231	20	2.44	1.4	20	20	0	21	20
6	Freq variation	Error	Error	157	211	20	2.63	1.3	20	20	0	21	10
7	Freq variation	0.322349	0.326432	157	211	20	2.63	1.3	20	20	0	21	20
8	Freq,purge variation	0.88249	0.88676	157	211	30	2.63	1.3	20	20	0	21	30

Gas, Med Tube 2

LONG TUBE
MED TUBE
SHORT TUBE

Sensors=1.079"=27.40mm

Run:	Layout Saved?	Event Start	Event End	O₂:	Pressures Fuel:	Purge(set):	O/F:	Ψ:	O₂ Fill:	Timing Fuel Fill:	Delay	Spark:	Freq:
9*	Did not do	NA	NA	157	162	20	3.42	1	20	20	0	21	20
10*	Did not do	NA	NA	157	178	20	3.11	1.1	20	20	0	21	20
11*	Did not do	NA	NA	157	197	20	2.85	1.2	20	20	0	21	20
12	Misc	0.072539	0.076474	157	211	20	2.63	1.3	20	20	0	21	20
13	Misc	0.322461	0.32641	157	231	20	2.44	1.4	20	20	0	21	20
14*	Did not do	NA	NA	157	211	20	2.63	1.3	20	20	0	21	10
15*	Did not do	NA	NA	157	211	20	2.63	1.3	20	20	0	21	20
16*	Did not do	NA	NA	157	211	30	2.63	1.3	20	20	0	21	30
17	Misc	0.241962	0.247038	157	234	40	2.43	1.4	40	40	0	41	10

*DND

Run:	Layout Saved?	Event Start	Event End	O₂:	Pressures Fuel:	Purge(set):	O/F:	Ψ:	O₂ Fill:	Timing Fuel Fill:	Delay	Spark:	Freq:
1	Phi variation	0.142672	0.147009	156	162	40	3.42	1	40	40	0	41	20
2	Phi variation	0.262072	0.264659	156	180	40	3.09	1.1	40	40	0	41	20
3	Phi variation	0.582589	0.586872	156	180	40	3.09	1.1	30	30	0	31	20
4	Phi variation	0.48234	0.487108	155	198	40	2.84	1.2	30	30	0	31	20
5	Phi variation	0.582392	0.586825	156	216	40	2.61	1.3	30	30	0	31	20
6	Phi variation	0.581847	0.586816	156	231	40	2.44	1.4	30	30	0	31	20
7	Freq, purge variation	0.132127	0.137046	156	213	40	2.64	1.3	30	30	0	31	10
8	Freq, purge variation	0.882572	0.886789	156	213	40	2.64	1.3	30	30	0	31	20
9	Freq, purge variation	0.288871	0.292837	156	213	50	2.64	1.3	20	20	0	21	30
10	Freq, purge variation	Bad data	Bad data	156	213	60	2.64	1.3	10	10	0	11	40

Liquid, Short Tube 2

LONG TUBE
MED TUBE
SHORT TUBE

Sensors=1.0309"=26.185mm

FileName:	Comments	Comments	Event Start	Event End	Run:	O₂:	Pressures Fuel:	Purge(set):	O/F:	Φ:	O₂ Fill:	Timing Fuel Fill:	Delay	Spark:	Freq:
Kerosene/RP-1															
PED_12_4_R1	Spark variation		0.435930	0.437460	1	175	1600	NA			28	7	29	33	5
PED_12_4_R2	Spark variation		Problems	Problems	2	175	1600	NA			28	7	29	35	5
PED_12_4_R3	Spark variation		0.800659	0.802400	3	175	1600	NA			28	7	29	33	5
PED_12_4_R4	Phi variation		0.434784	0.436439	4	200	1715	NA			28	7	29	33	5
PED_12_4_R5	Delay, spark vary	Solid Run	0.234732	0.236413	5	145	1715	NA			28	7	29	33	5
PED_12_4_R6	Delay, spark vary	~75%solid bangs	0.633781	0.635602	6	145	1730	NA			28	7	29	32	5
PED_12_4_R7	Delay, spark vary	Δ'd Wav1,2gain	0.038108	0.040263	7	145	1704	NA			28	7	29	34	5
PED_12_4_R8	Delay, spark vary	Bangs but No dets	0.637489	0.639954	8	145	1720	NA			28	7	29	35	5
PED_12_4_R9	Delay, spark vary	Poofs, no dets	0.038050	0.040152	9	145	1720	NA			28	7	28	33	5
PED_12_4_R10	Delay, spark vary	Dets every other shot	0.834684	0.836453	10	145	1720	NA			28	7	29	33	5
PED_12_4_R11	Delay, spark vary	Not quite dets	0.600751	0.603004	11	145	1720	NA			28	7	30	33	5
PED_12_4_R12	Delay, spark vary	Poofs	0.634576	0.637519	12	145	1720	NA			28	7	31	33	5
PED_12_4_R13	Phi variation	**Best case	0.400772	0.402500	13	157	1720	NA			28	7	29	33	5
PED_12_4_R14	Dito above	**Best case	0.234642	0.236466	14	157	1720	NA			28	7	29	33	5
PED_12_4_R15	Freq, purge variation	Solid dets	0.634733	0.636866	15	181	1725	NA			28	7	29	33	5
PED_12_4_R16	Freq, purge variation	Solid dets, sporatic	0.134636	0.136842	16	181	1725	NA			28	7	29	33	10
JP-10	** Amps at 300 **	** Amps at 300 **													
PED_12_5_R1	Phi vary @ best case	Mostly misses	0.643466	0.645643	1	181	1690	NA			28	7	29	33	5
PED_12_5_R2	Phi vary @ best case	Bangs every other	0.435142	0.437191	2	140	1690	NA			28	7	29	33	5
PED_12_5_R3	Phi vary @ best case	80% good bangs	0.800735	0.802680	3	160	1715	NA			28	7	29	33	5
PED_12_5_R4	Phi vary @ best case	Poofs, few bangs	0.800844	0.802904	4	200	1725	NA			28	7	29	33	5
PED_12_5_R5	Phi vary @ best case	Bangs every other	0.850117	0.852419	5	120	1730	NA			28	7	29	33	5
JP-10	**Removed solenoids	**Removed solenoids/Replaced with check valves**													
PED_12_6_R1	Various		NA	NA	1	321	1675	NA			28	7	29	33	20
PED_12_6_R2	Various		NA	NA	2	320	1700	NA			28	7	29	33	30
PED_12_6_R3	Various		NA	NA	3	357	1700	NA			28	7	29	33	30
PED_12_6_R4	Various	NoData	NA	NA	4	357	1710	NA			28	7	29	33	20
PED_12_6_R5	Various	NoData	NA	NA	5			NA			28	7	29	33	5

THIS PAGE INTENTIONALLY LEFT BLANK

APPENDIX D: FACILITY OPERATIONS

TEST CELL #2
STANDARD OPERATING PROCEDURES FOR *GASEOUS FUELS*

Facility Open Procedure

Test Cell

1. Turn on Amps 1-4.

Control Room

2. Verify emergency stop button is pushed in.
3. Turn on 24VDC power supply located in cabinet #1A.
4. Turn on control panel in cabinet #2.
5. Turn on warning lights.

Test Cell

6. Using hearing protection, turn on ignition system
(**Caution: Residual fuel in tube may ignite**).
7. Open high-pressure air. Ensure valve in Test Cell #1
is open.
8. Open shop air, O_2, N_2, and fuel bottles. Check for
leaks.

Control Room

9. On Roberto, control code:
     a. On desktop, open "PED_Code.EXE."
     b. Enter run conditions.
     c. Under facility operations open ball valves and
select "continuous", "spark", and "open facility".

10. Open data acquisition code.
     a. On desktop, open "HighspeedDAQ.vi."
     b. Set sample rate to 1,000,000 Hz.
     c. Set channels to 0:3.
     d. Set # of scans to 1,000,000.
     e. Set device to 2.

11. Ensure all RPCL personnel are in control room.
12. Reset emergency stop button.

Run Procedures

Control Room

1. Ensure all pressures and run conditions are set.
2. Ensure area is clear of golfers and all RPCL personnel are in control room.
3. Start VCRs.
4. Sound siren.
5. In control code, click on start run.
6. Once firing has begun, click on play in DAQ code.
7. In control code click on stop run.
8. Engage purge for 10-20 seconds.
9. Secure siren.
10. Secure VCRs
11. Engage emergency stop button.

Close Facility Procedure

Control Room

1. Ensure emergency stop button is engaged.
2. Close DAQ code.

Test Cell

3. Close/vent O_2 and shop air.
4. Close high-pressure air and fuel.
5. Secure ignition system.
6. Secure amps.

Control Room

7. Purge high-pressure air.
8. Purge fuel.
9. Secure warning lights.
10. Secure control code.
11. Secure control panel.
12. Secure 24VDC power supply.

TEST CELL #2
STANDARD OPERATING PROCEDURES FOR *LIQUID FUELS*

Facility Open Procedure

Test Cell

1. Turn on Amps 1-4.

Control Room

2. Verify emergency stop button is pushed in.
3. Turn on 24VDC power supply located in cabinet #1A.
4. Turn on control panel in cabinet #2.
5. Turn on warning lights.

Test Cell

6. Using hearing protection, turn on ignition system (**Caution: Residual fuel in tube may ignite**).
7. Ensure fuel and oil reservoirs are filled.
8. Open shop air, O_2, and N_2 bottles. Check for leaks.

Control Room

9. On Roberto, control code:
    a. On desktop, open "PED_Code.EXE."
    b. Enter run conditions.
    c. Under facility operations open ball valves and
select "continuous", "spark", and "open facility".

10. Open data acquisition code.
    a. On desktop, open "HighspeedDAQ.vi."
    b. Set sample rate to 1,000,000 Hz.
    c. Set channels to 0:3.
    d. Set # of scans to 1,000,000.
    e. Set device to 2.

11. Ensure all RPCL personnel are in control room.
12. Reset emergency stop button.

Run Procedures

Control Room

1. Ensure all pressures and run conditions are set.
2. Ensure area is clear of golfers and all RPCL personnel are in control room.
3. Start VCRs.
4. Sound siren.
5. In control code, click on start run.
6. Once firing has begun, click on play in DAQ code.
7. In control code click on stop run.
8. Open Ox valve 10-20 seconds.
9. Secure siren.
10. Secure VCRs
11. Engage emergency stop button.

Close Facility Procedure

Control Room

1. Ensure emergency stop button is engaged.
2. Close DAQ code.

Test Cell

3. Close/vent O_2, shop air, and N_2.
4. Close high-pressure air and fuel.
5. Secure ignition system.
6. Secure amps.

Control Room

7. Secure warning lights.
8. Secure control code.
9. Secure control panel.

10. Secure 24VDC power supply.

LIST OF REFERENCES

1. Glassman, I., <u>Combustion</u>, (1977), Academic Press, New York, NY.

2. <u>TEP™ for Windows- A Combustion Analysis Tool, Version User's Manual</u>, Software Engineering Associates, Inc., Carson City, NV.

3. Lederman, S., "Modern Diagnostics of Combustion," <u>Experimental Diagnostics in Gas Phase Combustion Systems</u>, <u>Progress in Astronautics and Aeronautics (AIAA)</u>, Vol. 53, 1976, New York, Page 479.

4. O'Shea, D.C., Callen, W.R., and Rhodes, W.T., <u>Introduction to Lasers and Their Applications</u>, (1978) Adison-Wesley Publishing Company, Reading, MA.

5. Rothe, E.W., An, H., and Hitchcock, L.M., "Rayleigh and Predissociative Fluorescence Imaging of Densities from an Internal Combustion Engine Using a Tunable KrF Laser," <u>Laser Applications in Combustion and Combustion Diagnostics II</u>, <u>SPIE-The International Society for Optical Engineering</u>, Vol. 2122, 1994, Los Angeles, Page 79.

6. Benedict, R. P., <u>Fundamentals of Temperature, Pressure, and Flow Measurements</u>, (1984), John Wiley & Sons, New York, NY.

7. Kuo, K. K., <u>Principles of Combustion</u>, (1986), John Wiley & Sons, New York, NY.

THIS PAGE INTENTIONALLY LEFT BLANK

INITIAL DISTRIBUTION LIST

1. Defense Technical Information Center
   8725 John J. Kingman Road, Suite 0944
   Ft. Belvoir, VA 22060-6218

2. Dudley Knox Library
   Naval Postgraduate School
   411 Dyer Road
   Monterey, CA 93943-5101

3. Marine Corps Representative
   Naval Postgraduate School
   411 Dyer Road
   Monterey, CA 93943

4. Director, Training and Education, MCCDC,
   Code C46
   Quantico, Virginia

5. Director, Marine Corps Research Center, MCCDC,
   Code C40RC
   Quantico, Virginia

6. Marine Corps Tactical Systems Support Activity
   (Attn: Operations Officer)
   Camp Pendleton, California

7. Maj Paul E. Damphousse
   212 Belden Street #6
   Monterey, CA 93940

8. Dr. Christoper M. Brophy, Code AA/BR
   Department of Aeronautics and Astronautics
   Naval Postgraduate School
   699 Dyer Road, Room 127
   Monterey, CA 93943-5106

9. Dr. Jose O. Sinibaldi, Code AA/SJ
   Department of Aeronautics and Astronautics
   Naval Postgraduate School
   699 Dyer Road, Room 127
   Monterey, CA 93943-5106